DESIGN AND ANALYSIS OF A WEARABLE PIEZORESISTIVE MEMS ACCELEROMETER WITH LOW CROSS-AXIS SENSITIVITY FOR NEUROLOGICAL DISEASE DIAGNOSIS

SONALI BISWAS

DESIGN AND ANALYSIS OF A WEARABLE PIEZORESISTIVE MEMS ACCELEROMETER WITH LOW CROSS-AXIS SENSITIVITY FOR NEUROLOGICAL DISEASE DIAGNOSIS

A

Thesis Submitted

in Partial Fulfilment of the Requirements

for the Degree of

DOCTOR OF PHILOSOPHY

By

SONALI BISWAS

Department of Electronics and Electrical Engineering

Indian Institute of Technology Guwahati

Guwahati-781 039, INDIA.

September, 2018

TH-2011_11610225

Certificate

This is to certify that the thesis entitled "**Design and Analysis of a Wearable Piezoresistive MEMS Accelerometer with Low Cross-axis Sensitivity For Neurological Disease Diagnosis**", submitted by **SONALI BISWAS** (11610225), a research scholar in the *Department of Electronics & Electrical Engineering, Indian Institute of Technology Guwahati*, for the award of the degree of **Doctor of Philosophy**, has been carried out by her under my supervision and guidance. The thesis has fulfilled all requirements as per the regulations of the institute and in my opinion has reached the standard needed for submission. The results embodied in this thesis have not been submitted to any other University or Institute for the award of any degree or diploma.

Dated:
Guwahati.

Prof. Anup kumar Gogoi
Dept. of Electronics & Electrical Engg.
Indian Institute of Technology Guwahati
Guwahati - 781039, Assam, India.

TH-2011_11610225

Acknowledgements

I would like to express my sincere gratitude to my supervisor, Prof. Anup Kumar Gogoi, for his advice, helpful discussions, support and encouragement throughout the course of this work. I would particularly like to thank him and Prof Uday. S Dixit for patiently and carefully correcting all my manuscripts and helping me with their constructive criticism.

I would like to thank my doctoral committee members Prof. Prabin Kumar Bora, Prof. R. Bhattacharjee and Prof. Uday. S Dixit for sparing their precious time to evaluate the progress of my work throughout these years and offering their valuable suggestions. I am deeply thankful to SCL team, Chandigarh for their thorough review, valuable suggestions and support for fabrication facility.

I had a great time with my many friends and labmates helping me with tools, discussing my courses and research work at IIT Guwahati, including (but not limited to) Pralay, Saroj, Mandar, Suman, Ansath, Rajib Jana, Shashank, Basudeb, Nama and Malathi. I sincerely thank Pawan, Arijit and Anoop for their ever ready help and encouragement. I thank my dearest friends Reena, Rajbir and Kakoli whose constant love and motivation helped me specially during adverse situations.

I am really thankful to my baby Divyansh, my all source of inspiration and deeply regret for all the sacrifices he made while I was at work. I express my deep appreciation to my beloved husband Dr Debasish Deb and am deeply sorry for the time we spent apart. I am really grateful to my beloved parents who actually made this research possible by letting me work peacefully by taking utmost care of my baby Divyansh. The love and support of my two sisters Dr Moushumi Biswas and Dr Barnali Biswas made this long cherished dream come true. I thank my brother-in-law Dr Debajit Das for helping me specially with the medical related areas in my work.

I am thankful to my uncle Manik and aunt Manju for their constant support and encouragement and all my little ones Debapriya, Debabani, and Kabir for their prayers, deep love and keeping me energetic. I am thankful to IIT Guwahati and all the people specially from Electronics and Electrical Engineering department who helped me directly or indirectly to complete my thesis work.

Finally, I would like to thank the Almighty God for bestowing upon me His choicest blessings and granting good health, wisdom and strength to enable its successful completion against all odds.

(Sonali Biswas)

TH-2011_11610225

Abstract

The aim of this thesis is to make the performance of Inertial MEMS (micro electro mechanical system) sensor suitable for neurological disease diagnosis. Different types of applications have different requirements. For example, some applications require higher performance in terms of sensitivity and precision whereas others may require sensors with smaller dimensions. Tremor (2 Hz−12 Hz) and seizure (0.5 Hz−29 Hz) are the symptoms of neurological disorders which require wearable sensors for continuous monitoring, specially for capturing feeble tremor. Therefore the sensors must have low mass, small size, high sensitivity and precision. Sensors which are very small, usually suffer poor resolution and sensitivity. A low mass sensor is required because it does not obstruct the motor task and can capture feeble signals for better performance with low noise floor. Usually, a single axis MEMS accelerometer if placed normal to the surface of the skin mainly the dorsum of the hand, can capture such feeble signals. It may be mentioned that the geometry of the structure may be responsible for slight rotation or tilt in the device. This gives rise to off axis acceleration being picked up by the accelerometer, which is responsible for cross axis sensitivity. The cross axis sensitivity must be as low as possible specially for detecting tremor jerks of the feeble type. The reduction of cross axis sensitivity has been done in two ways, first by geometric optimization and second by Wheatstone bridge scheme. In order to enhance the performance of the microsensor a noise reduction scheme has been proposed. The damping aspect of the proposed accelerometer has been investigated. An attempt has been made to design a low g wearable piezoresistive MEMS accelerometer of quad beam type of pure silicon, for the diagnosis of neurological disorders. The accelerometer designed here is to be used in strap-down medical diagnostic purpose for capturing feeble tremor having intensity which may be as low as 0 g signifying fall to maximum ±6 g signifying jerks. The sensitivity obtained for a dynamic range of ±6 g is 0.33 mV/V/g, noise floor is 7.65 $\mu g/\sqrt{\text{Hz}}$ and cross axis sensitivity is 0.48%.

TH-2011_11610225

Contents

TH-2011_11610225

TH-2011_11610225

TH-2011_11610225

List of Figures

TH-2011_11610225

TH-2011_11610225

TH-2011_11610225

List of Tables

TH-2011_11610225

Nomenclature

MEMS	Micro electro mechanical system
SUDEP	Sudden unexpected death in epilepsy
EEG	Electroencephalogram
FoG	Freezing of gait
DRIE	Deep reactive ion etching
FEA	Finite element analysis
SNR	Signal to noise ratio
SDM	Sigma delta modulator
NSD	Noise spectral density
ADC	Analog to digital converter
DAC	Digital to analog converter
CMOS	Complementary metal oxide semiconductor

TH-2011_11610225

Mathematical Notations

g	Acceleration due to gravity
M	Mass of the proofmass
k	Spring constant
D	Damping factor
Q	Quality factor
ϕ_s	work potential
V_b	Voltage applied between electrode pair
ω	Circular natural frequency
$\{\phi_i\}$	Eigen vector
λ_i	Eigen value
(ζ)	Damping ratio
$(\tau_{xy}, \tau_{yz}, \tau_{zx})$	shear stress
$(\sigma_{xx}, \sigma_{yy}, \sigma_{zz})$	Normal stress
ρ_0	Isotropic resistivity of unstressed crystal
ρ_1 to ρ_6	Independent components of the resistivity matrix
Π	Component of piezoresistance sensor
$s11, s22, s33, s23 = s32, s31 = s13, s12 = s21$	Six independent stress components
Π_{11} and Π_{12}	normal stress
Π_{44}	Shear stress
$[\Pi]$	Piezoresistive coefficient matrix
$[M]$	Mass matrix
$[K]$	Stiffness matrix
$\{U\}$	Deflection
$\{\phi_i\}$	Denotes i^{th} mode shape

TH-2011_11610225

ξ_i	Denotes i^{th} modal displacement
K_B	Boltzmann constant
R	Resistance
T	Temperature in Kelvin
R_m	Equivalent mechanical resistance of the sensor.
q	Electron charge
I	I is the current
ω_n	undamped frequency
a_n	rms value of the acceleration
z_c	Distance of the centre of mass from the surface
Mp	Maximum overshoot
t_s	Settling time
d	Dynamic viscosity
λ_0	Mean free path
Kn	Knudsen number
h_0	Gap height
P_0	Pressure

TH-2011_11610225

List of Publications

Journal Publications

1. S.Biswas and A.K.Gogoi, "A Wearable Piezoresistive Microaccelerometer with Low Cross-axis Sensitivity for Neurological Disease Diagnosis" *AEU- Int. J. of Electronics and Communications, vol. 99, no. 1, pp. 177-185, 2019.* https://doi.org/10.1016/j.aeue.2018.11.001

2. S.Biswas and A.K.Gogoi, "Design Issues of Piezoresistive MEMS Accelerometer for an Application Specific Medical Diagnostic System " *J. of IETE Tech. Review, vol.33, no.1, pp.11-16, 2016*

Conference Publications

1. S.Biswas, and A.K. Gogoi, "Design and Analysis of FEM based MEMS accelerometer for Detection of Postural Tremor in Thyrotoxicosis" *In Proc. of International Conf on Advanced Electronics System(ICAES). IEEEComputer Society pp. 113-116, Sep. 2013.*

2. S.Biswas, and A.K. Gogoi, "Design and Simulation of Piezoresistive MEMS Accelerometer for the Detection of Pathological Tremor" *In proc. of IEEE SoutheastCON, pp.1-5, Lexington, KY, Mar 2014*

3. S.Biswas and A.K.Gogoi, "Squeeze Film Damping Control of a Piezoresistive Micro Accelerometer for Neurological Disease Diagnosis" *In proc. Euromech conf of Dynamics of micro and nano electromechanical systems: multi-field modelling and analysis, 5 - 7 Sept. 2018, Porto, Portugal.*

Book Chapters

1. S.Biswas, and A.K. Gogoi, "Noise Performance and Design Optimization of a Piezoresistive MEMS Accelerometer Used in a Strapdown Medical Diagnostic System" *In Proc. of Advanced*

TH-2011_11610225

computing and communication Technologies , Advances in Intelligent Systems and Computing, Singapore: Springer, vol.562, pp.287-296, Jan 2018.

2. S.Biswas, and A.K. Gogoi, "Design of a Piezoresistive Microaccelerometer with High Sensitivity for Medical Diagnostic" *In Advances in Systems, Control and Automation, Lecture Notes in Electrical Engineering, Singapore: Springer vol.442, pp.481-490,2018.*

TH-2011_11610225

1

Introduction

Contents

TH-2011_11610225

TH-2011_11610225

1.1 Introduction

In the recent past, performance improvement of Inertial MEMS (micro electro mechanical system) sensors have attracted the attention of many researchers for various applications, and its impact in biomedical field is no exception [1], [2]. To cater to the need of a target application, inertial sensors with the required unique performance criteria has to be designed. Early diagnosis of several types of neurological disorders require continuous monitoring in order to ensure normal activity of an individual and reducing the mortality rates in extreme cases. Tremor(2 Hz-12 Hz) and Seizures(0.5 Hz-29 Hz) are the symptoms of various such nervous system disorders which need immediate attention [3]. Tremor is a rhythmic movement of the body parts occurring in patients suffering from neurodegenerative diseases like multiple sclerosis, Parkinsons disease, dystonia, serotonin toxicity etc. Neurodegenerative essentially means progressive loss of structures or functions of nerve cells resulting in tremor of body parts, rigidity, bradykinesia, postural instability etc. None of the pathologies that cause tremor are fully understood and epidemiological and neurophysiological studies are hampered by the lack of diagnostic methods other than purely clinical. Seizure occurs due to abnormal electrical activity in the brain and is the main symptom of epilepsy. The intensity varies from almost 0 g signifying fall to maximum $\pm$ 6 g signifying violent jerks [4]. Sometimes a person having epilepsy may have severe anxiety disorder and may die without a clear reason. This is called sudden unexpected death due to epilepsy (SUDEP). Unfortunately diagnosis of such neurological diseases are difficult mainly because these symptoms may occur suddenly and hence may not be recorded in a clinical set up and requires long term monitoring [5]. Usually seizure monitoring is done by Electroencephalogram (EEG) which requires large number of electrodes to be fitted on the scalp. This makes long term monitoring difficult specially for children and infants. In order to diagnose such type of neurological disorders, the design of the inertial sensors must fulfill two vital aspects. First, the sensor must have low mass and small size making it suitable for wearable purpose for continuous monitoring. Second, it shall be able to sense feeble tremor and jerks which makes low cross-axis sensitivity very important; this is an important design goal. Such sensors must be small and light weight so that they do not impede the motor task, can measure low frequency range and must have high sensitivity and resolution with minimum noise floor [1]. But sensors which are very small, usually suffer from poor resolution and sensitivity, hence design optimization is very important [6].

Among the different MEMS sensors available, accelerometer possess desirable features suitable

TH-2011_11610225

for emerging biomedical applications. MEMS accelerometers can be used for measuring tilt, body movement for given frequency range and amplitude of human body motion arising out of voluntary and involuntary actions. Miniaturization has made batch fabrication and low cost possible.

The performance factors of MEMS accelerometers depend on several aspects: geometric design, device sensing mechanism, scaling limitations, associated electronic circuits and fabrication aspects. There are different transduction mechanisms like capacitive, piezoelectric and piezoresistive which can be used for design of such accelerometers [6]. Stress based measurement generally use piezoresistive and piezoelectric principles whereas displacement based measurement usually use capacitive. Among the many technological alternatives available, the advantages of piezoresistive types are that they have a DC response, they have simple read out circuits and are capable of high sensitivity and reliability. Though it has the drawback of temperature dependency other than that they use simple principle of transduction and microfabrication as compared to other types.

Piezoresistive MEMS accelerometer has undergone many modifications by several researchers since its initial realization in 1979 [7].

Thus wearable MEMS accelerometer with light weight, high sensitivity remains an active area of research.

1.2 Brief Literature Survey

The existing body of the literature consist of different categories viz., i) study of neurological disorders which require immediate attention for early diagnosis ii) Sensing mechanism iii) relative comparison of different design configurations of the sensors iv) design optimization for performance enhancement in terms of reducing cross-axis sensitivity effect, noise and having adequate damping control. Micro sensors applied for biomedical applications must have sensitivity in one particular sensing axis and must be insensitive to the other axes. Thus reduction of cross-axis sensitivity is the most important consideration and the literature survey shows the reduction based on geometry and other schemes proposed by many researchers. The correct prediction of the squeeze-film air damping ratio is essential in MEMS devices design and the analysis has been discussed by several researchers. Miniaturization itself is a challenge and this makes signal to noise ratio improvement mandatory for high performance applications in medical diagnostics. The various noise sources and the methods for noise reduction are studied, which are active research area.

TH-2011_11610225

Tremor (2 Hz-12 Hz) and Seizures (0.5 Hz-29 Hz) occurs in patients suffering from various neurological disorders [3], [5]. Different types of neurodegenerative diseases where tremor occurs are Parkinson, essential tremor, epilepsy, stroke etc. There are different pathological tremor like rest tremor (3-6 Hz), kinetic tremor (4-1 2Hz) and postural tremor (2-7 Hz) [8]. Tremor is a roughly sinusoidal oscillatory movement and Seizure occurs due to abnormal electrical activity in the brain. The intensity varies from almost 0 signifying fall to maximum $\pm$ 6 g signifying jerks. Among the different MEMS sensors available accelerometer possess desirable features suitable for emerging applications in Biomedical applications [1]. Microaccelerometers with comparatively lower mass yet maintaining high sensitivity and minimum noise floor for low frequency applications has been a challenge [9], [10]. Piezoresistive microaccelerometers has to its credit both functional and manufacturing advantages [11]. There are several reasons for choosing piezoresistive method of transduction, mainly because of simplicity in structure, better sensing, easy fabrication and ruggedness. Throughout the time span various MEMS piezoresistive accelerometers have been developed for several applications in different emerging fields with respect to performance.

Micro accelerometer structures can have different configurations like doubly supported, quad beam and cross beam [12]. Though different designs have been presented but the proofmass structure with support beams arranged is still one of the most popular as reported in [10], [12] and [13]. The reason for choosing quad beam type is that the performance level is found better when compared to doubly supported and cross beam ones as reported by many researchers [12], [14].

Neurological disease diagnosis requires higher performance level specially for sensing tremor and jerks of the feeble type, and also to detect fall when vector sum of acceleration tends to be zero. Hence, attaining low cross-axis sensitivity is very important. The performance improvement by reducing cross-axis sensitivity was attempted by several researchers in various ways. The structural motion must be parallel to the prime axis sensing but sometimes it is seen that there is a coupled mode with other directions occuring due to translational or rotational effects or a combination of both where we get maximum errors. The reduction in cross-axis sensitivity is possible by increasing the lateral torsional stiffness. There may be several changes in geometries of the sensor structure for increasing the stiffness. The lateral stability of a quad beam structure and cross-axis sensitivity can be reduced by increasing the number of support beams [15] but it has the drawback that this demands high precision in mask alignment and etching control.

TH-2011_11610225

Apart from geometric modification another approach of increasing the stiffness was by depositing heavy metal on top of the proofmass. The proof-mass was electroplated with 20 μm thick gold on top of proofmass which reduced the cross-axis sensitivities in the lateral axes [13]and [16]. The primary axis sensitivity was improved and the resonant frequency was also affected as the equivalent mass was increased due to the gold deposition. In order to maintain the equivalent mass, the thickness of the proofmass was reduced and then the metal gold was deposited [17]. This improved the symmetry of the structure and gave a sufficient reduction in the cross-axis sensitivity. Cross-axis sensitivity can be eliminated by Wheatstone bridge technique because of the self cancelation of the resistance change occuring when lateral accelerations are applied. In a quad beam structure cross-axis sensitivity has been reduced by eliminating lateral accelerations [18] to almost 90%. Twin mass structure is another configuration for low cross-axis sensitivity which has a reduced lateral sensitivity. But as the centre of the mass and centre of the beams are not on the same plane, a lateral acceleration tends to cause the masses to tilt and thus brings about some output response [19]. Piezoresistive design of size 5 mm $\times$ 5 mm with self test was developed for multichip module with U shaped Proofmass and three beams [20]. Piezoresistive structure of size 5 mm $\times$ 5 mm was realized by reducing the thickness of the proofmass and electroplating with gold [17], [21]. A miniaturized accelerometer of size 3 mm $\times$ 3 mm, using twin mass and six axes claims to have high sensitivity upto 1.7 mV/V/g [22].

The main disadvantage of piezoresistors is that they are highly temperature sensitive and suffer from thermal drift [23] [24]. The piezoresistance coefficients depend on the doping concentration and temperature [25] and [26]. Hence the performance analysis of the device becomes very important for obtaining high sensitivity.

Just as the sensor structure itself, the interface electronics also plays a critical role in the overall system performance. In fact, noise analysis of the accelerometer, electronic circuit, and the overall system shows that as the device performance improves, the interface electronics sometimes limit the overall system resolution. The resolution is greatly affected by both electronic and mechanical noise floors [27]. Mechanical noise is due to the Brownian motion of the proof mass and is directly related to the sensing structure design and environment. However as shown in [28], this noise can be decreased down to 0.1 $\mu g/\sqrt{Hz}$. Mechanical sensitivity of higher level has been achieved by a microfabrication technique involving both surface and bulk micromachining. A high mechanical sensitivity can be achieved with a bulky proof-mass and flexible suspensions thus reducing the bandwidth and range.

TH-2011_11610225

Mechanical noise can also be reduced by reducing damping. Accelerometer damping can be decreased by using damping holes or vacuum packaging. By changing the hole density and geometry the damping factor can be controlled which further simplifies the closed loop circuit design. As the resolution depends both on mechanical noise and read out electronic circuits, attempts are made by several researchers to reduce electronic noise and hence enhance the resolution. The correct prediction of the squeeze-film air damping ratio is essential in MEMS devices design, and squeeze film damping was analysed by many researchers [10], [12] and [24]. It was observed that the squeeze film damping in MEMS devices varies with different pressure.

This work mainly focuses upon the miniaturized design of a wearable accelerometer for early diagnosis of neurological diseases. The proposed piezoresistive accelerometer has a lateral area of about 25 mm^2 having a mass of around 6 mg. Sensor optimization having better performance with small dimension, minimum weight and reduced noise is still under research [6], [9], [14]. Though different designs have been presented but the proof-mass structure with support beams is still one of the most popular as reported [10], [12]and [13].

Hence an attempt has been made to design a low g wearable MEMS sensor targeted to capture tremor as low as $\pm$ 0.04 g and seizure where acceleration value falls to almost 0 to maximum $\pm$ 6 g signifying jerks. The proposed accelerometer has a symmetrical structure so that off axis sensitivity is less and it is of pure silicon.

1.3 Motivation

Researchers are trying to tackle several design issues and challenges for both performance enhancement of the sensors and miniaturization. In addition to that, for capturing very feeble tremor occurring in patients suffering from neurodegenerative diseases and to detect fall for seizure affected people, the microsensor must have reduced cross-axis sensitivity. This is possible when the structural motion is accurately aligned with the primary sensing axis. However, the alignment of the primary sensing axis and the sensor motion is a design challenge and the accelerometer responds to signals in the lateral axes too. This motivated the work for design approach for suitable schemes for cross-axis sensitivity reduction. In order to enhance the performance of the microsensor a noise reduction scheme becomes important as with sensor miniaturization, resolution and sensitivity gets adversely affected. The proposal of noise reduction scheme at circuit level is motivated by the above fact. It is also very

TH-2011_11610225

important to look at the damping mechanism for such system; the work on squeeze film damping analysis aims towards that. The worst case cross-axis sensitivity of either axis (other than sensing axis) dictates the performance. The design to arrive at a suitable aspect ratio of the proof-mass for simultaneous reduction of cross-axis sensitivity in both the off axes is motivated by the same. Overall, the motivation is to design a wearable MEMS sensor for low g application with high sensitivity with low cross-axis sensitivity.

1.3.1 Gaps in the existing literature

From the survey of relevant literature, details of which are presented in next chapter, it is observed that MEMS accelerometer with all the desired features for biomedical application with specific emphasis for neuro degenerative disease has not yet received adequate studies. Noise reduction in circuit level is not known to be proposed for this kind of sensing mechanism in literature. Lowering of cross-axis sensitivity at circuit level is proposed in literature but simultaneous reduction at the sensor level is not studied in literature. It may be mentioned that the sensor design reported in [17] and [21] have smaller dimensions but performance in terms of sensitivity is too low to be used for tremor detection.

1.3.2 Problem statement of the research

The objective of the thesis work is to realize a piezoresistive MEMS accelerometer suitable for diagnosing feeble tremor signals ranging from almost 0 to maximum $\pm$ 6 g, having frequency range 0.5 Hz to almost 40 Hz. Cross-axis sensitivity has to be reduced based on two aspects viz geometric modification and Wheatstone bridge circuit implementation. We plan to study various aspects of performance enhancement schemes and perform damping and noise analysis and propose a noise reduction scheme.

1.4 Thesis Contribution

The following are the major contribution of the thesis:

(i) Proposed design of Piezoresistive MEMS accelerometer

(a) A quad beam type of piezoresistive microaccelerometer

TH-2011_11610225

(b) Design and analysis of different configurations for performance enhancement

(ii) Carried out reduction of cross-axis sensitivity

(a) Design Optimization of aspect ratio for simultaneous minimization of cross-axis sensitivities in both the off-axes of piezoresitive MEMS accelerometer

(b) Wheatstone bridge scheme for reduction in cross-axis sensitivity

(iii) Squeeze film damping analysis

(iv) Noise analysis and proposed scheme for noise reduction

1.5 Thesis Organization and summary of each chapter

First chapter brings out the brief survey of relevant literature followed by the motivation for the research. It also brings out the gaps in existing literature followed by the problem statement of the research and contribution of the current work. Chapter 2 brings out the detailed literature survey and state of the art in the field of the current research. As this work mainly aims at application in the field of medical diagnosis, a reasonable detail of the domain where the sensor is aimed to be used is also brought out. The topic wise contribution is brought out from Chapter 3 to Chapter 6. Conclusion and scope of further work is brought out in Chapter 7.

Chapter 3 discusses the modeling and details of the design configuration of the proposed structure. Various dimensions have been tailored to meet higher performance level required for neurological disease diagnosis. In this chapter modal analysis, stress analysis and sensitivity analysis have been done for the proposed structure. Also the proposed quad beam structure has been compared with a similar structure having difference in flexure positioning. In configuration 1 flexures are aligned with the proof-mass edge whereas in configuration 2 the flexures are placed non-aligned with the proof-mass Both the structures having same specifications and material but different geometric configurations have been designed, simulated and their performance have been compared.

In Chapter 4, the theoretical background of the damping analysis is given which is followed by the details of the squeeze film damping. Damping is provided by the thin air film on both sides of the proof mass, which is achieved by top and bottom capping layer to encapsulate the whole mechanical structure. Damping can be controlled by varying the air gap or air pressure between proof mass and

TH-2011_11610225

encapsulation. The Squeeze film damping effect is the interaction of the silicon proof-mass and the air film, trapped in the gap between mass and the encapsulation. In this chapter, the simulation is carried out to ascertain the design parameters for obtaining adequate damping. The damping ratio is predicted using existing models.

In Chapter 5, the performance enhancement by reduction in cross-axis sensitivity has been discussed. Here, two methods of reducing cross-axis sensitivity have been discussed. The first method is optimizing the aspect ratio of the proof-mass and the second method is by adopting Wheatstone bridge signal pick up. While carrying out the optimization of the proof-mass it is ensured that the mass of the proof-mass is kept same so that the prime axis sensitivity is not adversely affected. As piezoresistances are temperature sensitive, Wheatstone bridge helps in eliminating the temperature effect on the output.

Chapter 6 brings out the proposed technique for reduction of noise. It proposes reduction of noise at circuit level using sigma delta converter.

TH-2011_11610225

2

Literature Review

Contents

TH-2011_11610225

TH-2011_11610225

2.1 Extended Literature Survey

A brief discussion on the topics already studied in the existing literature has been brought out in the last chapter. This chapter will bring out the survey of literature in detail. There are many important aspects which are studied and investigated in the ongoing research activities. The existing body of literature spans the following areas.

- Wearable sensor for neurological disease diagnosis
- Structure, operation of MEMS accelerometer for disease diagnosis
- Different transduction mechanism and suitability of piezoresistive type
- Comparison between different configurations of quad beam type in terms of performance
- Sensor optimization for reduction of cross-axis sensitivity
- Noise reduction for performance improvement
- Damping analysis
- Nonlinear behaviour of MEMS.
- Fabrication

For any disease, the most important aspect is the diagnosis. Early diagnosis of several types of neurological disorders require continuous monitoring. Tremor and seizure are the symptoms of various such nervous system disorders which need immediate attention. Tremor is characterised by the frequency and the intensity. It is brought out in [3] and [5] that tremor frequency usually ranges from 2 Hz to 12 Hz and has intensity value for upper body part as low as 0.04 g for very feeble tremor to maximum $\pm$ 5 g signifying hand jerks. In certain cases, progressive neurological disorder may cause orthostatic tremor which occurs at frequency ranging from 13 Hz to 18 Hz. In [3], different types of tremor are listed viz., rest tremor [3-6 Hz], postural tremor [4-12 Hz] and kinetic tremor [2-7 Hz]. Unfortunately even today observation for coarse tremor is the only detection method available along with methods which use severity scales, where patients are asked to draw patterns [5]. Seizure which occur as small jerks besides having other characteristics, is a symptom of epilepsy. Seizure usually occurs due to abnormal electrical activity in the brain. The frequency of all types of seizure fall within a range

TH-2011_11610225

usually from 0.5 Hz to 29 Hz. Epileptic seizures mainly occur as paroxysmal events, which means that they occur at a sudden, unexpected timing. The frequency of the seizure varies from patient to patient. Some patients suffer from multiple seizures during the day and/or night, while others may have once in a month or so. Jerks at times may be so severe that a person may even fall. Fall is also very common in patients suffering from Parkinsons disease where freezing of gait (FOG) occurs. Unfortunately diagnosis of such neurological diseases are difficult mainly because these symptoms may occur suddenly and hence may not be recorded in a clinical set up. Myoclonic seizure monitoring using Electro-encephalogram (EEG) involves a large number of electrodes to be attached to the scalp, which poses difficulty for long term monitoring. Also it is difficult to monitor nocturnal seizure which occurs during sleep at night for children. Seizure monitoring is the most difficult specially for the elderly people and infants of age less than a year. It is seen that epilepsy if not properly diagnosed, it may lead to refractory epilepsy and the percentage of sudden unexpected death in epilepsy (SUDEP) may tend to increase. In order to diagnose such type of neurological disorders there is a need for wearable sensors. Wearable sensors help in continuous monitoring of the patients without hampering day to day activities. The requirements of such sensors are enlisted in [1]. It says that such a sensor must be small and light weight so that it does not impede the motor task, can measure low frequency range and must have high sensitivity and resolution with minimum noise floor. It is interesting to note that motion of our joints and muscles may be compared to the oscillatory movement of masses and springs of any mechanical structure. Neural activity follows rhythmic behavior. Among the different MEMS sensors available, accelerometer possess desirable features viz it can respond to frequency and intensity, measure tilt and body motion, hence are suitable for emerging applications in biomedical areas [1]. Though the most important aspect is miniaturization which has made batch fabrication and low-cost possible, it is brought out in [9], [10] that a microaccelerometer with comparatively lower mass yet maintaining high sensitivity and minimum noise floor for low frequency application is still challenging.

A MEMS accelerometer is a micro electromechanical device that measures acceleration forces. Demand for low cost, high resolution and high sensitivity micromachined accelerometers have been increasing to cater to the need in various fields. These accelerometers differ in their resolution, range and bandwidth as well as the principle of transduction and microfabrication as required by their applications. Miniaturized sensors usually suffer poor resolution and sensitivity, hence proper design

TH-2011_11610225

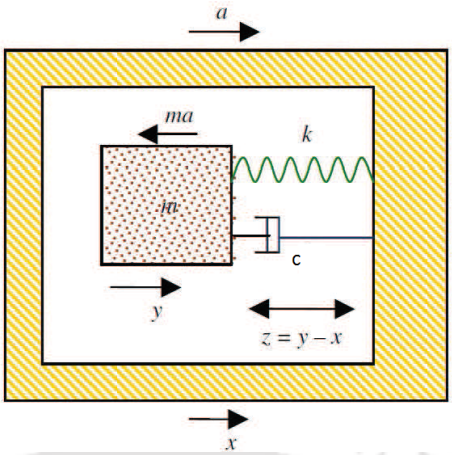

Figure 2.1: MEMS Accelerometer

optimization is very important. Researchers are trying to tackle several design issues and challenges for both miniaturization and performance enhancement of the sensors [6], [29].

A typical MEMS accelerometer consists of a proof mass suspended by beams anchored to a fixed frame. The proof mass has a mass of m, the suspension beams have an effective spring constant of k and there is a damping coefficient c, affecting the dynamic movement of the mass. The accelerometer can be modeled by a second order spring-mass damper system where both the relative displacement and suspension beam stress can be used as a measure of the external acceleration.

The basic principle and governing equations for MEMS accelerometer are studied in detail in literature [30]. For acceleration to be sensed most accelerometers convert the effect of acceleration to displacement and then transduce it to voltage so that it can be signal-conditioned and worked upon further. Accelerometers have a proof-mass which experiences an inertial force in the opposite direction of the acceleration to be measured. The deflection of the proof mass caused by this force is determined by the suspensions stiffness and is converted to a voltage using a suitable transduction principles. The acceleration of the frame a which is to be sensed manifests as the inertial force (mass $\times$ acceleration) on the mass. The movement of the frame is denoted by x and that of the mass by y. The net extension of the spring and damper will thus be $z = y - x$ as shown in the figure above. The equation of motion, by summing the forces-inertial, damping and spring forces-to zero is then given by 2.1.

$$m\ddot{y} + c(\dot{y} - \dot{x}) + k(y - x) = 0 \tag{2.1}$$

Once the structural model of the MEMS device is constructed, the performance of the structure can

TH-2011_11610225

be obtained through simulation tools which use finite element method.

The different transduction mechanisms of MEMS accelerometers are as follows and narrated at length in the literature.:

Piezoresitive Devices: These accelerometers incorporate silicon piezoresistors in their suspension beam. Bending of suspension beams due to proof-mass displacement produces strain in them. This is measured as a change in the resistance of a piezoresistor placed at the support end of the beam. These piezoresistors are generally placed at the edge of the support rim and proof mass where the stress variation is maximum. Change in resistance is measured by using a Wheatstone bridge configuration.

Capacitive Devices: The support frame of an accelerometer moves from its rest position in presence of an external acceleration, thus changing the capacitance between the proof mass and a fixed conductive electrode separated from it with a narrow gap. The capacitance is measured with a differential capacitance arrangement as it gives high sensitivity and good linearity. In the differential capacitance arrangement, the electrode attached to the proof-mass moves between two other static electrodes of opposite polarity [31].

Tunneling devices: Some microaccelerometers and high resolution physical sensors use a tunneling current between one tunneling tip and its counter electrode to sense displacement. It consist of two electrodes separated by a small distance d. When V_b voltage is applied between the electrode pairs we get a current flowing between them which is given by $I\alpha V_b e^{(-\alpha d\sqrt{\phi_s})}$, where $\alpha = 1.025\mathring{A}^{-1}\text{eV}^{-1/2}$ and ϕ_s is the work potential between the two surfaces through which tunneling takes place. For every 1^o displacement there is a corresponding current increase by an order of magnitude. Using this principle for accelerometers the moving electrode is attached to a proof-mass, while the static electrode is kept beneath it [31]. For tunneling to be effective the moving electrode is kept beneath it and the moving electrode has to have a very sharp tunneling tip. There are different types of tunneling accelerometers available which are sensitive and have a low noise floor but the challenge lies in fabrication because they require a sharp conducting tip and there is a chance of wear out of tunneling tip if there is a constant or intermittent contact. To overcome this, tunneling accelerometers are operated in force-re balance mode.

Thermal Devices: Thermal accelerometers use the principle that the temperature flux from a heater

TH-2011_11610225

to a heat-sink plate is inversely proportional to their separation [6]. If one plate can move relative to the other during the acceleration, the heat flow will change which affects the temperature of the heat sink. Therefore, by measuring the temperature using thermopiles the change in separation between plates can be measured which is a measure of the acceleration.

Others Devices: In addition to the above principles, accelerometers many use other principle including optical and electromagnetic. Recent trends are seen to combine optical and silicon micro machining to exploit the advantages of both thus developing miniature devices with very high linearity and noise immunity.

In [11], it is pointed out that, out of the different transduction methods available, piezoresistive MEMS accelerometer has to its credit both functional and manufacturing advantages. Though it has the drawback of temperature dependency; other than that it has to its credit a number of advantages. In general, there are several reasons for choosing piezoresistive method of transduction over others. These are mainly simplicity in structure, better sensing, easy fabrication and ruggedness. Piezoresistive MEMS accelerometers have undergone many modifications by several researchers since its initial realization in 1979.

Sensing methodologies utilized in inertial sensing generally fall under two categories viz., open loop and closed loop architectures. Closed loop control schemes relies on feedback to control the position of the seismic mass via a force feedback, or force rebalancing at its rest position. The force feedback required is proportional to the magnitude of the inertial load. High resolution accelerometers are generally operated in the closed loop mode to increase the bandwidth and range of operation. In this mode, the output voltage of the capacitance detection circuit is fed back to the proof-mass and an electrostatic force in a direction opposite to that of the acceleration is applied. This is studied in detail in [29]. In other sensing modes, a suitable actuation is necessary for providing the feedback. The feedback ensures that the deflection of the proof-mass is very small and thus it increases the range of operation. Additionally, the minute proof-mass movement improves the linearity of the system. Feedback improves the bandwidth by a factor equal to loop gain. Furthermore, feedback improves the dynamic range, drift, and temperature sensitivity. Open loop architectures straight forwardly measures the the changes in the sense signal whether it is piezoresistance or capacitance or other as a result of the inertial load displacing the seismic mass from its zero state position. These signals are typically amplified, compensated, filtered, buffered and output is analog or digital. These scheme

TH-2011_11610225

tends to be relatively immune to small production variation in the transducer element. These sensors are infact stable relying on no feedback signals and requires small die area. Sensitivity of an open-loop accelerometer is inversely proportional to the spring constant of its suspension. So, a small change in processing causes a large change in the sensitivity. By operating sensing element in electronic force feedback loop, strong dependence of accelerometer on processing parameters can be reduced substantially; this is brought out in [32]. However, operating in the closed-loop mode may make the system unstable for large feedback gains. There might also be a decrease in the sensitivity of the system.

Different configurations of micro accelerometer structures are brought out in [12]. The structures can have different configurations like doubly supported, quad beam and cross beam. Though different designs have been presented but the proofmass structure with support beams arranged is still one of the most popular as reported in [12], [10], [13]. The reason for choosing quad beam type is that the performance level is found better when compared to doubly supported and cross beam ones as reported by many researchers [12], [14].

In 1979, Roylance and Angel made the the first bulk micromachined piezoresistive z-axis accelerometer consisting of a cantilever support holding a huge proof mass with piezoresistors embedded at the support end where the maximum strain occurs. It was shown in [7], that using linear beam theory the stiffness can be obtained and further geometric design change like having two or more beams on either side of the mass can reduce the cross-axis sensitivity. In [33], a new approach was introduced to form the piezoresistors in the top surface of T shaped planar flexures but it was a complex structure. However the device geometry was free from the constraints by the anisotropic wet etch employed to form the flexure and proofmass. A new technology was developed by forming arbitrarily shaped planar flexures with vertical sidewalls by (deep reactive ion etching) DRIE process which gives optimal shape proof mass and flexures. This was followed by a new lateral planar accelerometer based on forming arbitrarily shaped planar flexures with vertical sidewalls by DRIE process [11]. This gave optimal shape proof mass and flexures. A triaxial piezoresistive accelerometer used for a biomechanical structure was proposed by using nano wires as piezoresistors [34]. This consideration has improved the resolution value being almost lower than 1 mg for all axes and higher sensitivity about 20.9 mV/g mainly because of higher stress on the nanowires. Hence proper design optimization of the piezoresistors is another very important step for resolution improvement.

TH-2011_11610225

As the diagnosis of neurological disorders require wearable accelerometers capable of sensing very low acceleration signals, sensing should be maximum in the prime axis and minimum possible in the off axes. The performance improvement by reducing cross-axis sensitivity was attempted by several researchers in various ways. The structural motion must be parallel to the prime axis sensing but sometimes it is seen that there is a coupled mode with other directions occuring due to translational or rotational effects or a combination of both where we get maximum errors. The reduction in cross-axis sensitivity is possible by increasing the lateral torsional stiffness. There may be several changes in geometries of the sensor structure for increasing the stiffness. The lateral stability of a quad beam structure and cross-axis sensitivity can be reduced by increasing the number of support beams. But it has the drawback that this demands high precision in mask alignment and etching control. These detailed aspects are brought out in [15].

When lateral acceleration is applied in a quad beam structure, we get larger rotations. This is caused by their low torsional stiffness. This can be improved by enlarging the distance between the central lines of beam and the proofmass. Also reducing the height difference between the beams and the proofmass, is another way of reducing the cross-axis sensitivity. The lateral stability of a quad beam structure can also be improved by aligning the proofmass edge with the beams. The MEMS structure having beams aligned with proofmass edge had better lateral stiffness compared to the mass with non aligned beams. This is reported in [14], [21] and [35].

Apart from geometric modification another approach of increasing the stiffness was by depositing heavy metal on top of the proofmass. In [13] and [16] it was proposed to electroplate the proofmass with 20μ m thick gold on top which reduced the cross-axis sensitivities in the lateral axes. The primary axis sensitivity was improved and the resonant frequency was also affected as the equivalent mass was increased due to the gold deposition. In order to maintain the equivalent mass, the thickness of the proofmass was reduced and then the metal gold was deposited [17]. This improved the symmetry of the structure and gave a sufficient reduction in the cross-axis sensitivity.

Another way to reduce cross-axis sensitivity is by arranging the piezoresistors in the form of a Wheatstone bridge where self cancelation of the resistance change occurs, when lateral accelerations are applied. In a quad beam structure cross-axis sensitivity can be reduced by eliminating lateral accelerations [24] to almost 90%. Twin mass structure is another configuration for low cross-axis sensitivity which can provide a reduced lateral sensitivity. But as the centre of the masses and centre

TH-2011_11610225

of the beams are not on the same plane, a lateral acceleration tends to cause the masses to tilt and thus brings about some output response [19]. Piezoresistive design of size 5 mm × 5 mm with self test was developed for multichip module with U shaped Proofmass and three beams as reported in [20]. Piezoresistive structure of size 5 mm × 5 mm was realized by reducing the thickness of the proofmass and electroplating with gold [17], [21]. A miniaturized accelerometer of size 3 mm × 3 mm, using twin mass and six axes claims to have high sensitivity upto 1.7 mV/Vg [22].

The main disadvantage of piezoresistors is that they are highly temperature sensitive and suffer from thermal drift [24] and [23]. The piezoresistance coefficients depend on the doping concentration and temperature [26], [25]. Hence the performance analysis of the device for various temperature becomes very important for obtaining high sensitivity.

Another aspect of such sensors is noise. Noise in accelerometer can occur due to the mechanical components and the electronic components. The actual noise which limits the resolution of the system noise depends upon its spectral density and the range of the operating frequencies, i.e., the bandwidth of the system. The spectral density (psd) of the noisefloor at the output of the accelerometer is expressed in V/$\sqrt{\text{Hz}}$. For a large bandwidth, the minimum detectable signal is large. This limits the resolution for a given noise-floor. The noise-floor is low for devices with low bandwidth. If the bandwidth of the system is small, then the resolution of the device improves [31]. This means that the devices with very low bandwidth would be able to resolve minute changes in acceleration better than those with large bandwidth. Naturally, the smallest signal that can be detected would have to be greater than the noise floor in the circuit.

In [27], the mechanical noise source for MEMS device is studied. The mechanical noise is due to the Brownian motion of the proof mass suspension or anchors. The total noise equivalent acceleration (TNEA) [m/s$^2\sqrt{\text{Hz}}$] is

$$TNEA = \frac{1}{M}\sqrt{4K_B}TD = \sqrt{\frac{4K_BTw_r}{QM}} \tag{2.2}$$

where K_B is the Boltzmann constant and T is the temperature in Kelvin. Here 2.2 clearly shows that to reduce mechanical noise , the quality factor and proof mass have to be increased. In the most general case the proof mass motion can have six degrees of freedom. But typically in a unidirectional accelerometer the geometrical design of the suspension is such that one of these is dominant and the device has low off-axis sensitivity. MEMS based accelerometers used as inertial sensors are typically specified by their sensitivity, maximum operation, frequency response, resolution, full scale linearity,

TH-2011_11610225

offset, off-axis sensitivity and shock survival. Noise analysis shows that not only the sensor, but the interface electronics associated with it also plays a critical role in the overall system performance. In fact, noise analysis of the accelerometer, electronic circuit, and the overall system shows that as the device performance improves, the interface electronics sometimes limit the overall system resolution. Mechanical noise is due to the Brownian motion of the proof mass and is directly related to the sensing structure design and environment. Fluctuation in mobility are the reasons for Hooge noise which is a frequency dependent non-equilibrium noise [28]. However, as shown in [28] this noise can be decreased down to 0.1 $\mu g/\sqrt{Hz}$. Mechanical noise can also be reduced by reducing damping. Accelerometer damping can be decreased by using damping holes or vacuum packaging. The noise and the damping factor are controlled and reduced by forming damping holes in the electrodes [35], [36]. As reported in most of the literatures as mechanical noise is dominant in deciding the overall noise performance, therefore on going efforts are made to improve upon the accelerometer itself rather than the interface electronics circuit associated. However as the resolution depends both on mechanical noise and read out electronic circuits, attempts are made by several researchers to reduce electronic noise and hence enhance the resolution [27]. The piezoresistive accelerometer designed is based on spring-mass-damper and efforts are still on for performance enhancement [6], [7].

Another aspect of such sensor design is damping. Damping plays important role in dynamic characteristics of the system. The dynamic characteristic of the device is mainly determined by the damping material and the spacing between the proofmass and the housing. There are different mechanisms of damping depending upon the the operating conditions and dimensions of the structure. At first, Newell [37] observed that air damping increases rapidly as the surface-mass ratio increases for a MEMS device. Squeeze film damping control in solid state accelerometers were at first given by J. Starr [38]. Soon after this, different researchers focussed on squeeze film air damping in MEMS [39], [40], [41], [42]. The most significant damping suitable in MEMS devices specially operating at atmospheric pressure and low frequency is the Squeeze film damping. For a specific value of air gap thickness, the various factors that affect squeeze film damping are the operating frequency of oscillations, surrounding pressure, viscosity of the medium, and dimensions of the structure [24]. The correct prediction of the squeeze-film air damping ratio is essential in MEMS device design. Squeeze film damping was analyzed by many researchers [12], [18]and [36].

TH-2011_11610225

There are many sources of non-linearities in MEMS which can be due to forcing, damping and stiffness [43]. Forcing can introduce non-linearities through actuation and detection mechanism such as the case of parallel plate electrostatic forces. Also, nonlinear forces can affect microstructures while in-use, such as in the case of capillary forces due to humidity. Many microstructures are compliant because of the large surface-to-volume ratio. When actuated, they undergo relatively large deformation, which amplifies the so-called geometric nonlinearities of the structures resulting in nonlinear stiffness effect. Also, the use of some materials can induce material and stiffness-related nonlinear behavior, such as piezoelectric materials, which are quadratic in nature. Linear theories fail to capture and explain many behaviors in MEMS, which are observed experimentally. The nonlinear theories and models need to be utilized for correct and accurate results [43]. It can be seen from the literature survey that for design of MEMS accelerometer one needs to look at various aspects viz., structure, sensing mechanism, cross-axis sensitivity, sensing circuitry, damping etc.

TH-2011_11610225

3

Proposed Design and Comparative Study of Different Design Configurations

Contents

TH-2011_11610225

TH-2011_11610225

3.1 Introduction

There is a demand for high performance, low cost micro electro mechanical system (MEMS) inertial sensors for vibration measurement in various fields such as automotive industry, aeronautical, tactical, biomedical, robotics and so on. Neurological disease diagnosis requires such inertial sensors which can capture feeble vibrations. In order to enhance the performance of such MEMS sensors, several design issues need special consideration. The resolution and sensitivity improvement of this micromachined inertial sensor has always been a challenge. The performance factors of MEMS accelerometers depend on several aspects of geometric design, device sensing mechanism, scaling limitations, associated electronic circuits and fabrication aspects. In developing these MEMS devices, Finite Element Analysis (FEA) is usually relied upon to study these microstructures in determining stress, deformation, resonance etc. The importance of Finite Element Analysis in MEMS cannot be denied since it is already acknowledged as the best way to optimize the performance of the MEMS devices. Microaccelerometers are one of the most important types of MEMS devices. MEMS accelerometers respond to frequency and intensity, measure tilt and body motion, and miniaturization has made batch fabrication and low-cost possible. Microaccelerometer with comparatively lower mass yet maintaining the sensitivity and minimum noise floor and better selectivity for low frequency applications has been a challenge [9] [10]. Piezoresistive microaccelerometers has to its credit both functional and manufacturing advantages [11]. There are several reasons for choosing piezoresistive method of transduction, viz., simplicity in structure, better sensing, easy fabrication and ruggedness. Since its inception, various MEMS piezoresistive accelerometers have been developed for several applications which span from a simple vibration monitoring system to a complex inertial navigation system. The development of piezoresistive MEMS applied for Biomedical purpose is gaining popularity starting from disease diagnosis to drug delivery.

3.2 Design Approach

The initial design procedure of any sensing element is based on the modeling of the device. The design methods adopted include the concept of structural mechanics where we first do the modal analysis. The design and appropriate placement of the piezoresistors are very important for maximum sensing.

TH-2011_11610225

3.2.1 Mathematical modeling

The proposed MEMS accelerometer structure consists of a solid quad beam type of structure made of silicon as shown in Fig. 3.1. The proof-mass has beams connected on either side of the proof-mass, at its edges. There are total four beams; the structure has p-doped piezoresistors placed at the junctions of (i) the mass and beam and (ii) the frame and beam. These positions have been identified as the points where maximum stress occurs. The entire structure is surrounded by a frame which is fixed. The beam end connected to the frame are fixed. The device is targeted to sense acceleration in a single axis (only z-axis). Hence no acceleration must be picked up in the other two axes. We consider that the four beams deform in the same way, the whole system is modelled as a single degree of freedom system. From [44], the expression for k_{eff} is given by Eq.

$$k_{eff} = 4\frac{Ebh^3}{l^3} \tag{3.1}$$

where b, h and l stand for beam width, height and length respectively and E is the Young's modulus. The factor of 4 in the above equation is because of quad beams used in the proposed structure. The reason for choosing quad beam type is that the performance level is found better when compared to doubly supported and cross beam ones as reported by many researchers [12], [14]. Whenever there is proof-mass displacement, the beams deflect and these cause strain on the piezoresistors, resulting in a change in resistivity. The proposed structure can be studied with the help of a simple spring-mass model as shown in Fig. 3.2, and the necessary fundamental equations in [44].

Let m, c and k denote the mass, damping coefficient and spring constant of a spring-mass system respectively. Let x be the displacement of the mass with respect to stationary frame and y be the displacement of the enclosure with respect to the same stationary frame. Let the enclosure be experiencing sinusoidal motion given by:

$$y = Asin(\omega t) \tag{3.2}$$

where A is the amplitude of the motion of the enclosure and ω is the frequency. The motion follows the following equation:

$$m\ddot{x} + c(\dot{x} - \dot{y}) + k(x - y) = 0 \tag{3.3}$$

TH-2011_11610225

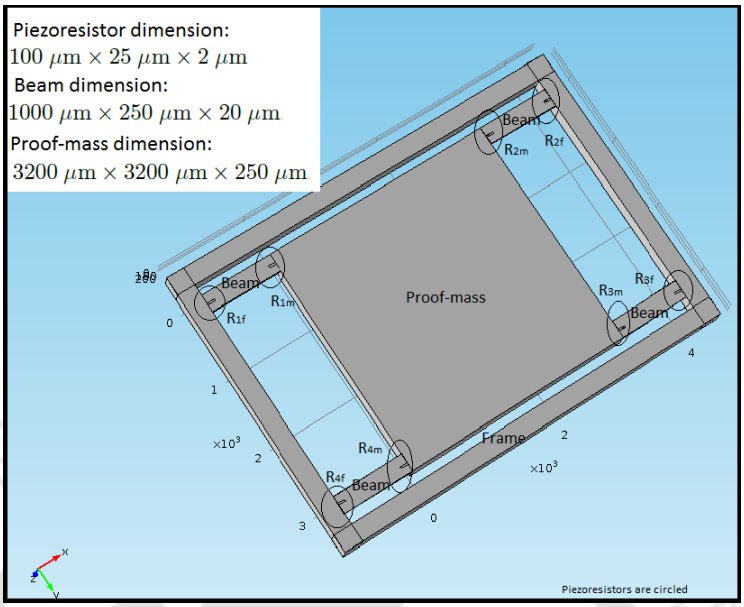

Figure 3.1: Proposed Quad beam Accelerometer

Let us use a intermediate variable z such that

$$z = x - y \tag{3.4}$$

z indicates the relative displacement of the mass with respect to the enclosure. With this intermediate variable and substitution of y, the Eq. 3.3 becomes

$$m\ddot{z} + c\dot{z} + kz = m\omega^2 A \sin \omega t \tag{3.5}$$

The steady state solution of the above equation is given in standard literature [30]

$$z(t) = Z \sin(\omega t - \phi) \tag{3.6}$$

where Z is the amplitude of relative motion of mass with respect to the enclosure and ϕ represents the lag of the movement of mass with respect to the movement of the enclosure. Z is given by

$$Z = A \frac{r^2}{\sqrt{(1 - r^2)^2 + (2\zeta r)^2}} \tag{3.7}$$

Here $r = \frac{\omega}{\omega_n}$, is the ratio of the frequency of excitation to the natural frequency. The phase angle ϕ

TH-2011_11610225

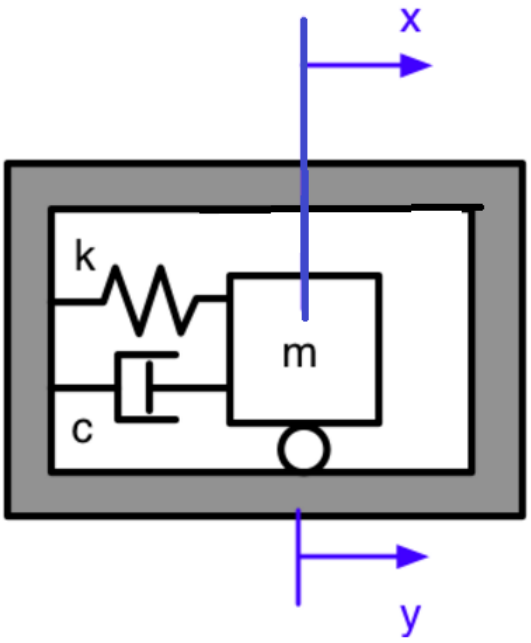

Figure 3.2: Spring-mass model

is given by

$$\phi = tan^{-1}\frac{2\zeta r}{1-r^2} \tag{3.8}$$

where ζ is the damping ratio and is given by

$$\zeta = \frac{c}{2\sqrt{(km)}} \tag{3.9}$$

As it can be seen from Eq. 3.2, the amplitude of the displacement of the enclosure is A. To find the input acceleration, we need to differentiate Eq. 3.2 twice.

$$\frac{d^2y}{dt^2} = \omega^2 Asin(\omega t) \tag{3.10}$$

Thus the amplitude of the input acceleration is $\omega^2 A$. Now rearranging the Eq. 3.7 we get

$$Z\omega_n^2 = \frac{\omega^2 A}{\sqrt{(1-r^2)^2 + (2\zeta r)^2}} \tag{3.11}$$

It is clear that the term $Z\omega_n^2$ is proportional to input acceleration $\omega^2 A$. For small value of r i.e., $\frac{\omega}{\omega_n}$, input acceleration is approximately equal to $\omega_n^2 Z$. This is the main design principle of accelerometer

TH-2011_11610225

which means the amplitude of input acceleration has to be sensed. It may also be pointed out that any other parameter proportional to the amplitude of the displacement (Z) may also be used to sense the acceleration.

3.2.2 Design of piezoresistors

Microaccelerometers of the piezoresistive type have always been a choice for many applications because of their structural and fabrication simplicity along with the simple read-out circuits [6]. However careful design geometry and sensing position of the implanted piezoresistors along with appropriate doping concentration are the prime concern for maximum sensing [10], [22] resulting in better performance. Single crystal silicon when doped with p or n type of material become p-type piezoresistors and n type piezoresistors respectively.

In this work, p-doped piezoresistor are chosen. It is observed that stress sensing is maximum when the piezoresistors are placed on both the beam ends i.e., one end which is connected to proof-mass and the other end which is connected to the frame. The piezoresistors dimension chosen in terms of length, breadth and height, all in micrometers are 100, 25 and 2 respectively.

The piezoresistive coefficients are influenced by doping concentration and the type of dopant used. For p-type and n-type silicon the value of piezoresistive coefficient decreases with increasing temperature and doping concentration. The quantity of dopant introduced, affects many electrical properties mainly the charge carrier concentration. As reported in [45] the longitudinal piezoresistive coefficient depends on the doping concentration and the operating temperature. At operating temperature that ranges between -75 to 75 ^{o}C, the piezoresistive coefficient decreases both with the increase in the doping concentration and with the increase in temperature.

There are approximately 5×10^{22} atoms/cm^3 in intrinsic crystalline silicon. In the present work, the doping concentration chosen is 5×10^{17} atoms/cm^3. This specification lies in the typical range for lightly doped that ranges from 10^{13} /cm^3 to 10^{18} /cm^3 [45]. The change in resistance can be obtained by initially considering the stress components. In a three dimensional space there are six independent stress components out of which three are normal stress ($\sigma_{xx}, \sigma_{yy}, \sigma_{zz}$) and three are shear stress ($\tau_{xy}, \tau_{yz}, \tau_{zx}$). Thus the various components of the stress tensor can be denoted as $\sigma_{xx} \rightarrow T_1$, $\sigma_{yy} \rightarrow T_2$, $\sigma_{zz} \rightarrow T_3$, $\sigma_{yz} \rightarrow T_4$, $\sigma_{xz} \rightarrow T_5$, $\sigma_{xy} \rightarrow T_6$. The relation between changes of resistivity and the applied stress and strain is given by 3.12, where ρ_0 is the isotropic resistivity of unstressed

TH-2011_11610225

crystal and ρ_1 to ρ_6 are the six independent components of the resistivity matrix, Π is the component of piezoresistance tensor and T is the component of stress tensor [46].

$$\begin{pmatrix} \Delta\rho_1/\rho_0 \\ \Delta\rho_2/\rho_0 \\ \Delta\rho_3/\rho_0 \\ \Delta\rho_4/\rho_0 \\ \Delta\rho_5/\rho_0 \\ \Delta\rho_6/\rho_0 \end{pmatrix} = \begin{pmatrix} \Pi \end{pmatrix} \begin{pmatrix} T \end{pmatrix} \tag{3.12}$$

$$= \begin{pmatrix} \Pi_{11} & \Pi_{12} & \Pi_{12} & 0 & 0 & 0 \\ \Pi_{12} & \Pi_{11} & \Pi_{12} & 0 & 0 & 0 \\ \Pi_{12} & \Pi_{12} & \Pi_{11} & 0 & 0 & 0 \\ 0 & 0 & 0 & \Pi_{44} & 0 & 0 \\ 0 & 0 & 0 & 0 & \Pi_{44} & 0 \\ 0 & 0 & 0 & 0 & 0 & \Pi_{44} \end{pmatrix} \begin{pmatrix} T_1 \\ T_2 \\ T_3 \\ T_4 \\ T_5 \\ T_6 \end{pmatrix} \tag{3.13}$$

Thus only three piezoresistive coefficient are required to be known. Out of these three piezoresistance coefficient, Π_{44} is more consistent and easy to measure [10]. The piezoresistive coefficients for n type and p type piezoresistors [46] are given in Table 3.1. Table 3.2 below shows the longitudinal and

Table 3.1: Piezoresistivity component for single crystal silicon

Piezoresistivity coefficient ($10^{-11}Pa^{-1}$)	n-type (Resistivity = 11.7 Ω cm)	p-type (Resistivity = 7.8 Ω cm)
Π_{11}	−102.2	6.6
Π_{12}	53.4	−1.1
Π_{44}	−13.6	138.1

transverse piezoresistive coefficient for some typical cases based on the direction of the strain and current direction eg., $< 100 >$, $< 110 >$, $< 111 >$ [46].

Change in resistivity of the piezoresistive material is directly proportional to the stress, hence it is important to place the piezoresistors in position where maximum stress can be sensed. In the present work the maximum stress positions are the junctions of the proof-mass and beams and the junction of the fixed frame and the beam. The maximum stress points have been obtained from simulation using

TH-2011_11610225

Table 3.2: Piezoresistive coefficients in various direction

Direction of strain	Direction of current	Configuration	Piezoresistive coefficient
$< 100 >$	$< 100 >$	longitudinal	Π_{11}
$< 100 >$	$< 010 >$	Transverse	Π_{12}
$< 110 >$	$< 110 >$	longitudinal	$(\Pi_{11} + \Pi_{12} + \Pi_{44})/2$
$< 110 >$	$< 110 >$	Transverse	$(\Pi_{11} + \Pi_{12} - \Pi_{44})/2$
$< 111 >$	$< 111 >$	longitudinal	$(\Pi_{11} + 2\Pi_{12} + 2\Pi_{44})/2$

FEM software. Once the resistance of piezoresistors change because of the stress induced owing to the applied acceleration, it needs to be sensed to ascertain the amplitude of the acceleration applied. The piezoresistors are connected in the form of a Wheatstone bridge signal pick up circuit. In order to achieve low off-axis sensitivity the eight piezoresistors are connected in such a manner that the bridge remains balanced during off-axis acceleration. This is done by observing the reduction and increase in resistance of piezoresistors based on applied acceleration. The piezoresistors undergo tension or compression based on the axis of applied acceleration. Meticulously, looking at the pattern of tension and compression of piezoresistors for acceleration applied in prime axis and off-axes, the resistance can be connected in Wheatstone bridge in such a way that the bridge remain balanced in case of off-axes acceleration as brought out in [10]. The bridge will be unbalanced for the accelerations along z- direction. Also, the beams are placed on the edge of the proof-mass unlike [10], hence there is low cross-axis sensitivity along y direction. Usually the piezoresistors are temperature sensitive and Wheatstone bridge is effective for nullifying the temperature coefficient of offset to some extent but the temperature coefficient of sensitivity has its influence [10]. The output voltage is proportional to the change of resistance of the piezoresistors. Depending on the direction of the piezoresistor, the piezoresistive coefficient, the direction of the stress and its value; the ratio of change in resistance to stress free resistance can be calculated. Let ΔR be the change in resistance, then the change in output voltage ΔV is given by Eq. 3.14, where V_s is the source voltage. Here it is assumed that all the piezoresistors undergo the same change in resistance for the proposed structure. In case the change in resistances are not exactly the same, a different equation needs to be used which is brought out in Section 3.4.

$$\Delta V = \frac{\Delta R}{R} V_s \tag{3.14}$$

TH-2011_11610225

where V_s is the wheatstone bridge supply voltage.

The sensitivity of the device is defined as the relative change of output voltage per unit differential acceleration Δg.

$$S = \frac{\Delta V}{\Delta g}\frac{1}{V_s} = \frac{\frac{\Delta R}{R}}{\Delta g} \tag{3.15}$$

3.2.3 Material Selection

The accelerometer structure has been designed with the above dimensions using Single crystal silicon material. Silicon wafers are extremely flat, can accept coatings and additional thin film layers for building microstructures. Silicon does not show mechanical hysteresis and therefore by using standard photolithography and etching techniques precise geometrical features can be realized. Electrically conductive silicon with resistivity 0.1 Ωcm is selected for the proof-mass. Also Pyrex 7740 glass is chosen for top and bottom wafers to provide required sealing. Using anodic bonding process, the glass wafers are bonded to the silicon wafer. Electrodes and electrical contact pads are realized by depositing submicron thickness Aluminium coating using E-beam evaporation process. The material properties of Silicon and Pyrex glass as given in [46] are shown in Table 3.3.

Table 3.3: Material properties of Silicon and Pyrex glass

Symbol	Material Property	Silicon	Pyrex Glass
σ_y	Yield strength (10^9N/m^2)	7	0.5 to 0.7
E	Youngs modulus(10^{11}N/m^2)	1.69	400
γ	Poisson's ratio	0.28	0.17
α	Thermal expansion Coefficient(10^{-6}m/m°C)	2.5	0.5
ρ	Density(g/cm^3)	2.3	2.225

3.3 Proposed Design configuration of the MEMS accelerometer

The design parameters of the proposed microaccelerometer are shown in Table 3.4 and that of piezoresistors are shown in Table 3.5. The parameters like natural frequency, maximum deflection for the proposed design is obtained using simulation tool which is given in Table 3.6. The piezoresistors are arranged in the form of a Wheatstone bridge as it reduces the cross axes sensitivity. Doping concentration is a very important factor for deciding the sensitivity and we have chosen it to be 5×10^{17} atoms/cm^3. The resistivity of Boron doped silicon at 300 °K is obtained for the known doping

TH-2011_11610225

concentration, using the logarthmic plot of resistivity vs input concentration as shown in Fig. 3.3. It has been observed that the sensitivity is maximum for this specification [10]. Also this specification lies in between the typical range for lightly doped that ranges from 10^{13} /cm^3 to 10^{18} /cm^3 [45]. The natural frequency of accelerometer is a very important parameter and needs to be ascertained. The dependency of natural frequency on various design parameters are demonstrated through simulation. The natural frequency of the proposed accelerometer for various beam dimensions are estimated using the FEM tool. The effective spring constant k_{eff} of the beam is given by Eq.3.1. The natural frequency is given by $\sqrt{\frac{k_{eff}}{m}}$ where m is the mass. The proposed beam dimensions gives a natural frequency which is much away from the frequency of operation. The beam dimensions also decide the sensitivity and stability which includes the factor of safety. In order to achieve better performance in terms of sensitivity the beam dimensions are chosen having narrow width, longer length and narrow thickness [22], [45]. The beam geometry has been optimized by choosing a natural frequency several times more than the bandwidth required.

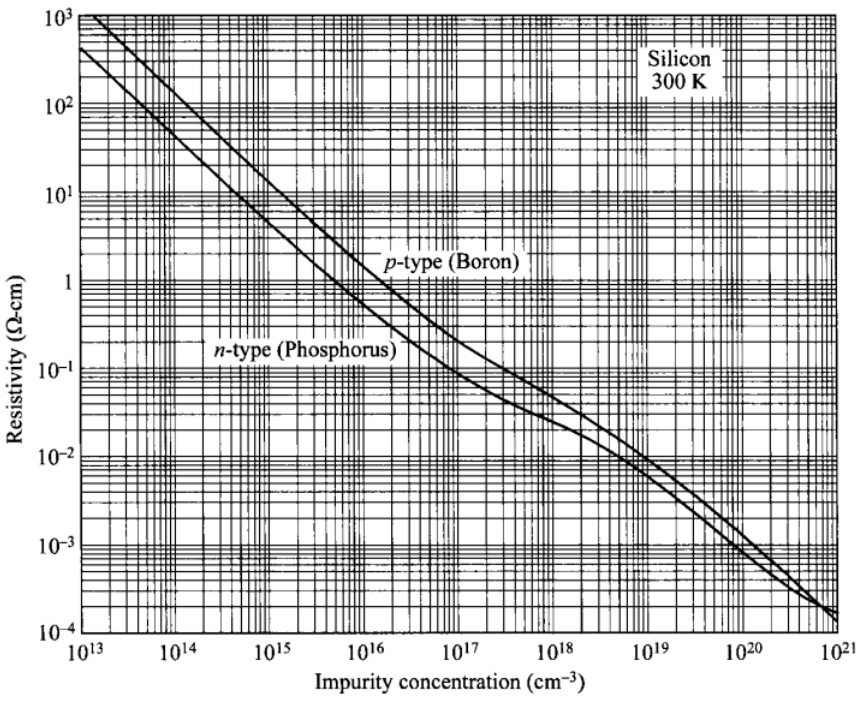

Figure 3.3: Resistivity vs impurity concentration for silicon at 300K

TH-2011_11610225

Table 3.4: Design parameters of the proposed microaccelerometer

Dimensions	**Design configuration**
Dimension of the proof-mass $(l \times b \times h)(\mu\text{m})^3$	$3200 \times 3200 \times 250$
Dimension of the beam $(l \times b \times h)(\mu\text{m})^3$	$1000 \times 250 \times 20$
Piezoresistor dimension $(l \times b \times h)(\mu\text{m})^3$	$100 \times 25 \times 2$
Dimension of the frame $(l \times b \times h)(\mu m)^3$	$5200 \times 230 \times 250$
Mass of the proof-mass (kg)	5.96×10^{-6}
Beam mass (kg)	1.15×10^{-5}
Density of proof-mass (kg/m^3)	2330
Spring constant of the microaccelerometer (N/m)	338
Effective mass of the microaccelerometer (kg)	5.9×10^{-6}
Effective spring constant of the microaccelerometer (N/m)	1352

Table 3.5: Design of the piezoresistors

Dimensions	**Design configuration**
Type of the piezoresistors	Single crystal silicon doped with p-type material
Location	Maximum stress position
Doping concentration	5×10^{17} atoms/cm^3
Resistivity	$\rho = 0.07198\ \Omega$cm
Sheet resistance,$\rho_s = \frac{\rho}{thickness}$	359.9 Ω/square
Resistance=$\rho_s \frac{length}{width}$	1439.6 Ω

Table 3.6: Design parameters obtained

Design Parameters	**Calculated values**	**Simulated values**
Natural frequency, ω_n (rad/s)	15061	15053
Natural frequency in Hz	2398	2397
Deflection for z-axis at 6 g(m)	2.59×10^{-7}	2.56×10^{-7}
Bandwidth (kHz)	2.39	2.39

TH-2011_11610225

3.3.1 Effect of beam thickness on sensitivity

The spring constant of the microaccelerometer is dependent upon the dimensions of the beam. The effective spring constant as shown in Eq. 3.1 has strong dependence on the thickness of the beam. Thus, to increase the sensitivity of the system, the stress induced on the accelerometer structure for different thickness of the beam is studied. The simulated displacement for thickness 10 μm, 20 μm, 30 μm and 40 μm for 6 g are shown in Fig. 3.4, Fig. 3.5, Fig. 3.6 and Fig. 3.7 respectively. The corresponding stress developed for same acceleration are shown in Fig. 3.8, Fig. 3.9, Fig. 3.10 and Fig. 3.11 respectively. Stress on surface gives us a distribution of electron density around surface atoms. This can be both positive (tensile) or negative (compressive). So it is important for MEMS devices and therefore shown in the figures.

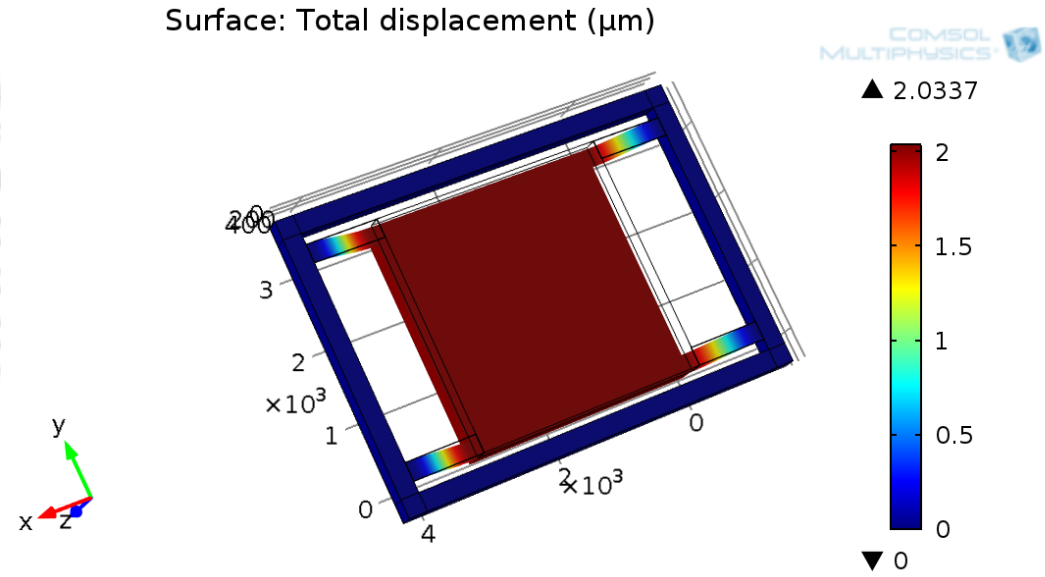

Figure 3.4: Simulated displacement in z-direction for beam thickness 10 μm

It can be seen that the stress induced decreases as the beam thickness increases which indicates that it is beneficial to reduce the thickness of the beam. At the same time, it is also pertinent to investigate the linearity of the stress developed with respect to the applied acceleration. Fig. 3.12 and Fig. 3.13 shows the displacement of the proof-mass vs. applied acceleration and the stress induced vs. applied acceleration respectively. To ascertain the linearity, a polynomial of higher order is fitted on this data and the coefficients of the polynomial are examined. The linearity is defined as the ratio of square of the coefficient of the 1st order term of the polynomial to sum of square of all coefficients except the constant term. For percentage linearity, the ratio is multiplied by 100.

TH-2011_11610225

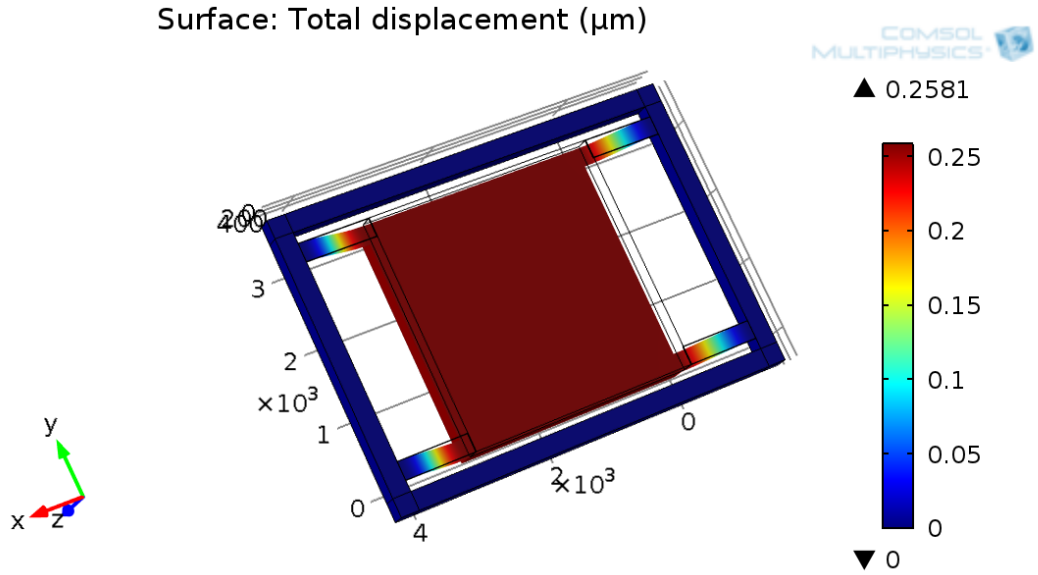

Figure 3.5: Simulated displacement in z-direction for beam thickness 20 μm

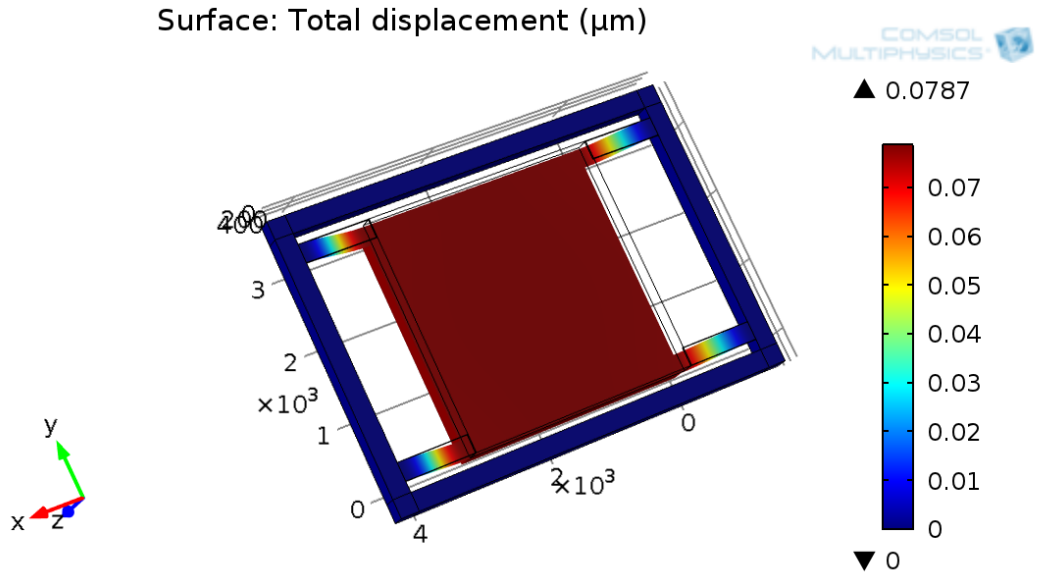

Figure 3.6: Simulated displacement in z-direction for beam thickness 30 μm

TH-2011_11610225

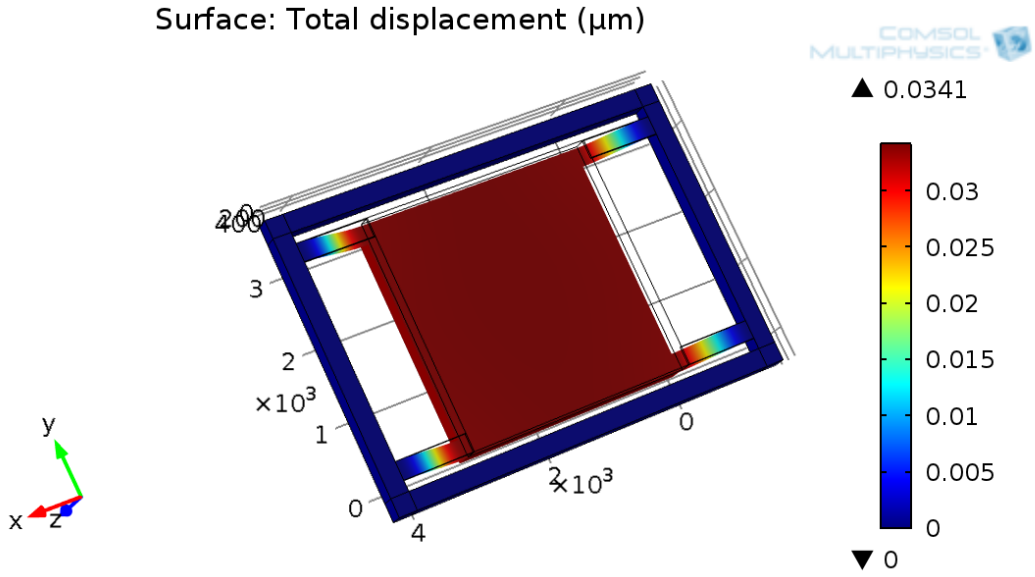

Figure 3.7: Simulated displacement for beam thickness 40 μm

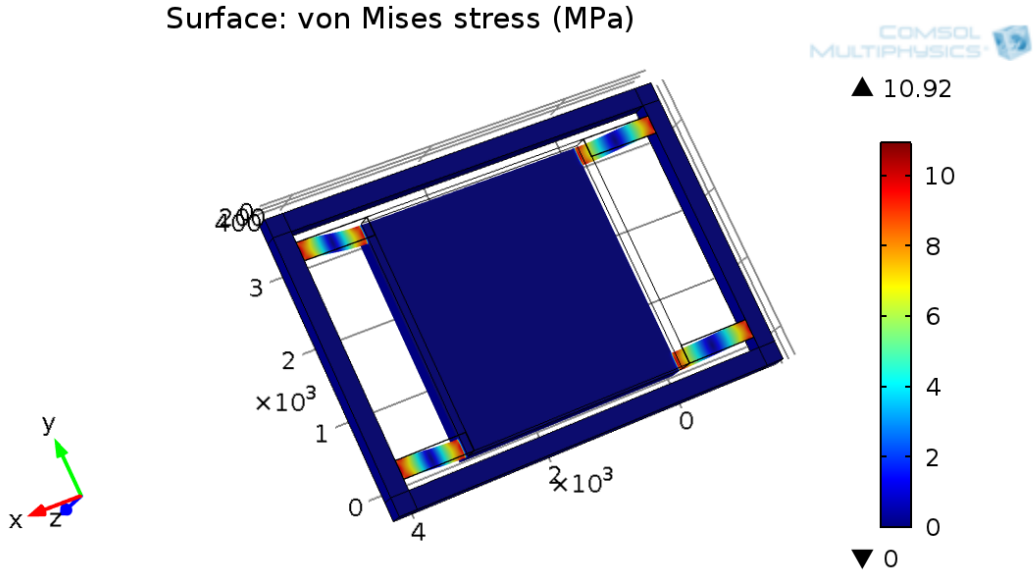

Figure 3.8: Simulated stress for beam thickness 10 μm

TH-2011_11610225

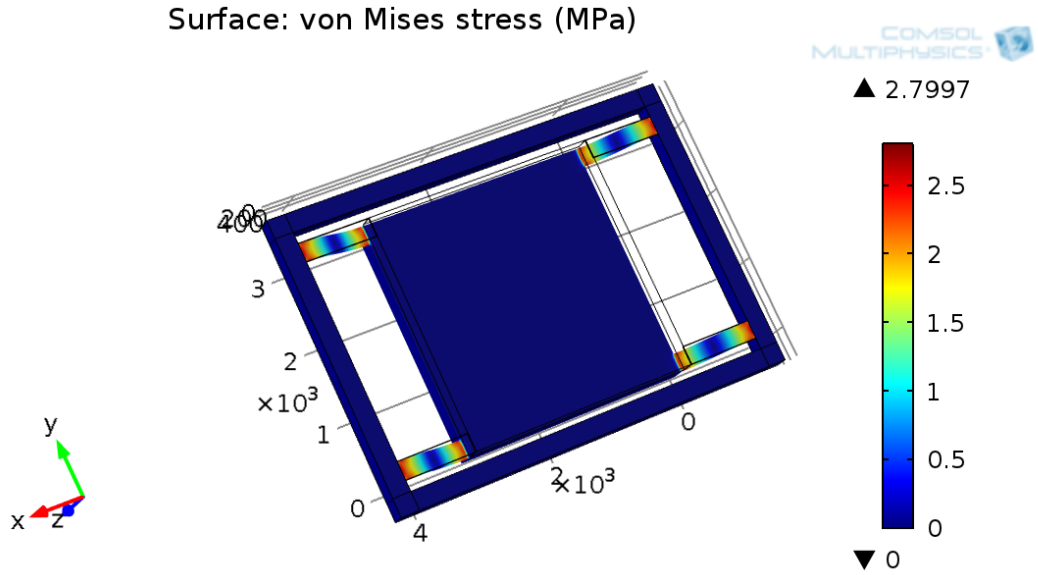

Figure 3.9: Simulated stress for beam thickness 20 μm

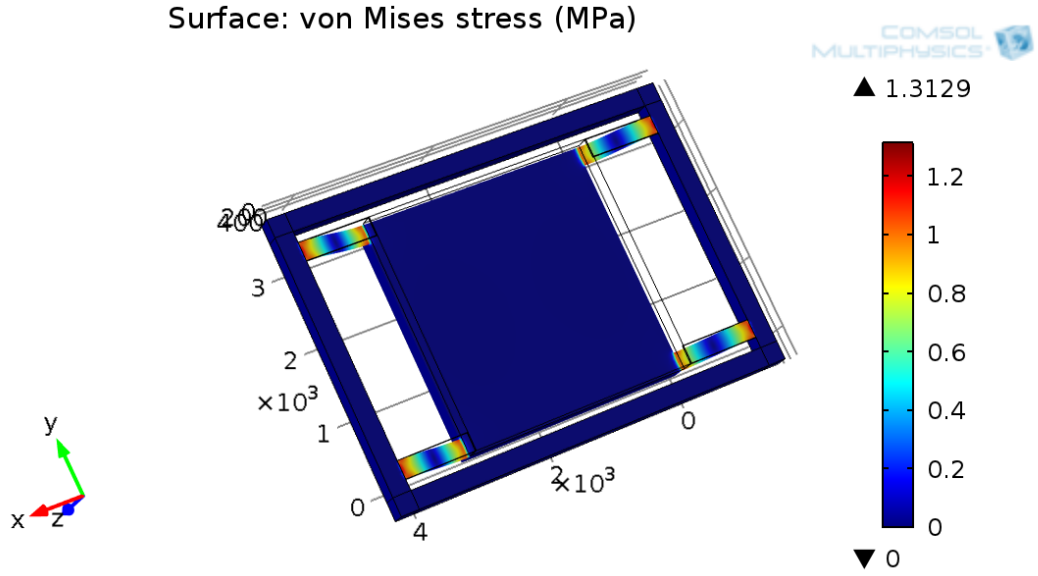

Figure 3.10: Simulated stress for beam thickness 30 μm

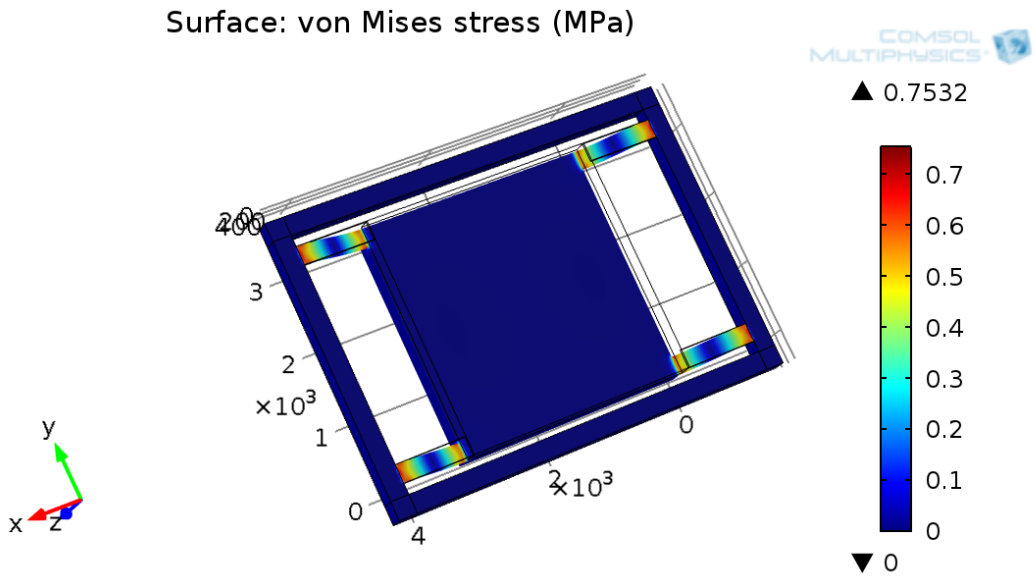

Figure 3.11: Simulated stress for beam thickness 40 μm

The linearity is evaluated for the displacement and stress induced. The values are given in Table 3.7.

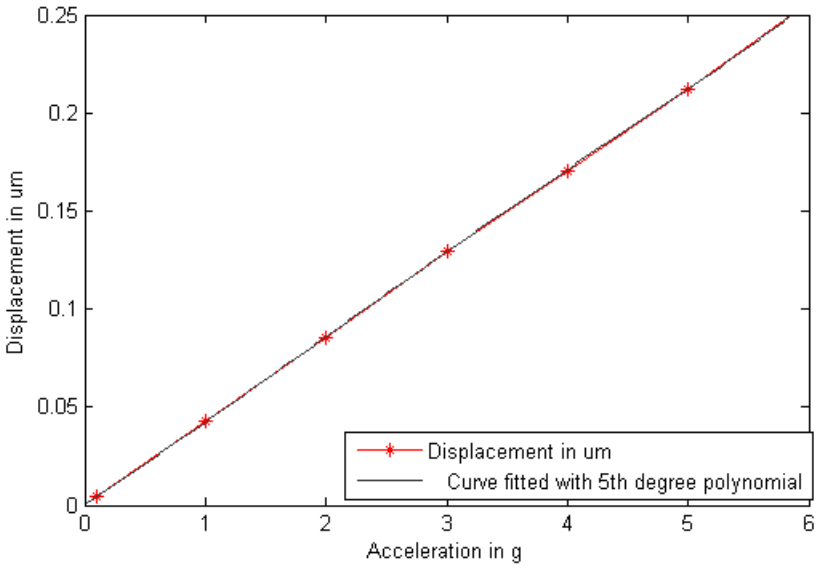

Figure 3.12: Plot showing displacement linearity for thickness 20 μm

It can be seen that there is marginal degradation in linearity if the beam thickness is taken as 10 μm. Beam thickness of 20 μm gives a linearity of 99.95% for displacement and 99.80% for stress. Beam thickness of 20 μm is chosen for our design.

TH-2011_11610225

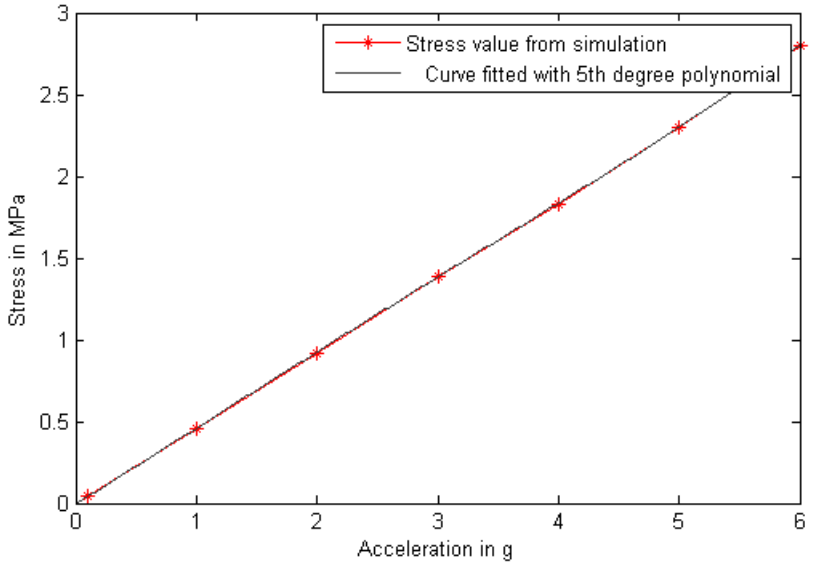

Figure 3.13: Plot showing stress linearity 20 μm

Table 3.7: Displacement and stress linearity

Beam thickness in μm	Displacement linearity (%)	Stress linearity(%)
10	98.84	98.83
20	99.95	99.80
30	98.91	99.91

TH-2011_11610225

3.3.2 Effect of positioning of Beams of accelerometer on sensitivity

The proposed design is based on the quad beam structure. In quad beam structure the placement of the beam plays a vital role. In this section, we investigate the impact of placement of the beam on the stress developed in turn on the sensitivity. It is also investigated to ascertain the impact of the placement of these beams on cross-axis sensitivity.

We have considered two different placement of the beams i) the beams are aligned with the edge of the proof-mass ii) wherein the beams are little inside from the edge of the proof-mass . Fig. 3.15 shows the placement of beam for case I and Fig. 3.14 shows the placement of beam for case II. The dimension for both: proof-mass 3200 μm $\times$ 3200 μm $\times$ 250 μm, beam 1000 μm $\times$ 250 μm $\times$ 20 μm, piezoresistors p-doped 100 μm $\times$ 25 μm $\times$ 2 μm. The difference is in the beams' positioning. Stress induced for both the structures when 6 g acceleration is applied in z-axis are shown in Fig. 3.16 and Fig. 3.17.

It can be clearly seen that the prime axis sensitivity of both the structures are almost the same. The proofmass is considered a rigid body. To investigate the impact on cross-axis sensitivity, the acceleration is applied in two off axes and the stress induced is evaluated using the simulation tool. The stress obtained for both the structures are tabulated in Table 3.8.

It can be seen from the table that the sensitivity in X axis is not effected much by the placement of the beams wherein the sensitivity in Y axis reduces when the beams are aligned to the proof-mass. In terms of percentage, the reduction of cross-axis sensitivity in Y axis is 36% when the beams are aligned to the proof-mass.

This is because the structure where beams are aligned with the proof mass edge, has better stiffness. Here stiffness is more because the distance from the centre of the proofmass to the edges where the beams are connected is larger. When lateral acceleration is applied, it causes rotation moment, the normalised parameters $\frac{k_{\theta x}}{k_z}$ and $\frac{k_{\theta y}}{k_z}$ increases. The higher the value of these parameters, the better is the device in terms of cross-axis sensitivity normalised with respect to prime-axis sensitivity. Thus, maximizing the distances from the centre of the proof-mass to the edges as given by a and b, as shown in figure3.14,there is a possibility of reducing cross-axis sensitivity. A detailed explanation is given in Chapter 5. Thus it is apparent from the above analysis that it is beneficial to go for structure with beam aligned to the edges of the proof-mass. The proposed structure thus puts the beams aligned with the edge of the proof-mass.

TH-2011_11610225

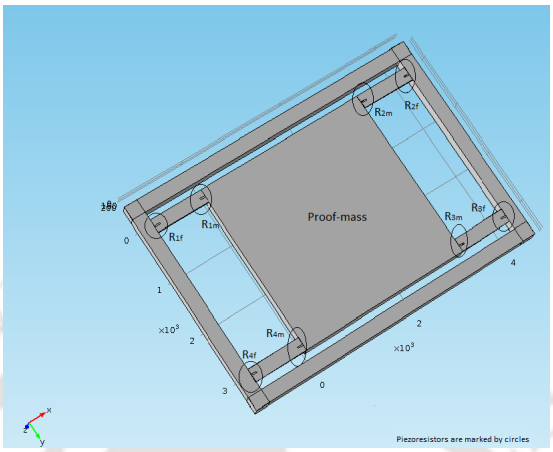

Figure 3.14: Accelerometer structure 2

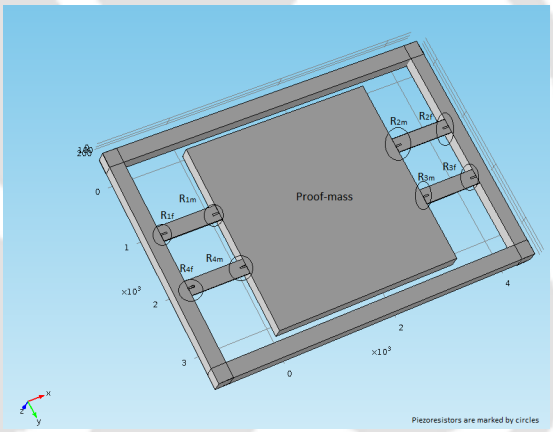

Figure 3.15: Accelerometer structure 1

Table 3.8: Design of the piezoresistors

Beams aligned/not aligned	von Mises stress (Prime axis acceleration)	von Mises stress (X axis acceleration)	von Mises stress (Y axis acceleration)
Aligned	2.7997 MPa	0.1854 MPa	0.7182 MPa
Not aligned	2.7118 MPa	0.1728 MPa	1.1138 MPa

TH-2011_11610225

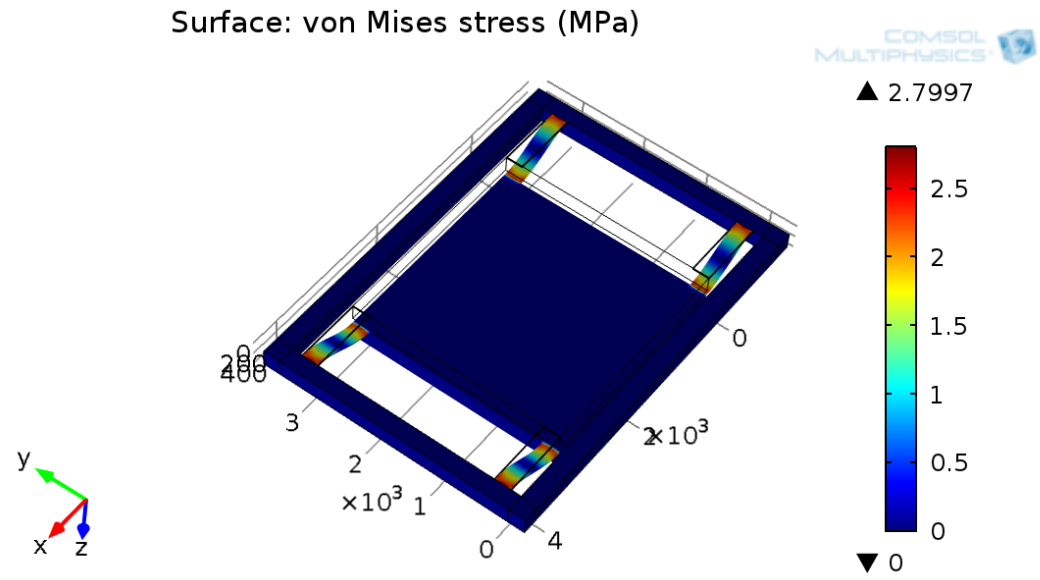

Figure 3.16: Stress for Structure 1 with beam thickness 20 μm

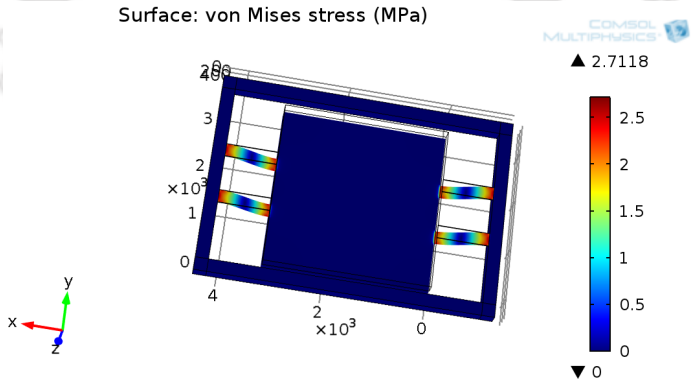

Figure 3.17: Stress for Structure 2 with beam thickness 20 μm

TH-2011_11610225

3.4 Wheatstone bridge as signal pick up circuit

Wheatstone Bridge is the most useful circuit with the help of which the change in resistance value of the piezoresistors can be sensed and the output voltage is obtained which is proportional to the change in resistance. The proposed accelerometer has total eight piezoresistors which are connected in the form of a Wheatstone bridge with two resistances on each arm. Eight piezoresistors are arranged in the wheatstone bridge in such a way that the sense of stress (Tensile or compressive) will ensure that the bridge becomes unbalanced only when the acceleration is applied in z direction and for other cases when acceleration is applied in other direction the bridge will remain balanced. This will ensure the differential output is available only when the acceleration is present in prime axis. In reality the magnitude of the stress developed will not be exactly same, thus there will be pick up at the circuit output even for off axes though very low.

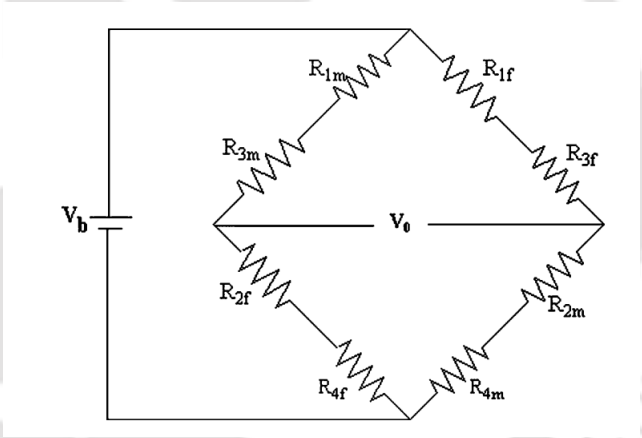

Figure 3.18: Wheatstone bridge circuit for signal pick-up

The exact position of the piezoresistors in the accelerometer structure vis-a-vis their position in Wheatstone Bridge can be seen by referring to Fig. 3.15 and Fig. 3.18. Let the output voltage be denoted by V_0 and the source voltage be V_s. Then we get Eq. 3.16.

$$V_0 = \left(\frac{R_{2f} + R_{4f}}{R_{2f} + R_{4f} + R_{1m} + R_{3m}} - \frac{R_{4m} + R_{2m}}{R_{4m} + R_{2m} + R_{3f} + R_{1f}} \right) V_s \tag{3.16}$$

For acceleration applied in Z direction, piezoresistors R_{1m}, R_{2m}, R_{3m} and R_{4m} undergoes compressive stress and R_{1f}, R_{2f}, R_{3f} and R_{4f} undergoes tensile stress. The resistance of piezoresistors increase when they undergo tensile stress and the resistance decrease when they undergo compressive stress. Let ΔR_{im} and ΔR_{if} denote the magnitude of change of resistance of R_{im} and R_{if} respectively. With

TH-2011_11610225

these we get Eq. 3.17.

$$V_0 = \left(\frac{R_{2f} + \Delta R_{2f} + R_{4f} + \Delta R_{4f}}{R_{2f} + \Delta R_{2f} + R_{4f} + \Delta R_{2f} + R_{1m} - \Delta R_{1m} + R_{3m} - \Delta R_{3m}} - \frac{R_{4m} - \Delta R_{4m} + R_{2m} - \Delta R_{2m}}{R_{4m} - \Delta R_{4m} + R_{2m} - \Delta R_{2m} + R_{3f} + \Delta R_{3f} + R_{1f} + \Delta R_{1f}} \right) V_s \tag{3.17}$$

Let us assume that the magnitude of the stress is same for all the resistors and let the magnitude of change of resistance be denoted by ΔR. And let us also assume that the stress free resistance of all the piezoresistors are the same and is denoted by R. In that case the above equation reduces to

$$V_0 = \frac{\Delta R}{R} V_s \tag{3.18}$$

In practical cases, the change in resistances will not be exactly the same, in that case Eq. 3.17 shall be used to find out the voltage output.

3.5 Simulation Results and Analysis

The analysis of the proposed MEMS accelerometer structure is carried out by FEM tool (COMSOL). The modes of vibrations, displacement, stress analysis and sensitivity has been simulated for the structure.The software is based on finite-element method. At first the model is set to 3 axis geometry and then the physics is added. This is followed by setting the global definition like parameter or variables or functions etc. The material of the structure is defined as silicon (by defining properties like Young's modulus, refractive index etc) and p-type doping is selected for piezoresistors (by defining Poisson's ratio, relative permittivity, density etc). Then choosing solid mechanics module, the boundary conditions are applied at the frame end faces of the beam. The frame is kept fixed in all the direction. The simulation is performed with proofmass weighing 5.96×10^{-6}kg, and the beam dimensions of 1000μm $\times$ 250μm $\times$ 20μm. After setting the design geometry, meshing is done using tetrahedral elements. To perform the modal analysis, eigen modes shapes are simulated. The eigen mode analysis is followed by frequency domain analysis and Time dependent analysis. After simulating with all the geometry, boundary condition, physics etc the necessary parameters like displacement, stress etc can be evaluated in the results section of the software.

TH-2011_11610225

Table 3.9: Verification of Deflection values calculated and simulated

Acceleration on z-axis	**Calculated Deflection** (μm)	**Simulated Deflection** (μm)
1 g	0.0427	0.0425
2 g	0.0854	0.0854
3 g	0.1281	0.1296
4 g	0.1708	0.1706
5 g	0.213	0.2123
6 g	0.2592	0.2562

3.5.1 Displacement

Let us assume that the accelerometer is subjected to a acceleration having an amplitude of a_z. It can be seen from Eq. 3.11, that, if Z is the amplitude of the displacement of the proof-mass than for small $'r'$, $Z\omega_n^2$ is equal to a_z (in Eq. 3.11, the amplitude acceleration was $\omega^2 A$). Thus, we can write

$$\omega_n^2 Z = a_z \tag{3.19}$$

Using $\omega_n = \sqrt{\frac{k_{eff}}{m}}$ where k_{eff} is the effective spring constant of the beams of rectangular cross section, of the mass spring system.

$$Z = \frac{ma_z}{k_{eff}} \tag{3.20}$$

Now substituting the expression for k_{eff} as given in Eq. 3.1, we obtain Eq. 3.20 becomes

$$Z = \frac{ma_z l^3}{4Ebh^3} \tag{3.21}$$

The deflection is evaluated analytically using the above formula and is simulated for different accelerations applied in the z-axis and is given in Table 3.9. The accelerometer has been subjected to different accelerations applied in the z-axis from 1 g to 6 g. The values obtained from simulation shows very good agreement with the values obtained analytically. The displacement obtained from simulation for different values of acceleration is shown in Fig. 3.19−3.24.

TH-2011_11610225

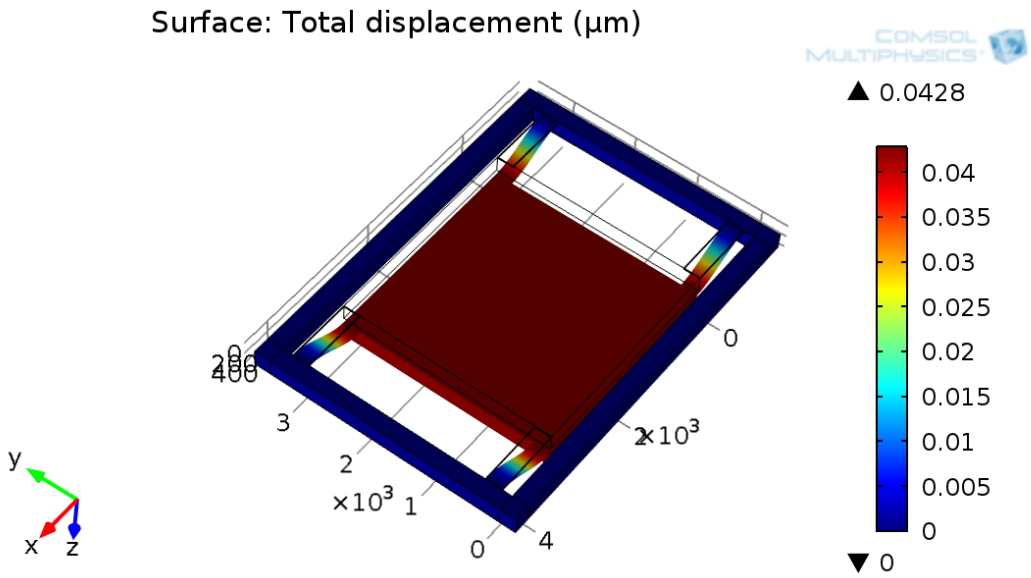

Figure 3.19: Simulated displacement for 1 g acceleration

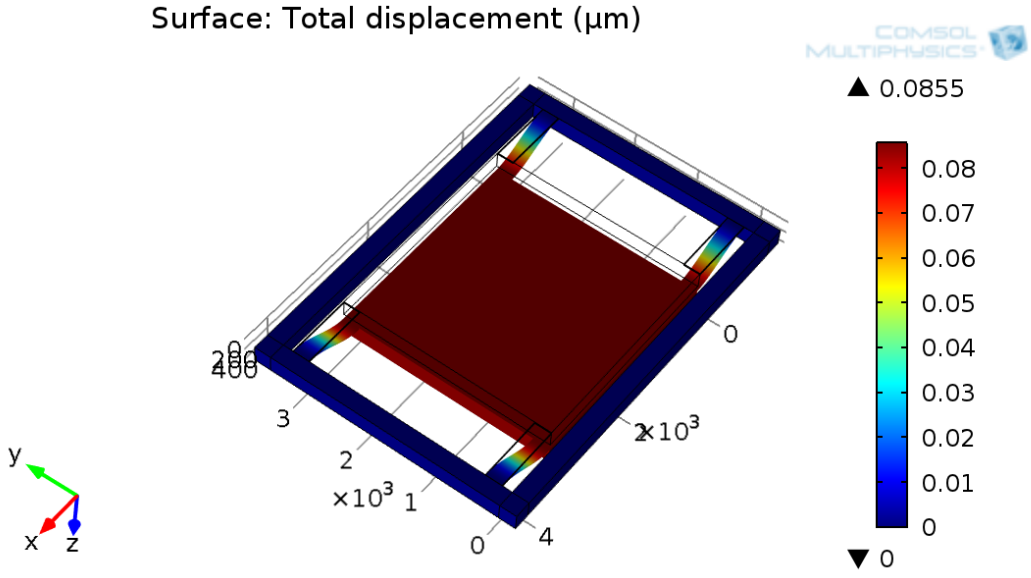

Figure 3.20: Simulated displacement for 2 g acceleration

TH-2011_11610225

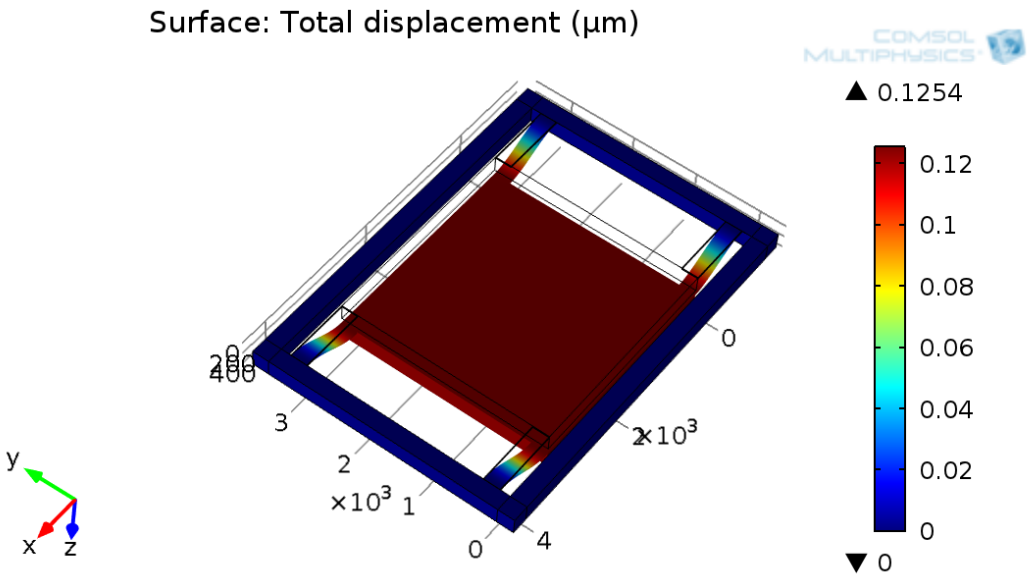

Figure 3.21: Simulated displacement for 3 g acceleration

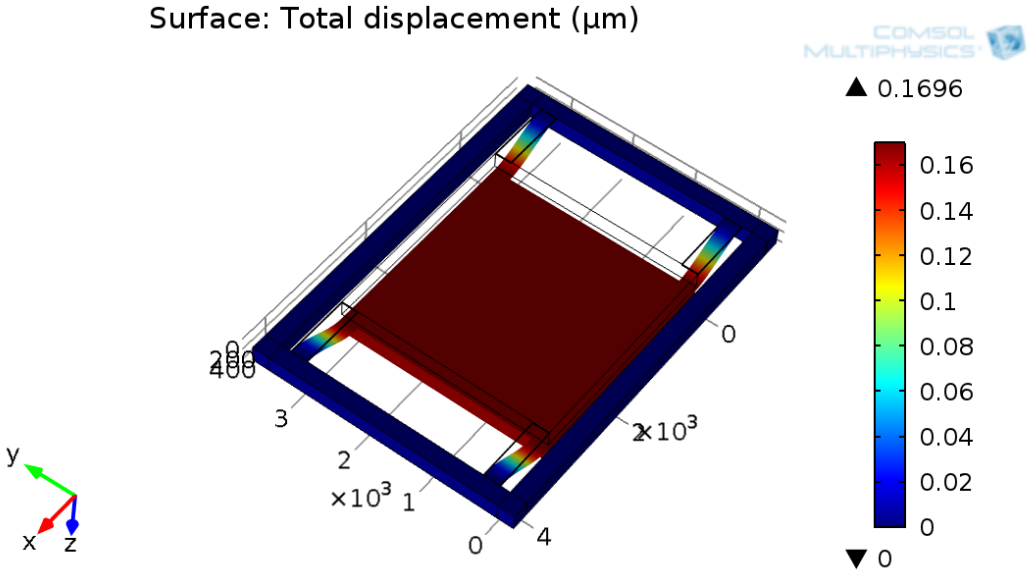

Figure 3.22: Simulated displacement for 4 g acceleration

TH-2011_11610225

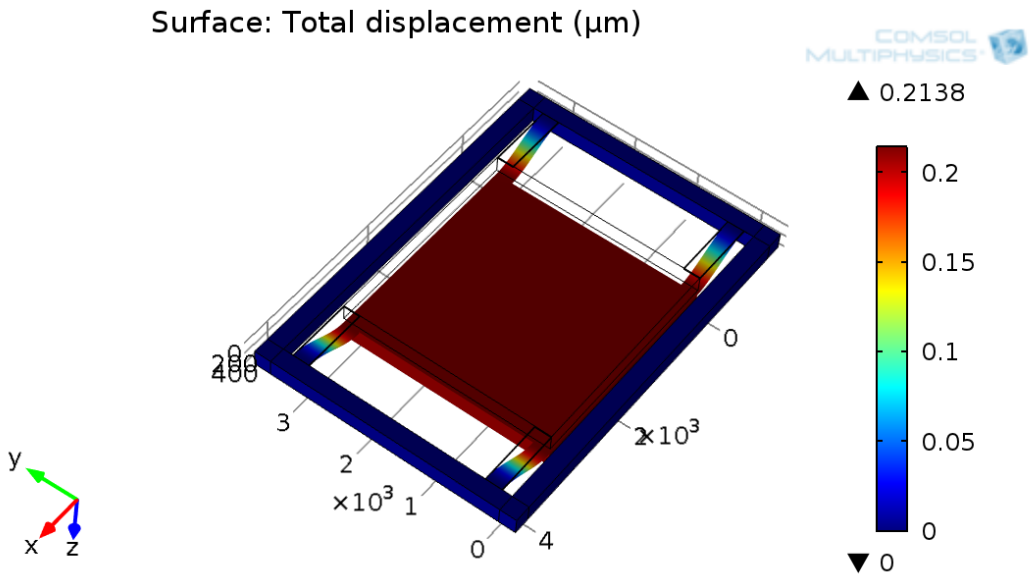

Figure 3.23: Simulated displacement for 5 g acceleration

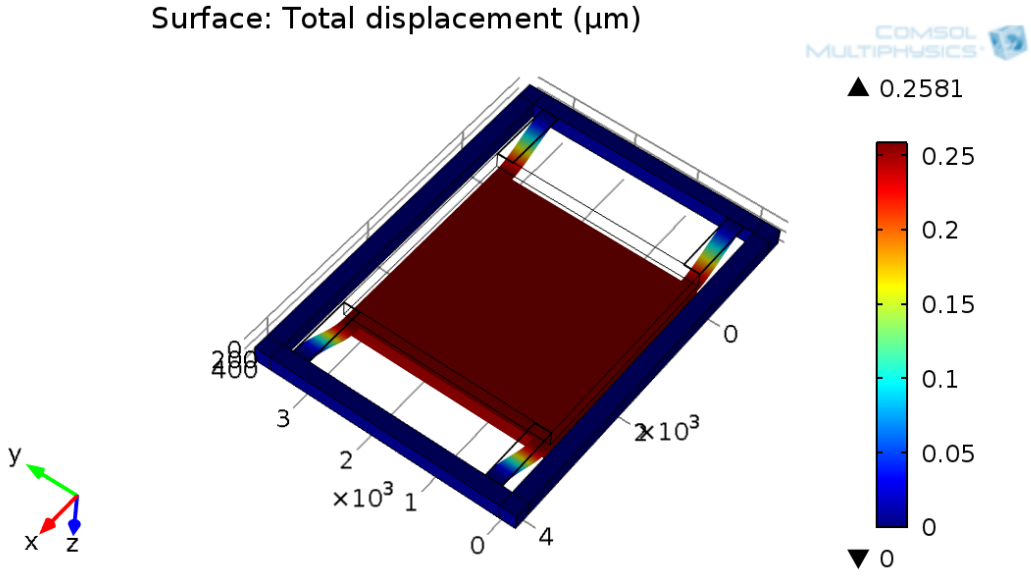

Figure 3.24: Simulated displacement for 6 g acceleration

TH-2011_11610225

Table 3.10: Stress simulated when acceleration applied on z-axis

Acceleration on z-axis 'g'	**Simulated Stress (MPa)**
1g	0.46
2g	0.92
3g	1.39
4g	1.83
5g	2.3
6g	2.8

3.5.2 Stress Analysis

In the piezoresistive sensing mechanism, whenever there is a change in the resistance value, this change is proportional to the developed stress which in turn is proportional to the displacement of the proof-mass. Hence for maximum sensitivity it is important to locate the maximum stress regions to place the piezoresistors for maximum stress sensing. For the fixed doping concentration, first the change in the resistance value of each piezoresistor has to be found out. Then the change in current through each piezoresistor is obtained and the new resistance value of each piezoresistor is obtained for a particular acceleration. The sensitivity is the relative change of the output voltage per differential acceleration. The stress has been observed for different g value ranging from 1 g to 6 g, applied on z-axis (out of plane). Thus, the simulated stress is shown in Table 3.10 and in Fig. 3.25−3.30. The von Mises stress helps in checking if the microstructure is able to withstand the induced stress or a failure occurs if it reaches the yield strength of the material. Under normal acceleration the beams bend in such a way that they are convex in shape near the frame end and concave near the proof-mass end. This will depend on the direction of acceleration whether upward or downward. The longitudinal stress values are obtained to be maximum near the fixed ends and minimum at the middle of the beams. When acceleration is applied on z-axis, the resistors located near the frame end suffer tensile stress and those near the proof-mass end suffer compressive stress.

3.5.3 Modal analysis

The rhythmic pattern or oscillations of tremor can be related to the movement of the mass and spring [3]. Hence the microstructure can be modeled by a spring-mass system and is governed by the

TH-2011_11610225

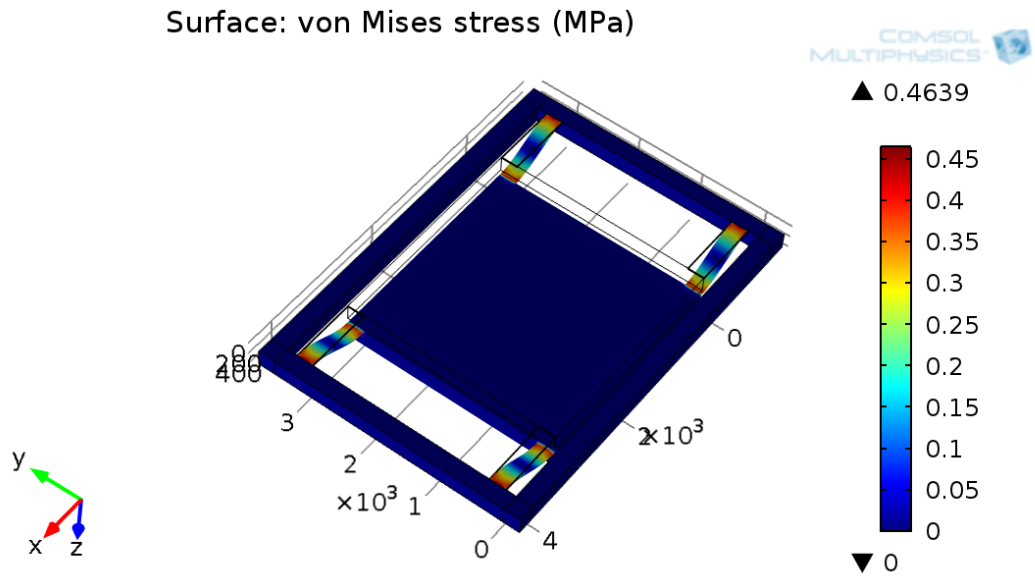

Figure 3.25: Simulated stress for 1 g acceleration

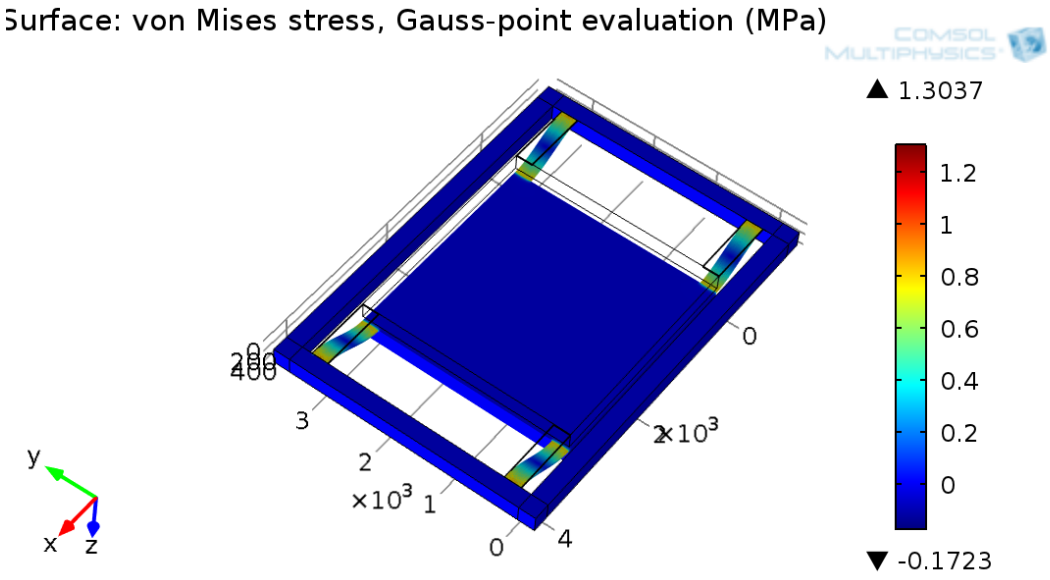

Figure 3.26: Simulated stress for 2 g acceleration

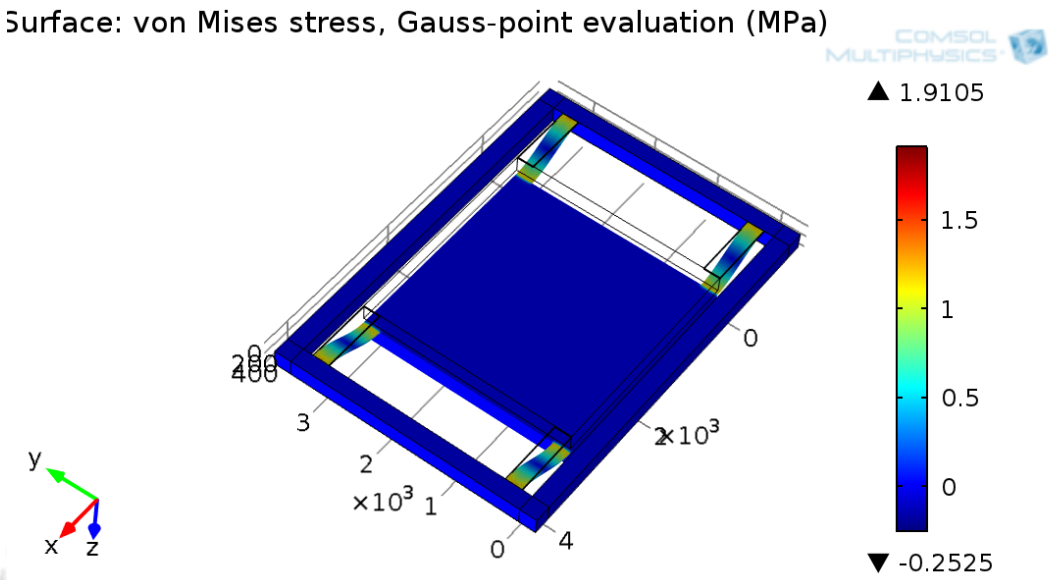

Figure 3.27: Simulated stress for 3 g acceleration

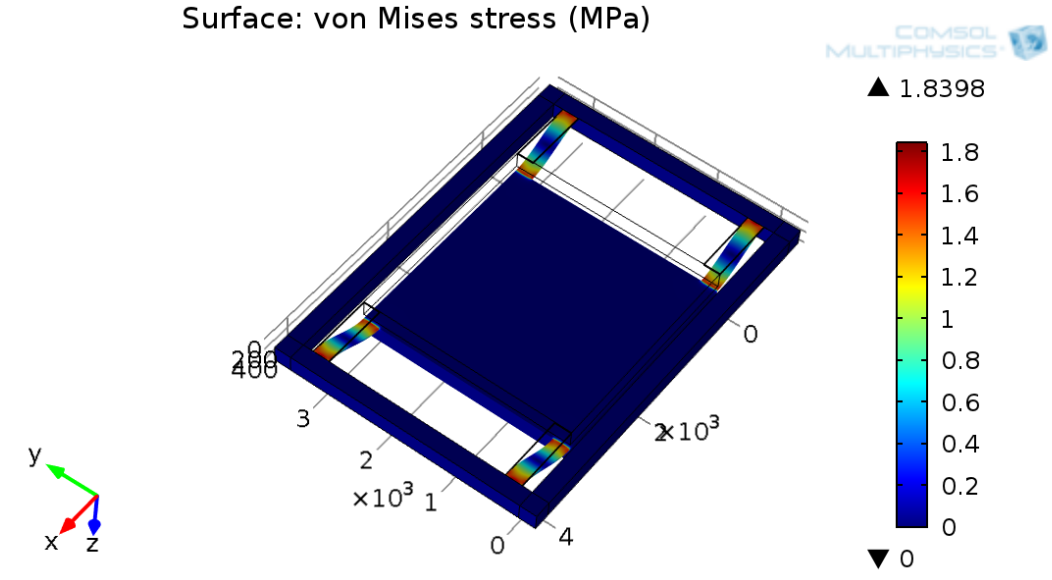

Figure 3.28: Simulated stress for 4 g acceleration

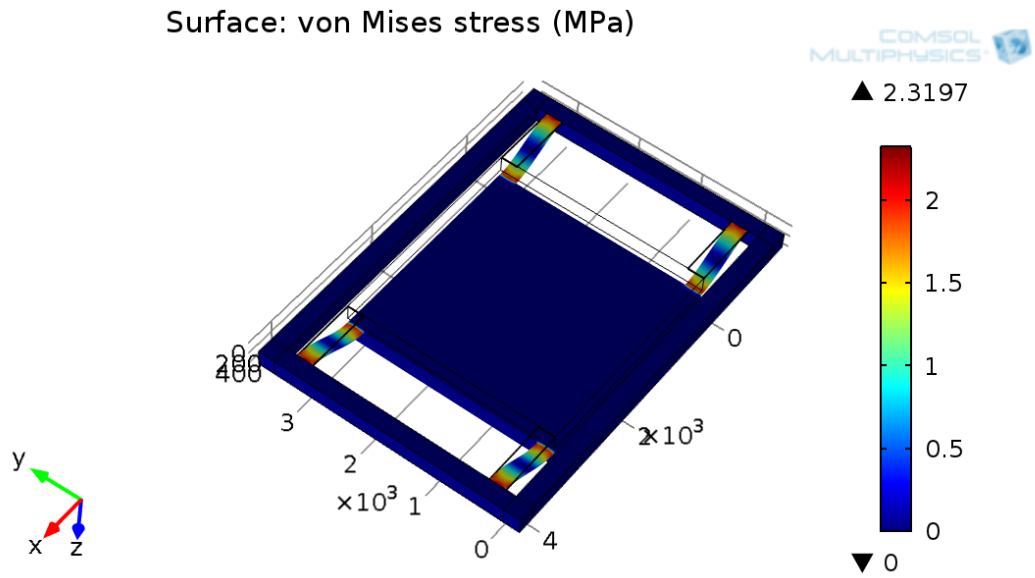

Figure 3.29: Simulated stress for 5 g acceleration

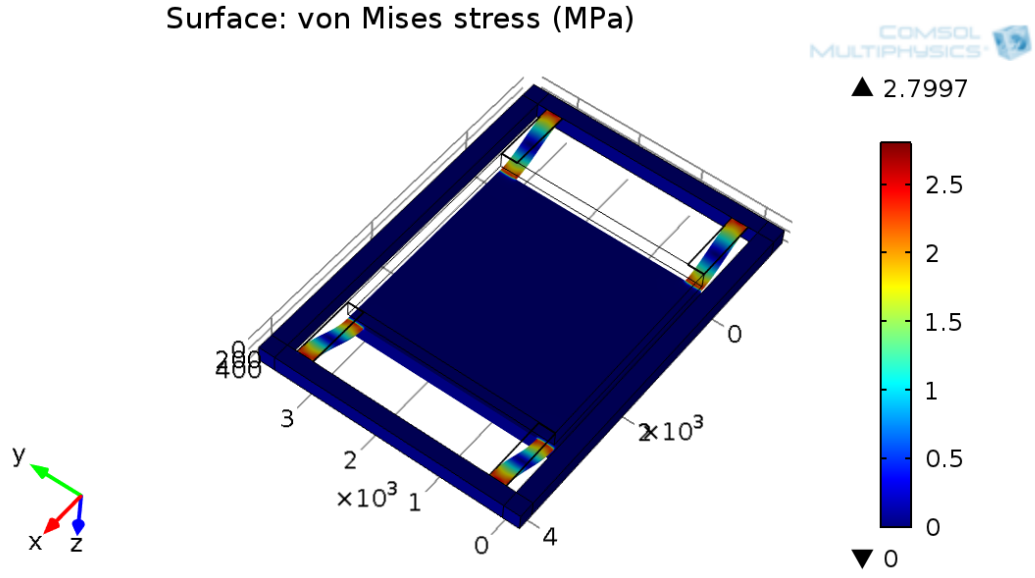

Figure 3.30: Simulated stress for 6 g acceleration

TH-2011_11610225

second order differential equation of motion [46]

$$[M]\{\ddot{U}\} + [K]\{U\} = 0 \tag{3.22}$$

where $[M]$, $[K]$ and $\{U\}$ represent mass matrix, stiffness matrix and deflection respectively. Here both K and M are symmetric and real. The deflection which occurs due to the free or forced vibration of the microaccelerometer is actually a combination of all its normal modes and may be given as

$$\{U\} = \Sigma_i\{\phi_i\}\xi_i \tag{3.23}$$

where $\{U\}$ stands for physical displacement, $\{\phi_i\}$ stands for i^{th} mode shape and ξ_i denotes i^{th} modal displacement. The dynamic analysis is important and therefore we need to do the eigenmode analysis. The eigenvalue analysis for no load condition is given by

$$[K] - \omega_n^2[M]\{\phi\} = 0 \tag{3.24}$$

where the natural frequency ω_n=$2\pi f$ gives the frequency of vibration in rad/sec, f denotes one of the n natural frequencies of vibration in hertz, $\{\phi\}$ is the eigenvector which denotes the different mode shapes or free mode vibration. The most important condition of the accelerometer design is that the natural frequency must be at least three times the operating frequency in order to ensure that there is no interference nor any chance of structural damage. However too high a natural frequency may give reduced selectivity and precision for low bandwidth operations. Thus it is important to perform the normal mode analysis, determine natural frequencies and mode shapes for all types of dynamic analysis of the microstructure. The modal analysis has been carried out where the first six eigenmodes have been obtained as shown in Table 3.11 having different mode shapes as shown in Fig. 3.31−3.36. The natural frequency and different vibration modes shapes are obtained which are the function of the spring constant of the spring and the mass of the proof-mass.

3.5.4 Sensitivity Analysis

Sensitivity of the accelerometer, sometimes referred to as the scale factor of the accelerometer, is the ratio of the sensors electrical output to mechanical input. A transducer generally is defined as a device that converts one form of energy to another. An accelerometer simply is a transducer that

TH-2011_11610225

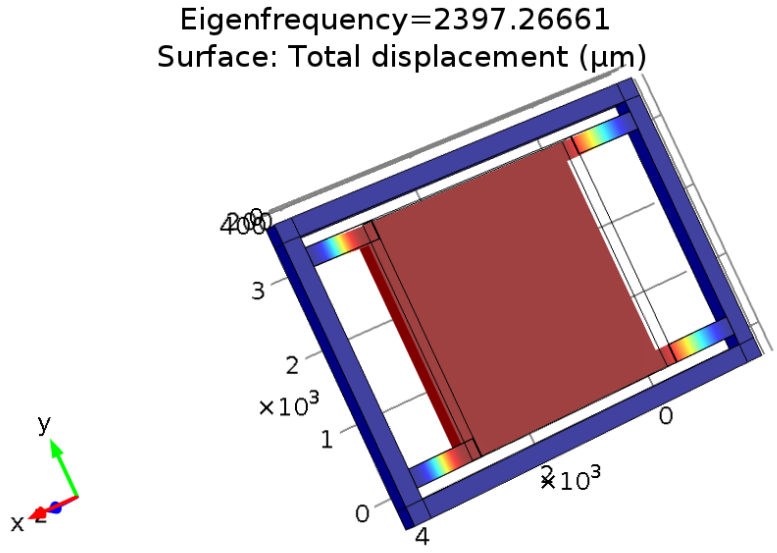

Figure 3.31: Mode 1 represent the sensing in the desired axis (z-axis) and natural frequency 2397 Hz

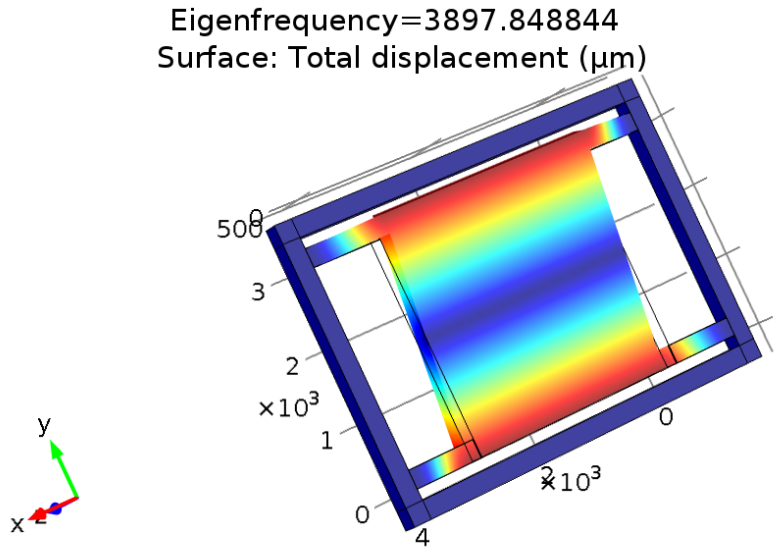

Figure 3.32: Mode 2 obtained at the frequency 3897 Hz

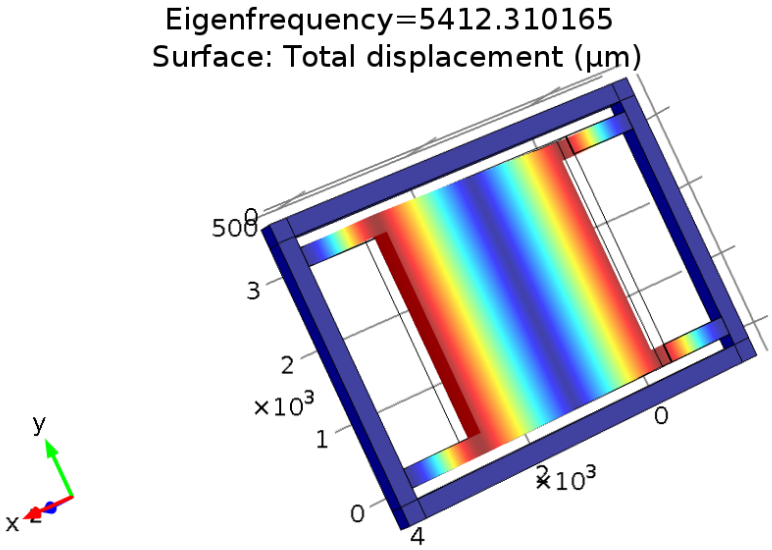

Figure 3.33: Mode 3 obtained at frequency 5412 Hz

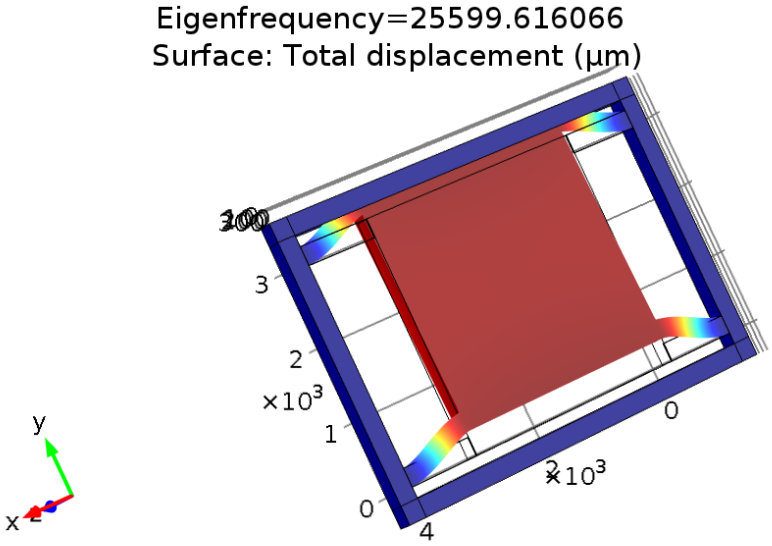

Figure 3.34: Mode 4 obtained at frequency 25599 Hz

TH-2011_11610225

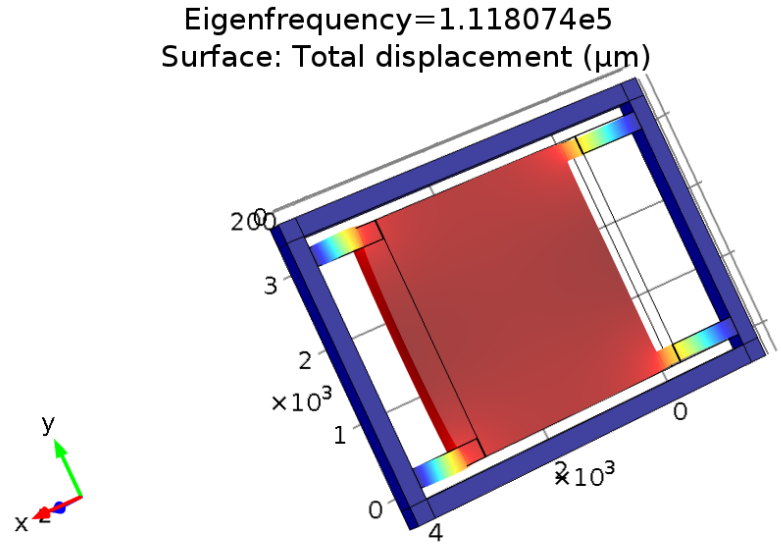

Figure 3.35: Mode 5 obtained at frequency 1.11×10^5 Hz

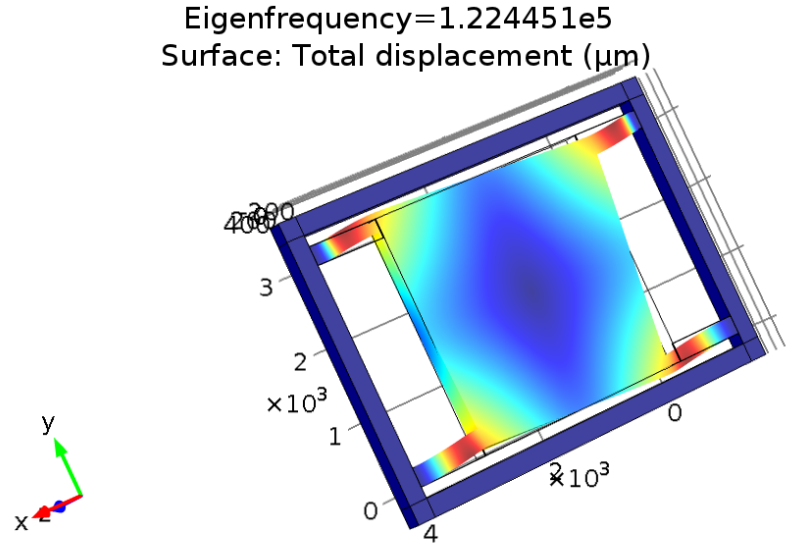

Figure 3.36: Mode 6 obtained at frequency 1.22×10^5 Hz

TH-2011_11610225

Table 3.11: Simulated Eigenvalues

Eigen modes	**Frequency values (Hz)**
Mode 1	2397
Mode 2	3897
Mode 3	5412
Mode 4	25599
Mode 5	1.11×10^5
Mode 6	1.22×10^5

converts mechanical acceleration into a proportional electrical signal. Sensitivity is determined by the relative change in output per applied differential acceleration per input voltage. The piezoresistors are connected in the form of a Wheatstone bridge signal pick up circuit. The change in resistance of the piezoresistor is linearly related to the induced stress. The piezoresistive coefficients of a doped single-crystal silicon piezoresistor are influenced by its relative orientation to crystallographic directions. Appropriate doping concentrations must be carefully selected when designing silicon piezoresistors. A successful design must balance the needs to have an appreciable resistance value, to maximize the gauge factor, and to minimize temperature effects. The temperature coefficient of resistance of a piezoresistor ideally should be as small as possible to minimize effects of temperature variation. For both p- and n-type silicon, the value of the piezoresistive coefficient decreases with increasing temperature and doping concentrations. Different coefficients π_{11} , π_{12}, and π_{44} are affected differently by temperature and doping concentrations. If stress is applied in the longitudinal direction, the change in resistance is given as Δ R/R_0=$\pi_l\sigma_l$ [45] where R_0 is the initial resistance, π_l is the longitudinal piezoresistive coefficient and $\sigma_l$is the longitudinal stress. The piezoresistive coefficient for the piezoresistors along the (110) direction is given by 1/2[π_{11}+π_{12}+π_{44}]. For single crystal silicon different piezoresistivity components exist for different doping concentrations.

For the purpose of ascertaining the sensitivity we need to find out the output voltage for an applied acceleration. In this simulation, an acceleration of 6 g is applied in the prime-axis direction. The stress induced was noted to be 2.8 MPa. Therefore, referring to Eq.5.9, we need to determine $\frac{\Delta R}{R}$ to arrive at the output voltage. The value of source voltage V_s is 5 volts. Considering the values for piezoresistive coefficients ($\pi_{11} = 6.5 \times 10^{-11}$, $\pi_{12} = -1.1 \times 10^{-11}$ and $\pi_{44} = 138 \times 10^{-11}$) and stress induced of 2.8 MPa for the applied acceleration; the ratio $\frac{\Delta R}{R}$ is found out to be 2.01×10^{-3}. This gives rise to $V_0 = 10.05 \times 10^{-3}$ Volt. From this sensitivity can be calculated by dividing the value by amplitude of

TH-2011_11610225

acceleration applied and source voltage which gives rise to a value of 0.33 mV/V/g.

3.6 Conclusion

In this chapter, the design of microaccelerometer is brought out. The modeling and design analysis of the proposed accelerometer is carried out using FEM based software COMSOL. Various design issues are discussed and the proposed structure is compared with similar structure having difference in beam positioning. The detailed analysis of the same including the effect of thickness of the beam, positioning of the beam on the sensitivity are brought out. The linearity of observed parameter with respect to the parameter to be sensed i.e., acceleration is also very important. The same is studied in this chapter. It is important to investigate the displacement, stress induced on the structure for different values of applied acceleration. The material selection and their parameter selection for piezoresistor is detailed in this chapter along with their position in the microaccelerometer. The signal pick-up circuit and connection of the piezoresistors in Wheatstone bridge for reduction of cross-axis sensitivity is brought out. Modal analysis establishes the mode shapes and resonance frequencies of vibration. The same is studied here for the proposed structure.

TH-2011_11610225

TH-2011_11610225

4

Damping Analysis

Contents

TH-2011_11610225

TH-2011_11610225

4.1 Introduction

Inertial MEMS (micro electro mechanical system) accelerometers require adequate damping control for high performance applications. Damping is basically a phenomenon by which we get a reduction in the amplitude of undesired oscillation as a result of energy being drained from the system to overcome any resistive forces. Damping of the proof-mass is a fundamental consideration in the design of accelerometers. Damping is one of the characteristic that determines the dynamic behaviour. Air damping is very important in this case unlike conventional machines where energy dissipated by air damping is much smaller than the energy dissipated by other mechanisms. In any micro device, there is large surface area to volume ratio of the moving parts. This is one of the reasons which makes dynamic performance analysis important [24]. The energy consumed by air damping must be minimized so that with a limited energy supply, the motion of the mechanical parts can be maximized. Also in order to have an optimum dynamic performance, air damping has to be controlled. Thus, one of the most important design steps is estimating the damping effect in MEMS accelerometer as like any other micro mechanical device.

The dynamic characteristic of the device is mainly determined by the damping material (air here) and the spacing between the proof-mass and the housing. There are different mechanisms of damping depending upon the the operating conditions and dimensions of the structure. At first, Newell [37] observed that air damping increases rapidly as the surface to mass ratio increases for a MEMS device. Soon after this, different researchers focussed on squeeze film air damping in MEMS [39], [40], [41], [42]. The most significant damping suitable in MEMS devices specially operating at atmospheric pressure and low frequency is the Squeeze film damping. For a specific value of air gap thickness, the various factors that affect squeeze film damping are the operating frequency of oscillations, surrounding pressure, viscosity of the medium, and dimensions of the structure [24]. It is desirable for any MEMS device to achieve a flat response over a wide range of frequencies. Micromachining has significantly enhanced different damping provisions as silicon technology has grown significantly. It has made possible for the damping material to be a very thin layer of air instead of oil, which is less temperature dependent due to its smaller relative change in viscosity compared to oil. The air damping, however requires a more precise control of gap dimension in a reproducible way. Different types of analysis and studies have been made on Squeeze film damping. The adiabatic squeeze films have been studied by Langlois [47]. Squeeze film damping control in solid state accelerometers were at first given by

TH-2011_11610225

Starr [38]. Bao has detailed the squeeze film air damping of thick holes made on the plate, assuming the holes in the plate are of equal cross sectional area. The most widely used technique used by most of the researchers is perforation on proof-mass [35], [36]. The squeeze film analysis of most of the MEMS devices is generally performed using the 2D isothermal compressible Reynolds equation [36]and [38]. Different mathematical models with different assumptions have been proposed by different researchers for determining the squeeze film damping model [48] and [49]. As the dynamic behaviour is significantly affected by the squeeze film air damping, correct prediction of damping ratio becomes significantly important. The squeeze film damping effect has been simulated in this Chapter.

4.2 Theoretical Background

In this section, the theoretical aspects are brought out. The different models used for predicting the damping in squeeze film damping coefficient are also brought out.

4.2.1 Damping of second order system

The MEMS accelerometer can be modeled as a mass-spring-damper where the proof-mass deflects relative to the supporting frame with the input acceleration, forming a second order system. The accelerometer can be modeled by a second order mass-spring-damper system where both the relative displacement and suspension beam stress can be used as a measure of the external acceleration. Let z be the displacement of the mass m relative to the casing.

The equation of motion is

$$m\ddot{z} + c\dot{z} + kz = -ma \tag{4.1}$$

where c, k and a denote the damping coefficient, spring constant and acceleration of the base respectively. The dynamic behavior is determined by the natural frequency and damping ratio, thus the equation of motion becomes

$$\ddot{z} + 2\zeta\omega_n\dot{z} + \omega_n^2 z = -a \tag{4.2}$$

where

$\omega_n = \sqrt{(\frac{k}{m})}$

$\zeta = \frac{c}{C_c}$

C_c is critical damping coefficient and is equal to $2\sqrt{(km)}$

TH-2011_11610225

The mechanical transfer function can be written as.

$$H(s) = \frac{\omega_n^2}{s^2 + 2\zeta\omega_n s + \omega_n^2} \tag{4.3}$$

For a second order underdamped system we have $\zeta < 1$ and its requirement for step response can be expressed by settling time and overshoot as illustrated in Figure. 4.1. The time history of the step

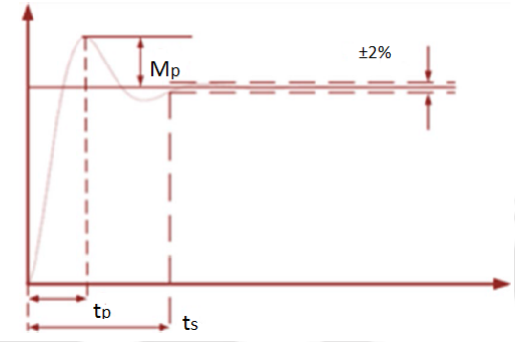

Figure 4.1: Definition of settling time and maximum overshoot

response of a second-order system found from the inverse Laplace transform of H(s)/s is given as [50].

$$z(t) = 1 - \frac{1}{\sqrt{1-\zeta^2}} e^{-\zeta\omega_n t} sin(\omega_d t + \beta) \tag{4.4}$$

where

$\omega_d = \omega_n\sqrt{1-\zeta^2)}$ is the damped frequency of oscillation

β is the phase lag

Maximum overshoot Mp may be defined as the difference between the magnitude of the highest peak of time response and magnitude of its steady state. At the peak time, the response curve reaches its maximum value. Hence at that point, the derivative of Eq. 4.4 becomes equal to zero. The expression for maximum overshoot is given as

$$Mp = e^{-\frac{\pi\zeta}{\sqrt{1-\zeta^2}}} \tag{4.5}$$

From Eq. 4.5, the damping ratio can be calculated by taking logarithm on both sides

$$\zeta = \frac{|\ln(Mp)|}{\pi^2 + [\ln(Mp)]^2} \tag{4.6}$$

TH-2011_11610225

The peak time is given by

$$tp = \frac{\pi}{\omega_d} \tag{4.7}$$

where ω_d is damped natural frequency and equals $\omega_n\sqrt{1-\zeta^2}$. The overshoot disappears as the damping ratio increases to a certain value. The damping ratio can also be calculated from the settling time. For a second-order underdamped linear system, the envelope curve of its step response is given as

$$z(t) = 1 \pm \frac{e^{-\zeta\omega_n t}}{\sqrt{1-\zeta^2}} \tag{4.8}$$

The settling time t_s is the time taken by the system to settle down to steady state value with an error percentage of 2% to 5%.

For 2% error the damping ratio

$$\zeta \approx \frac{4.2}{t_s\omega_n} \tag{4.9}$$

For 5% error the damping ratio

$$\zeta \approx \frac{3.5}{t_s\omega_n} \tag{4.10}$$

Therefore the damping ratio caused by the squeezed film air can be obtained by measuring the M_p and t_s from the step response of the mass spring damper system. Damping is also related to Quality factor or Q factor of such system. Q factor determines the behaviour of damped system. A system having low Quality factor i.e. less than 0.5 is overdamped system, with Q higher than 0.5 is underdamped and system with value of Q equal to 0.5 is critically damped. Q is related to the damping ratio as follows:

$$Q = \frac{1}{2\zeta}. \tag{4.11}$$

4.2.2 Squeeze film damping

In Squeeze film damping, the freely moving structure is separated from a larger structure that is stationary by a thin layer or gas or air. When the freely moving structure is in motion, two things can happen. (i) The motion increases the pressure and squeezes the gas out of the gap (ii) decreases the pressure and draws the gas into the gap. Due to the viscous behaviour of the gas, the movement of the

TH-2011_11610225

mass is resisted which results in a pressure gradient inside the gas film. This pressure gradient opposes the movement of the seismic mass. Hence, the faster the mass moves, the larger the pressure gradient and therewith the reaction force. Here, the work done by the plate is consumed by the viscous flow of the air and transformed into heat. The air film acts as the damper and this type of damping is called the Squeeze film air damping. The damping force of squeeze-film air damping is thus dependent on the gap distance; the smaller the gap, the larger the damping force. When the plate is very far away from the wall, the pressure build-up is negligible and the damping force is mainly due to the drag force. The squeeze-film air damping has significant effects on the dynamic behavior of microstructures. In many cases, it should be reduced and, in some other cases, it should be controlled to an expected level.

The Squeeze film damping effect is the interaction of the silicon proof-mass and the air film, trapped in the gap between mass and the encapsulation. The schematic of the Squeeze film damping is shown in Figure. 4.2.

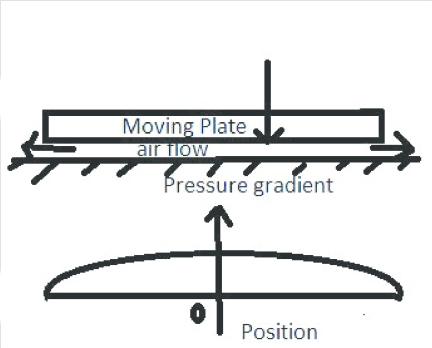

Figure 4.2: Schematic of the Squeeze film damping with the obtained pressure gradient.

It is important to predict the performance of squeeze film damping. For this purpose, we need to have a theoretical model based on which the damping coefficient can be predicted for a given structure and related parameters. In literature many models are provided [51], [52], [53] where they provide the prediction with varying level of precision [53]. In [51], the study is carried out by providing experimental data for validating squeeze film damping (SFD) models. There are continuum and non continuum models for prediction of squeeze film damping. Continuum-based models assume that the gas is a continuum, meaning that the pressure gradient is continuous throughout the gas. Continuum based squeeze film damping models are based on the linearized Reynolds equation. The continuum based models may break down when the mean free path is larger than the thickness of the gap. In free

TH-2011_11610225

molecular regime, it is suggested by researchers not to use the continuum models [51]. The regime of gas damping is defined by Knudsen number(K_n). The ratio of molecular mean free path (λ) to the thickness of the gap (h) defines the Knudsen number. The Knudsen number is defined as

$$K_n = 1.016\lambda/h \tag{4.12}$$

A value of Knudsen number greater than 10 indicates the free molecular regime. Under continuum based models, the Blechs model [47]and [51], Andrews et al's model [51] and Veijola model [49] are used for predicting the squeeze film damping coefficient of MEMS structures. A brief description of the above models is brought out here. All the symbols used in these models are brought out in Table 4.1. **Blech's model** [47]:

Table 4.1: meaning of different symbols

Symbol Name	**Meaning**
a	Plate width
b	Plate length
h	Height of the gap (Squeeze film)
P	Ambient pressure
μ	Viscosity
ρ	Gas density
j	$\sqrt{-1}$
λ	Mean free path
σ	Squeeze number
ω	Angular frequency of operation

This model assumes the following:

(i) Rigid plate

(ii) Small gap

(iii) Small displacement

(iv) Small pressure variation

(v) Isothermal process

(vi) Pressure at outside plate edge equals ambient pressure

TH-2011_11610225

(vii) Small molecular mean free path

(viii) No inertial effects of gas moving in and out of the gap.

The damping coefficient given by this model depends on the Squeeze number, σ [51]. The damping coefficient is given by:

$$C^{Blech}(\omega) = \frac{768a^3b}{\pi^6h^3}\mu\Sigma_{(m,nodd)}\frac{m^2+n^2(\frac{a}{b})^2}{m^2n^2[m^2+n^2(\frac{a}{b})^2]^2+\frac{\sigma^2}{\pi^4}} \tag{4.13}$$

The summation for odd values of m and n shall be done for sufficient number of terms to have reasonable precision. The squeeze number is given as

$$\sigma = 12\mu\left(\frac{a}{h}\right)^2\left(\frac{\omega}{P}\right) \tag{4.14}$$

Andrews et al's Model:

This model is proposed for low squeeze numbers [51]. The damping coefficient is given by:

$$C^{Andrews} = \beta(b/a)\frac{a^2b^2\mu}{h^3} \tag{4.15}$$

where $\beta(b/a)$ is a correction factor which depends on the aspect ratio of the structure. For square proof-mass the value is 0.42.

Veijola's model:

In this model [49] and [52], the trivial boundary condition was replaced with a boundary condition that gives a much more accurate transition from the pressure in the gas film into the ambient pressure away from the plate. This is the major improvement over Blech's and other models. The damping coefficient is given by:

$$C^{Veijola}(\omega) = \mathrm{Re}\left[\Sigma_{m=1,3,..}\Sigma_{n=1,3,...}\frac{1}{Q_{pr}G_{mn}+j\omega C_{mn}}\right] \tag{4.16}$$

where

$$C_{mn} = \frac{\pi^4h(mn)^2}{64abP}$$

$$G_{mn} = \frac{\pi^6h^3(mn)^2}{768\mu ab}\left(\frac{m^2}{a^2}+\frac{n^2}{b^2}\right)$$

TH-2011_11610225

$$Q_{pr} = \frac{1 + 6K_n}{1 + j\omega \frac{\rho h^2 (1+10K_n+30{K_n}^2)}{10\eta(1+6K_n)}}$$

Re[.] indicates real part.

4.3 Analysis of damping for the proposed structure

The damping ratio is mainly determined by the dimensions of the accelerometer structure, mass of the proof-mass, pressure, density, and viscosity of the gas in the enclosed volume of the accelerometer module. Thus, the gas in the gap between the mass and the encapsulation provides the necessary damping through the squeeze film damping mechanism. For the proposed design, the gap between the proof-mass and the encapsulation is designed to achieve a damping ratio of 0.7. Damping is provided by the thin air film (h) on both sides of the proof-mass, which is achieved by top and bottom capping layer to encapsulate the whole mechanical structure. The squeeze film damping effect is the interaction of the silicon proof-mass and the air film, trapped in the gap between mass and the encapsulation.

It is reported in literature [51], the accuracy of prediction of damping ratio varies from one model to the other. Hence to obtain a damping ratio of the proposed structure, we need to first calculate the height of the gap of thin film to obtain at an approximate value of the gap and carry out the simulation to obtain at the value of damping ratio. The parameters are chosen as per Table.4.2. From Andrews et al's model, for the proposed structure, the gap of the thin film is worked out to be 18.6 μm. With this gap value, the damping coefficient is calculated using other models and also evaluated from simulation. When the proposed structure with this height was simulated, it produced a damping higher than it. As the damping decreases with increase in height, the simulation was repeated with higher height to achieve a damping ratio of around 0.7. The damping ratio obtained for different heights from model and simulation are tabulated in Table 4.3.

The damping coefficients from simulation is calculated by observing the step response of the system. From the step response the peak time is ascertained, from the peak time the damping ratio is obtained using the relation given in Eq. 4.7. The gap of 23.5 μm produced damping ratio of nearly 0.7 from simulation and is used for final design.

The displacements of the proof-mass as obtained from the simulation for thin film height of 18.6 μm, 23.5 μm and 30 μm are shown in Figure. 4.3, Figure. 4.4 and Figure. 4.5, respectively. The forces

TH-2011_11610225

Table 4.2: Design parameters chosen for damping control

Design Parameters chosen	values
Dynamic Viscosity of air (N/m^2s)	1.85×10^{-5}
Atmospheric Pressure (Pa)	1.013×10^5
Height of the proof-mass (μm)	250
Natural Frequency (rad/sec)	15061
(Design 1) Proof-mass area (μm^2)	3200×3200

Table 4.3: Comparison of damping ratios from different models and simulation.

Height of the air gap (μm)	Blech's model	Andrews et al's model	Veijola's model	From simulation
18.6	1.34	0.7088	0.7112	≥ 1
23.5	0.6686	0.3515	0.3527	0.69
30	0.3214	0.1689	0.1695	0.31

on the plate for the same heights are shown in Figure. 4.6, Figure. 4.7 and Figure. 4.8 respectively. It can be seen that the damping ratio obtained through simulation is closer to the one predicted by Blech Model. The theories and the numerical procedure applied in COMSOL for modeling damping are given in appendix A.1.

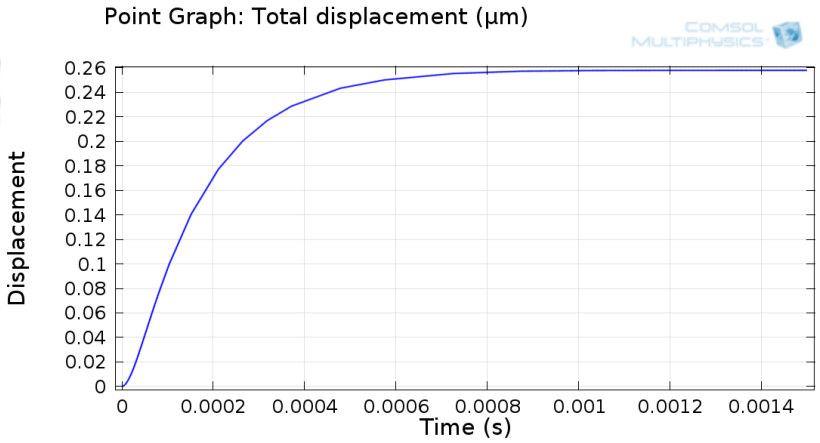

Figure 4.3: Displacement obtained with air gap height of 18.6 μm

TH-2011_11610225

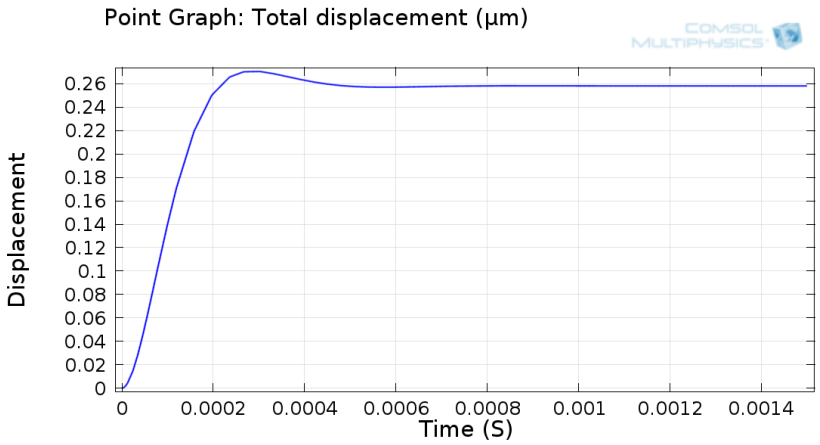

Figure 4.4: Displacement obtained with air gap height of 23.5 μm

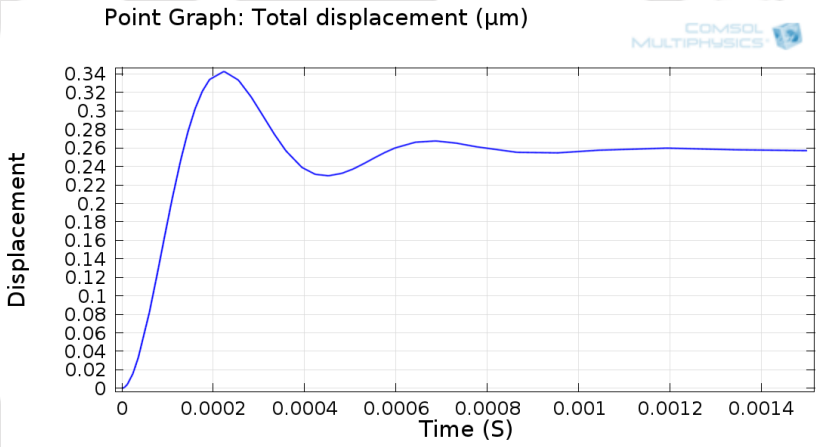

Figure 4.5: Displacement obtained with air gap height of 30 μm

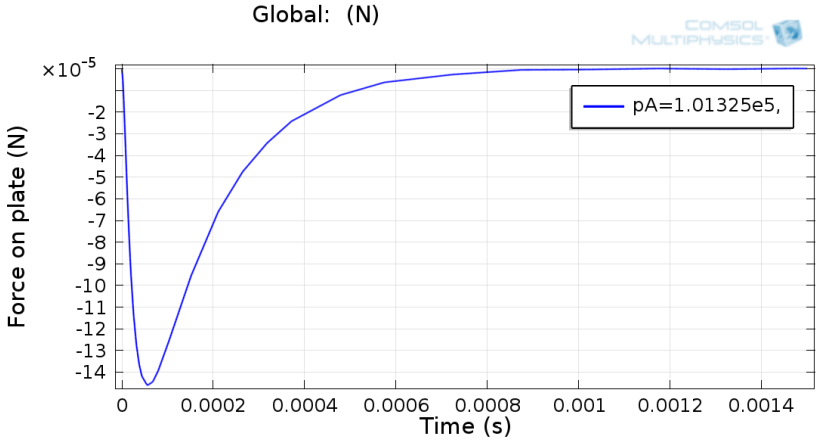

Figure 4.6: Force obtained on the plate with air gap height of 18.6 μm

TH-2011_11610225

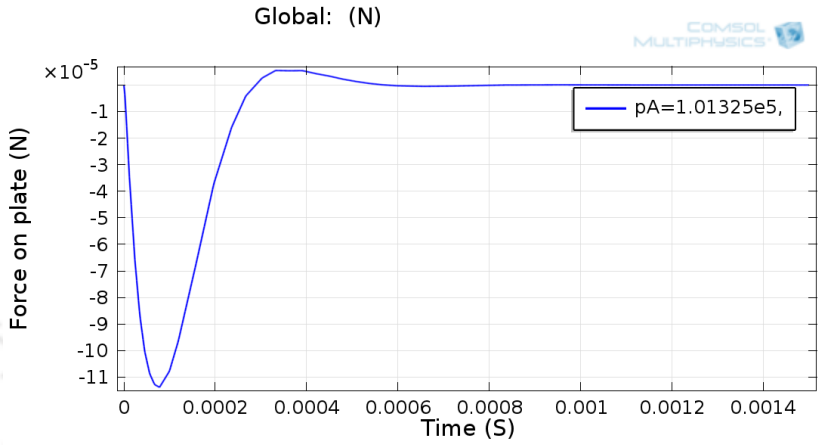

Figure 4.7: Force obtained on the plate with air gap height of 23.5 μm

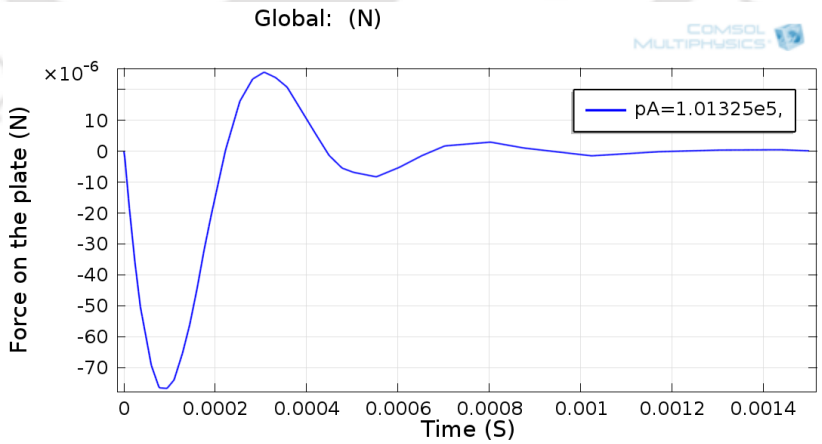

Figure 4.8: Force obtained on the plate with air gap height of 30 μm

TH-2011_11610225

4.4 Time domain Analysis

In addition to the analysis of free vibration and response to step input, it is also important to evaluate the performance of the accelerometer to sinusoidal input. An external force is explicitly dependent upon time, hence time dependent analysis is very important for understanding the performance of the device. It is known that the steady state response of a linear system is sinusoidal with a phase shift when the external excitation is sinusoidal. However, before reaching the steady state there will be a transient in the response. The transient response depends on the initial conditions of the system. The transient and the steady state response together describes the total response of the system. In order to estimate the device sensitivity and response time to the applied acceleration, the transient analysis is done. For a second order system (spring-mass damper) the total response is given by

$$z = Ce^{-\zeta\omega_n t}\sin(\omega_d t + \alpha) + A\sin(\omega t + \phi) \tag{4.17}$$

where z is displacement, ω_d is the frequency of damped oscillation, ζ is the damping ratio, ω_n is the natural frequency, ω is the frequency of external excitation, C is the amplitude of transient part of the response, A is the amplitude of steady state part of the response, α is the phase lag for transient response and ϕ is the phase difference between external excitation and the steady state response. The value of C and α depends upon the initial conditions. The first term on the right hand side of the above equation is the transient response of the system whereas the second term is the steady state response. It can be seen that the transient response dies exponentially with time and at a reasonable large time the steady state response dominates and the transient response becomes negligible. For a system with a large natural frequency compared to the frequency of forced excitation (which is generally the typical frequency of application of accelerometers), the transient response dies even before a fraction of the excitation signals time period. It may also be noted that a system with very low damping will have a transient of longer duration. Thus, it is important to have adequate damping. The time domain response (total response including both transient and steady state) for the proposed structure with very low damping (thin film gap height of 40μm) is simulated and shown in Figure. 4.9 for time duration of 0.025 sec for signal of frequency of 40 Hz. The time domain response with the designed damping (thin film gap height of 23.5 μm) is simulated for the proposed structure for a duration of 0.025 sec and is depicted in Figure. 4.10. It can be seen from Figure. 4.9 that there are very small

TH-2011_11610225

overriding oscillations on top of the sinusoidal response whereas the response of the proposed structure with adequate damping is free from such overriding oscillations.

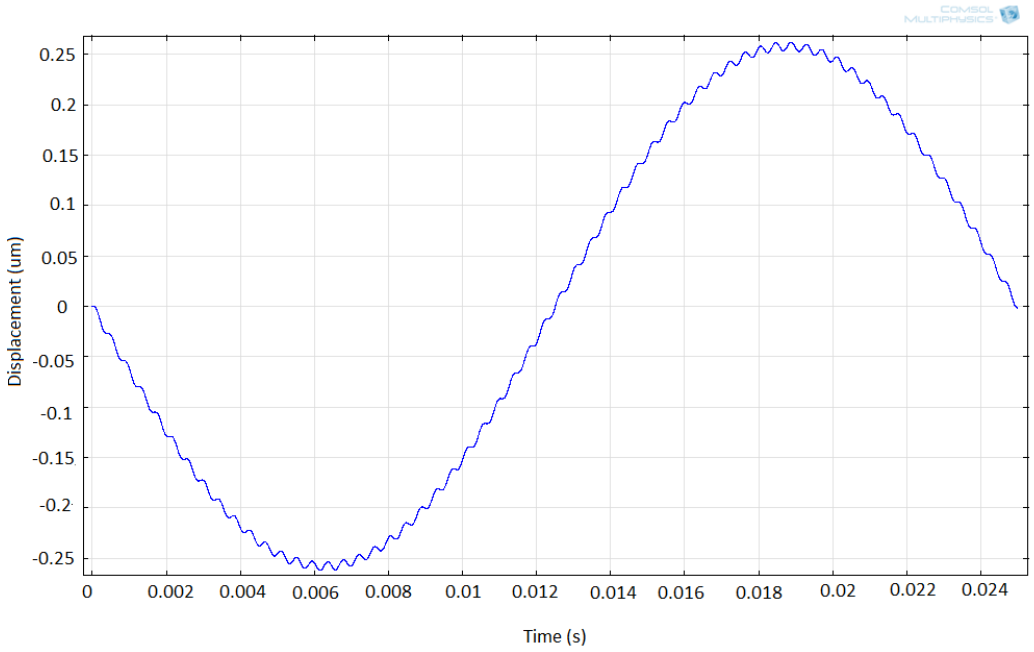

Figure 4.9: Time domain response to sinusoidal input for very low damping

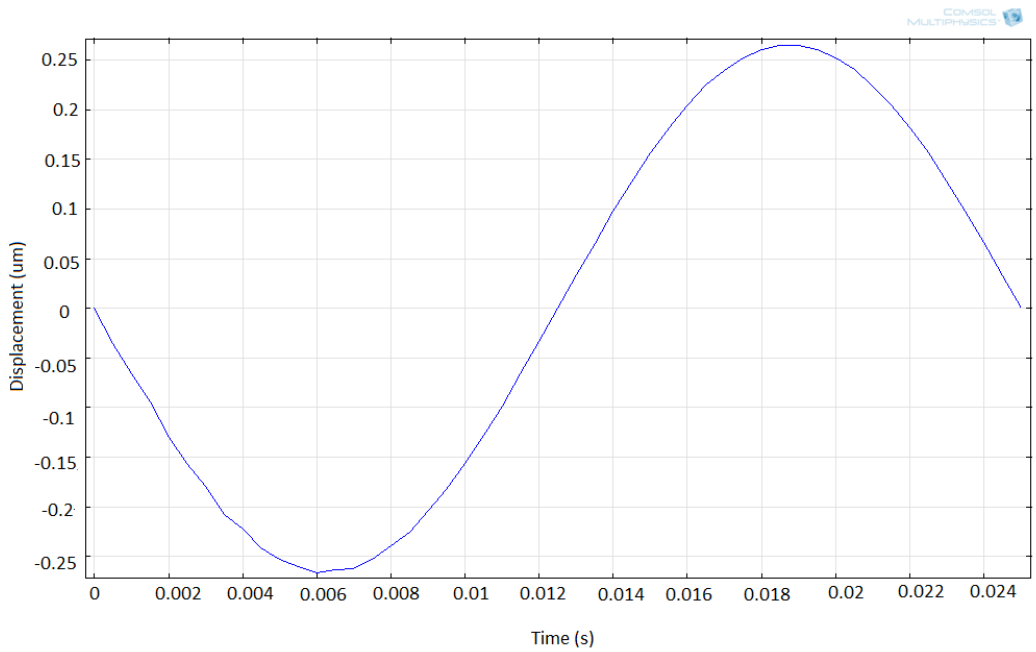

Figure 4.10: Time domain response of the proposed structure to sinusoidal input

TH-2011_11610225

4.5 Conclusion

In this chapter, a detailed investigation on the damping aspect for the proposed micro accelerometer is carried out. It is shown that for a height of thin film 23.5 μm, approximately the desired damping ratio of 0.7 is achieved. The exact value from simulation is 0.6947. The damping ratio achievable for different height of the gap of thin film is also investigated and tabulated. The time dependent analysis is also carried out for the proposed structure with intended damping and very low damping. The time domain analysis include the transient and steady state response both.

TH-2011_11610225

5

Proposed Scheme for Cross-axis Sensitivity Reduction

Contents

TH-2011_11610225

TH-2011_11610225

5.1 Introduction

Cross-axis sensitivity is one of the most critical issues in microaccelerometers, which require higher precision for medical diagnostics. Cross-axis sensitivity means how much perpendicular acceleration is coupled and it mainly depends upon the sensor geometry. It is important that a single axis MEMS accelerometer must be designed such that it senses and measures acceleration in a particular axis and does not respond to acceleration in the other two off-axes. However, the geometry of the structure may be responsible for slight rotation or tilt in the device. This gives rise to off axis acceleration being picked up by the accelerometer, which is responsible for cross-axis sensitivity [12]. The diagnosis of neurological disorders requires very low acceleration signals to be measured, hence sensing should be maximum in the prime axis and minimum possible in the off axes. Accelerometers are transducers used to measure the vibration responses of structures. The accelerometer designed here to be used in strapdown medical diagnostic purpose for capturing feeble tremor having intensity which may be as low almost as 0 g signifying fall to maximum ±6 g signifying jerks. The frequency range for such tremor and seizures which occur in patients suffering from different types of neurological disorders have frequency range from 0.5 Hz to 29 Hz [1]and [3],. In order to capture such signals there should be minimum cross-axis sensitivity as possible. This can be possible only by proper design consideration of the sensor structure where there is alignment of the structural motion with the prime axis sensing. Though the structural motion must be parallel to the prime axis sensing but sometimes it is seen that there is a coupled mode with other direction occuring due to translational or rotational effects or a combination of both where we get maximum errors. The actual response when decomposed into translational motion and rotational motion, the normal component of the rotational motion gets merged with the primary sensing axis while the tangential component represents the accelerometers cross-axis sensitivity.

Different design modifications and schemes for reducing cross-axis sensitivity have been proposed since the initial realization. Cross-axis sensitivity is caused by the three dimensional effect of sensor geometry. The reduction in cross-axis sensitivity is possible by increasing the lateral torsional stiffness. There may be several changes in geometries of the sensor structure for increasing the stiffness. When lateral acceleration is applied in a quad beam structure, we get a larger rotational displacement. This is caused by their low torsional stiffness. This can be improved by enlarging the distance between the central lines of beam and the proof-mass. Also reducing the height difference between the beams

TH-2011_11610225

and the proof-mass, is another way of reducing the cross-axis sensitivity. The lateral stability of a quad beam structure can also be improved by aligning the proof-mass edge with the beams. The MEMS structure having beams aligned with proof-mass edge had better lateral stiffness compared to the mass with non aligned beams. This similar arrangement has been found in many other quad beam structure [14] and [21].

Apart from geometric modification another approach of increasing the stiffness was by depositing heavy metal on top of the proof-mass. Higher stiffness ensures that the rotation of mass is reduced when lateral acceleration is applied which causes reduction of cross-axis sensitivity. In [13] and [16], the top of proof-mass was electroplated with 20μm thick gold which reduced the cross-axis sensitivities in the lateral axes. The primary sensitivity was improved and the resonant frequency was also affected as the equivalent mass was increased due to the gold deposition. In order to maintain the equivalent mass, the thickness of the proof-mass was reduced and then the metal gold was deposited [17]. This improved the symmetry of the structure and gave a sufficient reduction in the cross-axis sensitivity. Cross-axis sensitivity can be reduced and we can have better sensing in a particular axis.

Increasing the stiffness without electroplating with any costly metal requires a new design approach. In the present work an attempt has been made to reduce the cross-axis sensitivity without the use of any costly metal. The stiffness of the silicon accelerometer has been increased by geometric optimization of the aspect ratio of the proof-mass and having the proof-mass edge aligned with the beams. Also, further reduction of cross-axis sensitivity is done by adopting Wheatstone bridge circuit as signal pick-up by the piezoresistive elements. The proof-mass aspect ratio chosen gives equal and reduced cross-axis sensitivity on both x and y-axis simultaneously.

5.2 Theoretical Background

Cross-axis sensitivity is a critical issue and it mainly depends upon the design geometry of the sensor. Investigations based on aspect ratio optimization is done. Aspect ratio of the proof-mass plays an important role in deciding the cross-axis sensitivity.

Different types of geometric configurations have been given by different researchers out of which quad beam type is the most popular in terms of performance as reported [12], [13]and [54]. However, the cross-axis sensitivity reduction is considered as a serious issue and still a challenge. The proposed design is a quad beam type having a proof-mass with four beams as shown in the Fig. 5.1.

TH-2011_11610225

The cross-axis sensitivity of the proposed accelerometer has been evaluated based on the theory given

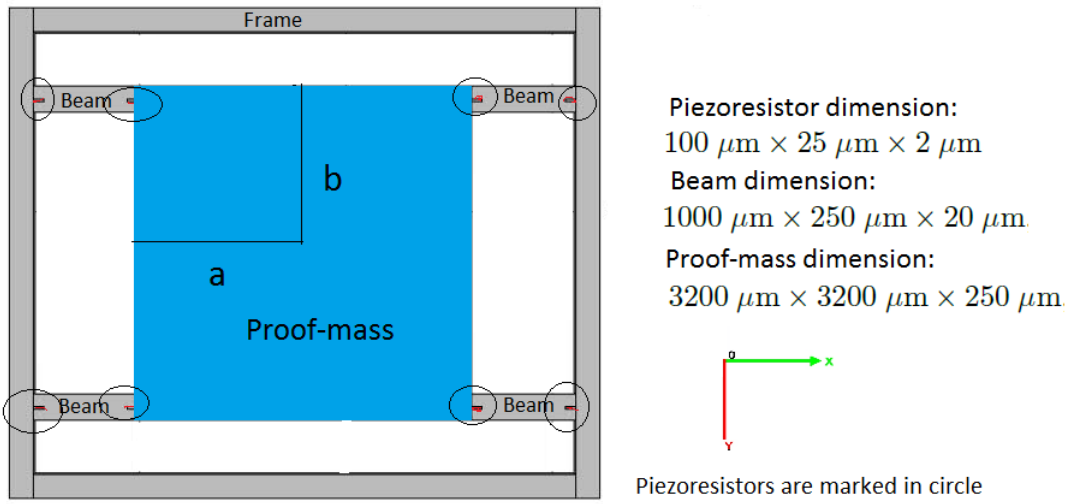

Figure 5.1: Proposed Design structure of the microaccelerometer structure

in [12]. Displacement of the proof-mass Δz is given by:

$$\Delta z = \frac{ma_z}{k_z} \tag{5.1}$$

Here Δz denotes the vertical displacement of the mass m, when normal acceleration a_z is applied and k_z is the stiffness in Z direction. The lateral acceleration causes rotation moment, and this causes the mass to tilt or rotate until the sum of all reaction forces and moments are zero. Rotation of the mass around x-axis is given by

$$\theta_x = \frac{ma_y z_c}{k_{\theta_x}} \tag{5.2}$$

where z_c is the distance of the centre of mass from the surface, a_y is the acceleration applied in Y direction and k_x is the stiffness of beam in X direction. Similarly rotation of the mass around y-axis,

$$\theta_y = \frac{ma_x z_c}{k_{\theta_y}} \tag{5.3}$$

Stiffness(N/m) [12] is

$$k_z = 4 \times \frac{Ebh^3}{l^3} \tag{5.4}$$

where E is the Youngs modulus, width, height and length of the beam are given by b, h and l respectively. Stiffness of beam in Y direction normalised with respect to stiffness in prime-axis is

TH-2011_11610225

given by (m^2/rad)

$$\frac{k_{\theta y}}{k_z} = \frac{l^2 + 3al + 3a^2}{3} \tag{5.5}$$

Stiffness of beam in X direction normalised with respect to stiffness in prime-axis is given by (m^2/rad)

$$\frac{k_{\theta x}}{k_z} = b^2 \tag{5.6}$$

Here, a and b are the distances shown in Fig. 5.1. To increase the sensitivity in prime-axis, the stiffness in the axis needs to be reduced and to reduce the cross-axis sensitivity, the stiffness of beams in those direction needs to be increased. Thus to ascertain the figure of merit of the device in terms of higher prime axis sensitivity and lower cross-axis sensitivity, the normalised parameters $\frac{k_{\theta x}}{k_z}$ and $\frac{k_{\theta y}}{k_z}$ are used. The higher the value of these parameters, the better is the device in terms of cross-axis sensitivity normalised with respect to prime-axis sensitivity. Thus, maximizing the distances from the centre of the proof-mass to the edges as given by a and b, there is a possibility of reducing cross-axis sensitivity.

Also, cross-axis sensitivity can be reduced by arranging the piezoresistors in the form of a Wheatstone bridge where self cancelation of the resistance change occurs, when lateral accelerations are applied. As the piezoresistors are highly temperature sensitive the Wheatstone bridge configuration also helps in reducing and nullifying the temperature effect.

5.3 Proposed aspect ratio for simultaneous reduction in cross-axis sensitivity

The proposed design configuration has proof-mass dimension of 3200 × 3200 × 250 μm^3, beam dimension 1000 × 250 × 20 μm^3 and piezoresistors of 100 × 25 × 2 μm^3 as shown in Figure. 5.1. The stiffness of the beam in z direction is 1352 N/m. The cross-axis sensitivity obtained in this case with aspect ratio 1:1 is not equal for both x and y-axis. The normalised stiffness (m^2/rad), from (5.5) and (5.6) for x-axis and y-axis are obtained as $Cx = 2.5 \times 10^{-6}$ and $Cy = 4.49 \times 10^{-6}$ respectively.

As the cross-axis sensitivity is a serious issue specially where precise sensing is required in medical diagnostics, we need to propose a design such that the cross-axis sensitivity for both x and y-axis are equal. Several investigations on cross-axis effect are done by altering the dimension of the proof-mass

TH-2011_11610225

in x, y and both x and y direction, keeping mass constant. The aspect ratio is altered keeping the mass i.e. 5.96×10^{-6}kg, constant and same beam length 1000 μm. This maintains the natural frequency and sensitivity same as the initial design with 1:1 aspect ratio. The design proposed has a dimension similar to the one shown in figure.5.1 only with the proofmass dimension being different, which is $3800 \times 2700 \times 250$ μm^3.

Figure. 5.2 shows the cross-axis sensitivity obtained. The design with aspect ratio 1.4:1 is the proposed

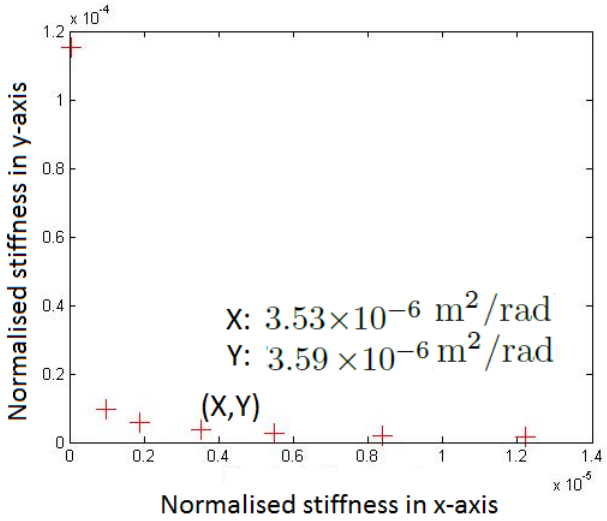

Figure 5.2: Cross-axis sensitivity in both axis for constant beam length

proof-mass design having equal cross-axis sensitivity on both x and y-axis. The normalised stiffness in (m^2/rad) on x and y-axis are 3.53×10^{-6} and 3.59×10^{-6} respectively. It is clear that they are almost equal.

5.4 Proposed Scheme for further reducing Cross-axis Sensitivity by Wheatstone bridge

The cross-axis sensitivity shows how much perpendicular acceleration is coupled. This value should be minimum and for this the beam are edge-aligned with the proof-mass and the dimensions are chosen such that it gives high stiffness. As piezoresistances are temperature sensitive, Wheatstone bridge helps in eliminating the temperature effect on the output. Thus cross-axis sensitivity can be reduced and we can have better sensing in a particular axis. Thus Wheatstone bridge helps us serve both the purpose of enhancement of desired axis signals and auto-cancelation of the off-axis perturbations and

TH-2011_11610225

auto compensation of the temperature variations. The eight piezoresistors connected in the form of the Wheatstone bridge are as shown in Figure. 5.3.

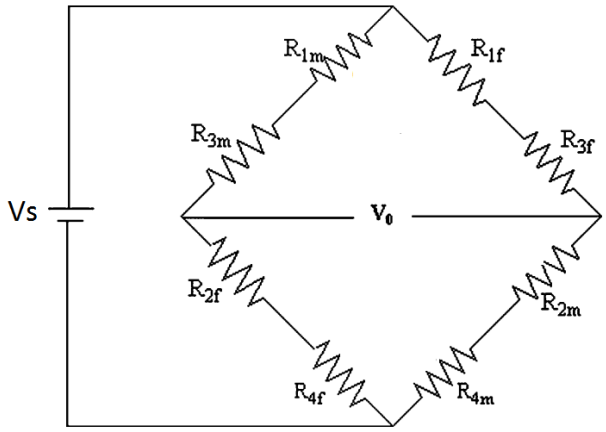

Figure 5.3: Wheatstone bridge structure with stress free resistance

It has been observed from simulation that for a particular doping concentration, the ratio of change in resistance to resistance value ($\frac{\Delta R}{R}$) decreases with increasing beam thickness. For the same beam thickness it has been observed that the value of ($\frac{\Delta R}{R}$) is maximum for a doping of the order of 10^{17} atoms/cm^3 and reduces gradually with the increase in the doping concentration [55]. Considering the p type single crystal silicon as the piezoresistive sensing element with orientation $< 110 >$ we choose the piezoresistive coefficient namely Π_{11}, Π_{12} and Π_{44} and obtain the longitudinal coefficient. Based on the simulation results the geometric dimensions are fixed for achieving desired performance. Here the resistors R_{im} and R_{if} denote the sensing element near to the mass and near to the frame respectively. The piezoresistors have been labeled in the proposed structure as shown in the Figure. 5.1.

When acceleration is applied in z direction, there is proof-mass deflection and stress is induced. For downward deflection of the proof-mass, compressive stress is induced near the proof-mass end and resistance values $R_{1m}, R_{2m}, R_{3m}, R_{4m}$ decrease, whereas tensile stress induced near the frame end and resistance values $R_{1f}, R_{2f}, R_{3f}, R_{4f}$ increase. Thus four resistors are in tension and four in compression. Because of this opposite nature we can connect these piezoresistors in the form of a Wheatstone bridge as shown in Fig. 5.3. The nature of stress developed on the piezoresistors for application of stress in z, x, y-axis may be compressive or tensile as shown in Table 5.1 and in Fig.

TH-2011_11610225

5.4–5.11.

The voltage output V_0 for the Wheatstone bridge is given by

$$V_0 = \left(\frac{R_{2f} + R_{4f}}{R_{2f} + R_{4f} + R_{1m} + R_{3m}} - \frac{R_{4m} + R_{2m}}{R_{4m} + R_{2m} + R_{3f} + R_{1f}} \right) V_s \tag{5.7}$$

For acceleration applied in z direction, piezoresistors R_{1m}, R_{2m}, R_{3m} and R_{4m} undergoes compressive stress and R_{1f}, R_{2f}, R_{3f} and R_{4f} undergoes tensile stress as shown in Fig. 5.4.

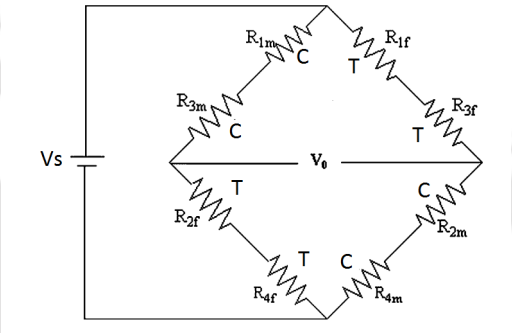

Figure 5.4: Wheatstone bridge structure with acceleration on z-axis

The resistance of piezoresistors increase when they undergo tensile stress and the resistance decrease when they undergo compressive stress. Let ΔR_{im} and ΔR_{if} denote the magnitude of change of resistance of R_{im} and R_{if} respectively. With these we get Eq. 5.8.

$$V_0 = \left(\frac{R_{2f} + \Delta R_{2f} + R_{4f} + \Delta R_{4f}}{R_{2f} + \Delta R_{2f} + R_{4f} + \Delta R_{4f} + R_{1m} - \Delta R_{1m} + R_{3m} - \Delta R_{3m}} - \frac{R_{4m} - \Delta R_{4m} + R_{2m} - \Delta R_{2m}}{R_{4m} - \Delta R_{4m} + R_{2m} - \Delta R_{2m} + R_{3f} + \Delta R_{3f} + R_{1f} + \Delta R_{1f}} \right) V_s \tag{5.8}$$

Let us assume that magnitude of the stresses are same for all the resistors and let the magnitude of change of resistance be denoted by ΔR. And let us also assume that the stress free resistance of all the piezoresistors are the same and is denoted by R. In that case the above equation reduces to

$$V_0 = \frac{\Delta R}{R} V_s \tag{5.9}$$

When the acceleration is applied in x direction R_{1f}, R_{2m}, R_{3m} and R_{4f} undergoes tension and R_{1m}, R_{2f}, R_{3f} and R_{4m} undergoes compression as shown Fig. 5.5. Then the Eq. 5.8 becomes

TH-2011_11610225

Table 5.1: Piezoresistor under compression and tension as an effect of acceleration along different axes

Piezoresistors	Δ R for X axis	Δ R for Y axis	Δ R for Z axis
R_{1f}	+ve	+ve	+ve
R_{1m}	−ve	−ve	−ve
R_{2f}	−ve	+ve	+ve
R_{2m}	+ve	−ve	−ve
R_{3f}	−ve	−ve	+ve
R_{3m}	+ve	+ve	−ve
R_{4f}	+ve	−ve	+ve
R_{4m}	−ve	+ve	−ve

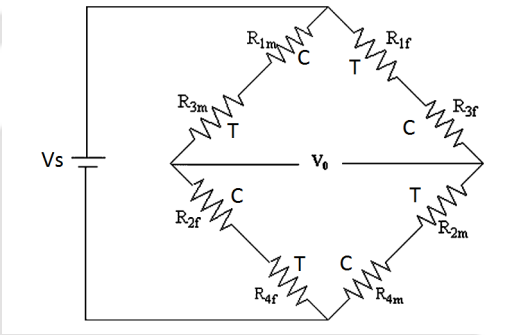

Figure 5.5: Wheatstone bridge structure with acceleration on x-axis

$$V_0 = \left(\frac{R_{2f} - \Delta R_{2f} + R_{4f} + \Delta R_{4f}}{R_{2f} - \Delta R_{2f} + R_{4f} + \Delta R_{4f} + R_{1m} - \Delta R_{1m} + R_{3m} + \Delta R_{3m}} - \frac{R_{4m} - \Delta R_{4m} + R_{2m} + \Delta R_{2m}}{R_{4m} - \Delta R_{4m} + R_{2m} + \Delta R_{2m} + R_{3f} - \Delta R_{3f} + R_{1f} + \Delta R_{1f}} \right) V_s \tag{5.10}$$

It can be seen that if the magnitude of resistance changes for all piezoresistors are equal than V_0 will be equal to 0.

When the acceleration is applied in y direction R_{1f}, R_{2f}, R_{3m} and R_{4m} undergoes tension and R_{1m}, R_{2m}, R_{3f} and R_{4f} undergoes compression as shown in Fig. 5.6. Then the Eq. 5.8 becomes

$$V_0 = \left(\frac{R_{2f} + \Delta R_{2f} + R_{4f} - \Delta R_{4f}}{R_{2f} + \Delta R_{2f} + R_{4f} - \Delta R_{4f} + R_{1m} - \Delta R_{1m} + R_{3m} + \Delta R_{3m}} - \frac{R_{4m} + \Delta R_{4m} + R_{2m} - \Delta R_{2m}}{R_{4m} + \Delta R_{4m} + R_{2m} - \Delta R_{2m} + R_{3f} - \Delta R_{3f} + R_{1f} + \Delta R_{1f}} \right) V_s \tag{5.11}$$

It can be seen that if the magnitude of resistance changes for all piezoresistors are equal than V_0 will be equal to 0. Thus it can be seen that, even if stress is induced in microaccelerometer when there is

TH-2011_11610225

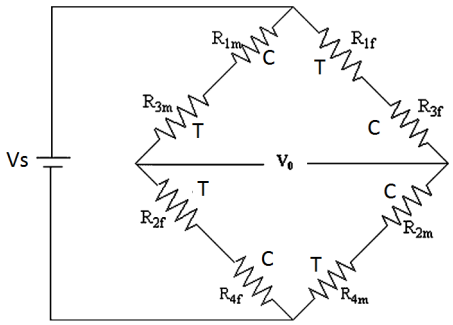

Figure 5.6: Wheatstone bridge structure with acceleration on y axis

acceleration applied in lateral axis, if the magnitude of the stresses induced are equal the Wheatstone bridge will remain balanced and the output will be zero. In practical cases, the stress induced will not be exactly equal in magnitude, thus there will be very small output. This helps in reducing cross-axis sensitivity even when there is stress induced in the structure with application of acceleration in off axis.

For the proposed structure, in order to obtain the sensitivity, stress was observed on application of ± 6 g acceleration in all three axes. From this, the change in resistance was calculated which in turn using Eq. 5.8 we obtain the V_0 as 10mV. Thus prime axis sensitivity is 0.33 mV/V/g. For x-axis putting the value of change in resistances in Eq. 5.10, V_0 is found to be 0.0125 mV, thus cross- axis sensitivity is 0.0004 mV/V/g. Now putting change in resistances for y-axis in Eq. 5.11, V_0 is found to be 0.049 mV, thus cross-axis sensitivity is 0.0016 mV/V/g

5.5 Conclusion

The wearable piezoresistive microaccelerometer designed has small size and high sensitivity performance when compared to the reported ones as shown in Table 5.2. The frequency ratio is small and the natural frequency obtained is 2397 Hz, thus the fundamental criteria of the microaccelerometer has been achieved. It may be mentioned that the sensors designed which are reported in [17] and [21] have smaller dimensions and low cross axis sensitivity, but performance in terms of prime axis sensitivity is too low to be used for tremor detection. The cross-axis sensitivity has been reduced by wheatstone bridge arrangement and is the lowest as compared to other reported ones [56] [20] [54] [17] [21] [22]as shown in Table 5.2. Thus, the proposed miniaturized design has a low mass of around 6 mg, small

TH-2011_11610225

Table 5.2: Comparison with a few low g piezoresistive microaccelerometers

Ref	(±g) value	Size in ($mm \times mm$)	Fundamental natural freq(kHz)	Prime axis Sensitivity (mV/V/g)	Cross-axis sensitivity %	Approx. proof-mass weight (mg)
[20]	±1.5	5.5x5.5	0.53	0.56	9.3	≃ 88
[20]	±2.5	5.5x5.5	0.72	0.43	10.2	≃88
[20]	±10	5.5x5.5	0.32	1.03	8.1	≃ 88
[54]	±13	8x8	1.65	0.106	<8	7.25
[17]	±13	≃5x5	3.3	0.085	0.316	≃7
[21]	±13	≃5x5	2.94	0.12	0.62	≃7.25
[22]	±10	3x3	0.300	1.77	<4	-
Present work	±6	5X5	2.39	0.33	0.48	≃6.0

size of 5×5 mm^2, has dynamic range of ±6 g, sensitivity of 0.33 mV/V/g and cross-axis sensitivity of 0.0016 mV/V/g. The mini size further helps the sensors combine with low power CMOS circuits, making smart modules having multiple functionality possible. The size, mass and performance level makes it suitable as a wearable sensor for neurological disorder diagnostic purposes.

TH-2011_11610225

6

Noise Performance and Proposed Noise Reduction Scheme

Contents

TH-2011_11610225

TH-2011_11610225

6.1 Introduction

Microaccelerometers and other microsensors have been a boon in various fields and the cost has been reduced because of batch fabrication. However the smaller the device the lower is the signal to noise ratio [57]. With the objective of increasing the performance of the system an attempt has been made to study the sources of noise and thereby propose the design parameters considering the challenges. The acceleromometer designed is of the piezoresistive type and the desired properties include high sensitivity and resolution, maximum operating range, wide frequency response, good linearity, low cross-axis sensitivity and high signal to noise ratio. The first accelerometer work [7] was followed by various acceleration sensing by different types of piezoresistive accelerometers by many researchers all having its merits and demerits. There are several reasons for choosing piezoresistive method of transduction, mainly because of simplicity in structure, better sensing, easy fabrication and ruggedness. Throughout the time span various MEMS piezoresistive accelerometers have been developed for several applications in different emerging fields with respect to performance. However miniaturization itself is a challenge which makes signal to noise ratio improvement a must for high performance activities. This chapter concentrates on the analysis of the different sources of noise and the mechanical-thermal noise has been evaluated for the designed piezoresistive MEMS accelerometer used in a strapdown physiological tremor diagnostic system. The noise analysis gives an idea of several design constraints that has to be considered for improving the signal to noise ratio (SNR). In order to enhance the sensor performance a noise reduction model has been proposed using a sigma delta modulator.

6.1.1 Noise sources

Noise is an unwanted signal and sometimes high noise floor can make measurement of the signal of interest very difficult. The intrinsic non-deterministic noise which originates from the device itself, can neither be neglected nor avoided by shielding. Noise being a random process, for measurement purpose we take the power spectral density function, which gives the magnitude of the random signal squared over a range of frequencies. The fundamental noise mechanisms that potentially limit the performance of the piezoresistive MEMS sensors are thermo-mechanical noise, Johnson noise, Hooge noise or 1/f noise, and shot noise. Miniaturization is attractive for many applications but the small moving parts are especially susceptible to mechanical noise resulting from molecular agitation. Any

TH-2011_11610225

molecular agitation even through solid structure like springs and support can cause random motion of an object which is called the Brownian motion. The mechanical thermal noise depends on the temperature and the magnitude of mechanical damping. Johnson noise is independent of frequency and it occurs due to thermal energy in a resistor. Johnson noise describes voltage fluctuations at the terminal of a conductor or semiconductor at equilibrium and is caused by the random vibrations of charge carriers in equilibrium with the lattice at a particular temperature. The expression of the thermal noise power spectral density in [V^2/Hz] as units have been reported in [58] [59] and is given by Eq.(6.1)

$$S_J = 4K_B RT \tag{6.1}$$

where K_B is the Boltzmann constant, R is the resistance, and T is the temperature in Kelvin. Electrical thermal noise is caused by the agitation of the charge carriers by thermal lattice vibrations and is present regardless of bias voltage. However, higher temperature induces more agitation of the carriers, hence the Johnson noise is temperature dependent. Moreover as the lattice vibrations are random and not related to any single time constant therefore Johnson noise is frequency independent. The mechanical thermal noise depends on the temperature and the magnitude of mechanical damping. Mechanical thermal noise is analogous to electrical thermal noise. The fluctuation-dissipation theorem says that there must be a fluctuation force to maintain the energy balance and the thermal equilibrium, if there exists mechanical damping in any dissipative mechanism [59]. The mechanical thermal noise equation analogous to the above equation is given by Eq.(6.2) and its units is in [N^2/Hz].

$$S_m = 4K_B R_m T \tag{6.2}$$

Here R_m is the equivalent mechanical resistance of the sensor. Low Frequency noise also known as $1/f$ noise or Hooge is a frequency dependent non-equilibrium noise. Though the main reasons are the fluctuation in mobility and carriers [28], still it is an active research area. In a semiconductor, when charge carriers cross a potential barrier independently and randomly, fluctuations which occur in the average current give rise to shot noise which is a non-equilibrium noise. The shot noise power spectral density in [A^2/Hz] as units is given by Eq.(6.3)

TH-2011_11610225

$$S_I = 2qI \tag{6.3}$$

where q is the electron charge and I is the current. The shot noise is frequency independent. In this chapter the mechanical thermal noise for the designed piezoresistive accelerometer has been derived under thermal equilibrium and by adding a force generator alongside the damper. Solving the accelerometer for noise response we get an idea of the various dependent design parameters we need to consider to increase the signal to noise ratio. The dissipation mechanism has been studied which gives an idea to choose appropriate damping mechanism and the damping ratio. The low frequency dominant noise has been reduced by suitable doping concentration thus enhancing the resolution and sensitivity. Thus taking into consideration the various design and process parameters and the necessary tradeoffs, a sigma delta noise reduction model has been proposed for the high performance.

6.1.2 Tremor Diagnostic System Architecture and the Device configuration

A modern strap down pathological tremor diagnostic system can be described in the form of a block diagram as shown in the Fig. 6.1. The system consist of mobile unit and Hospital unit

1) The mobile unit is set up around the patient to acquire the patient's tremor data and to receive medical recommendations and

2) The hospital unit, which enables the medical staff to telemonitor the patient's condition in order to send medical recommendations.

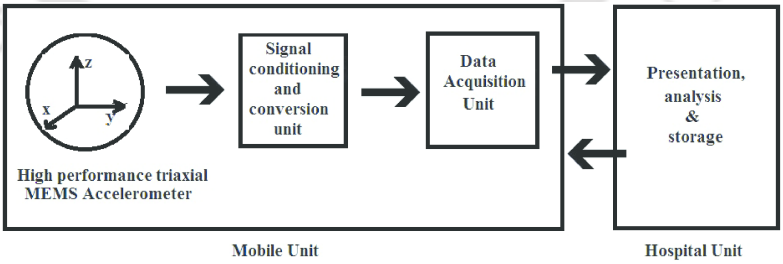

Figure 6.1: Block diagram of modern Strapdown Pathological Tremor diagnostic system

The microaccelerometer designed has a silicon square proof-mass with four beams, two on either side of the proof-mass.The entire structure is surrounded by a fixed frame. Eight p doped single crystal silicon piezoresistors are implanted, four on the junction of the beam and proof-mass and the other four on the junction of the beam and fixed frame. The chosen geometric dimensions: proof-mass

TH-2011_11610225

$3200\mu m \times 3200\mu m \times 250\mu m$, beams-1000 μm $\times$ 250 μm $\times$ 20 μm, Frame-5200 mum $\times$ 230 μm $\times$ 250 μm, piezoresistors 100 μm $\times$ 25 μm $\times$ 2 μm. The structure has been simulated using finite element tool COMSOL 4.3. Here the effective spring constant is taken for parallel beams which is given by four times the spring constant for each. The design parameters obtained has been shown in Table 6.1. The signal pick up circuit is the Wheatstone bridge where all the eight piezoresistors form the arms of the bridge, this helps in reducing the cross-axis sensitivity. The voltage output is directly proportional to the applied acceleration.

Table 6.1: The device design parameters

Design parameter	units	symbol	value
Proof-mass weight	Kg	m	5.96×10^{-6}
Effective spring constant	N/m	k_{eff}	1352
Undamped natural frequency	rad/s	ω_0	15061

6.2 Noise in the accelerometer

The performance and the design of the MEMS accelerometer can be made from the accelerometer noise [57]. Considering thermal equilibrium, the equation of motion is Eq.(6.4). We know from fluctuation-dissipation theorem, the energy lost by the system through damping is statistically balanced by the energy brought into the system by the equivalent noise forces. For the overall noise analysis of the structure we use the equipartition and Nyquist theorems.

$$m\frac{\mathrm{d}^2 z}{\mathrm{dt}^2} + c\frac{\mathrm{d}z}{\mathrm{dt}} + kz = F_n \tag{6.4}$$

The above equation in terms of velocity v taking v=dz/dt, can be written as

$$m\frac{\mathrm{d}v}{\mathrm{dt}} + cv + kz = F_n \tag{6.5}$$

Now using Laplace transform we can write the above equation as

$$msv + cv + kv/s = F_n \tag{6.6}$$

TH-2011_11610225

The mean square velocity due to the noise generator is given by Eq.(6.7)

$$v^2 = \frac{\bar{F}_n^2}{c^2 + (\omega m - k/\omega)^2} \tag{6.7}$$

We know that the natural undamped frequency is given by

$$\omega_n = \sqrt{\frac{k}{m}} \tag{6.8}$$

and the ratio of the peak amplitude to the amplitude at low frequency is referred to as Q, the quality factor.

$$Q = \frac{\omega_n m}{c} \tag{6.9}$$

The Eq. 6.7 can be rewritten in terms of the ω_n and Q as in Eq.(6.10)

$$v^2 = \frac{1}{c^2} \frac{\bar{F}_n^2}{1 + Q^2 \left(\frac{\omega}{\omega_n} - \frac{\omega_n}{\omega}\right)^2} \tag{6.10}$$

The kinetic energy stored therefore is given by Eq.(6.11)

$$E = \frac{1}{2} m \bar{v}_n^2 = \frac{1}{4\pi c} \int_0^\infty \frac{\bar{F}_n^2 Q d\left(\frac{f}{f_n}\right)}{1 + Q^2 \left(\frac{f}{f_n} - \frac{f_n}{f}\right)^2} \tag{6.11}$$

Considering high value of Q, it can be assumed that most of the energy is confined near ω_n and $\bar{F}_n^2 = \bar{F}_n^2(f_n)$. Thus

$$E = \frac{\bar{F}_n^2(f_n)}{4\pi c} \int_0^\infty \frac{Q d\left(\frac{f}{f_n}\right)}{1 + Q^2 \left(\frac{f}{f_n} - \frac{f_n}{f}\right)^2} \tag{6.12}$$

The integration evaluates to $\pi/2$. So

$$E = \frac{\bar{F}_n^2(f_n)}{8c} \tag{6.13}$$

Considering thermal energy as $\frac{1}{2} K_B T$ where K_B and T are Boltzman constant and absolute temperature respectively. The expression for $\bar{F}_n^2(f_n)$ becomes

$$\bar{F}_n^2(f_n) = 4 K_B c T \tag{6.14}$$

TH-2011_11610225

As the result does not depend on frequency, the spectral density of the fluctuating noise force related to damping is given

$$\bar{F_n^2} = 4K_B cT \tag{6.15}$$

In the microaccelerometer, using the Eq. 6.15, the acceleration noise a_n can be written as

$$< a_n >= \frac{\sqrt{4K_B cT}}{m} \tag{6.16}$$

For the designed Piezoresistive MEMS accelerometer the accelerometer noise obtained from equation Eq. 6.16 is 7.65 μm/s^2/$\sqrt{\text{Hz}}$.The noise equation 6.16 can be rewritten in terms of the Quality factor as in Eq.(6.17)

$$< a_n >= \sqrt{\frac{4K_B T\omega_n}{mQ}} \tag{6.17}$$

6.3 Proposed model for noise reduction

The accelerometer designed has piezoresistors at the edges of the beams to sense maximum stress. The sensor has to be placed on the plane normal to the tremor affected area of the patient. Usually, the single axis accelerometer if placed normal to the surface of the skin mainly the dorsum of the hand, can sufficiently capture feeble tremor as majority of the nerve fibres are connected. Whenever acceleration is applied, there is proof-mass displacement, and the suspension beams deflect, and this causes strain on the piezoresistors. The effect of applied stress is to change the number and mobility of the charge carriers within a material. This causes large change in resistivity. All the eight piezoresistors are connected in a manner that they form the arms of a Wheatstone bridge with each arm having two piezoresistors. Thus, the change in output voltage of the bridge is directly proportional to the applied acceleration. This analog output obtained from the MEMS accelerometer with the Wheatstone bridge circuit is then taken and fed to a sigma-delta converter. Here basically oversampling, noise shaping using sigma delta modulator, digital filtering and decimation are the stages the analog signal goes through for reduction of noise.

Oversampling is the process of taking more samples per second than required on the basis of the Nyquist-Shannon criterion. When we change the sampling rate the signal power and total quantization noise power is not affected. Therefore, the signal to quantization noise ratio is not changed. However, the quantization noise is spread over a larger frequency range, reducing the spectral density of the

TH-2011_11610225

quantization noise. If now only the original Nyquist band is considered, the quantization noise power is reduced by 3 dB for every doubling of the oversampling ratio and the signal to quantization noise ratio is improved accordingly. In this manner we get an increased efficiency since now the quantization noise can be pushed to frequencies far from the signal band. This effect is illustrated in Fig. 6.2 for an oversampling ratio of 1, 2, and 4 times.

Noise shaping is applied as a second step to improve the signal to quantization noise ratio. In this

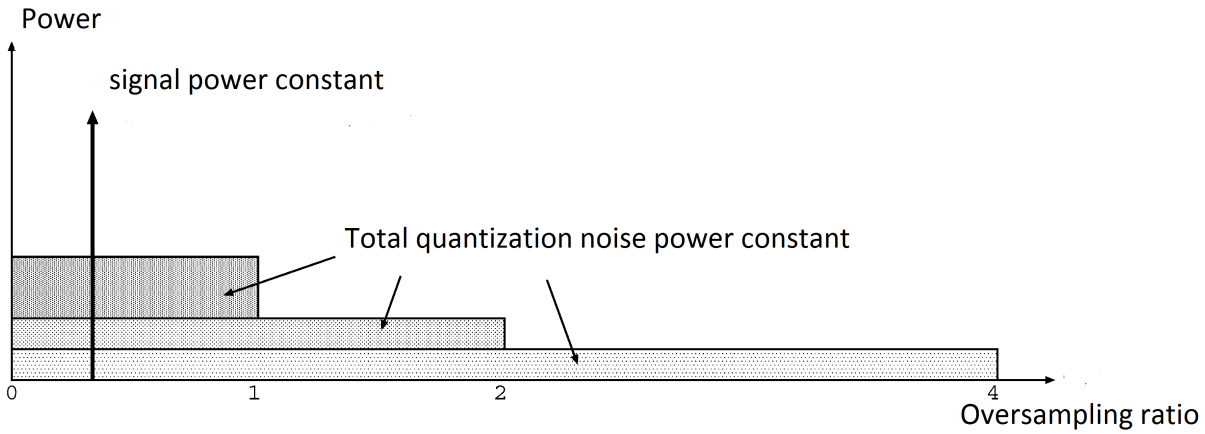

Figure 6.2: Illustration to show oversampling reduces noise spectral density

process the frequency distribution of the quantization noise is altered such that the quantization noise density reduces in the signal band. As a result the noise density increases at other frequencies where the noise is less harmful. This effect is depicted in Fig. 6.3 where low frequency noise is pushed to high frequencies. The amount of quantization noise is not changed by this process but the signal-to-noise ratio is increased in the low frequency area of the spectrum. In a sigma-delta modulator (SDM) the techniques of oversampling and noise shaping are combined, resulting in an increased efficiency since now the quantization noise can be pushed to frequencies far from the signal band. First, the sigma delta converter converts the analog signal into digital with a very low resolution analog to digital converter(ADC). The effective resolution is increased by using oversampling techniques in conjunction with noise shaping and digital filter. The digital filter is used to attenuate signals and noise that are outside the band of interest followed by decimation. During decimation the data rate is reduced from the oversampling rate without losing any necessary information. The proposed model for noise reduction is given in Fig. 6.4

As shown in Fig. 6.5, in the sigma delta modulator, the analog input signal is first fed via a

TH-2011_11610225

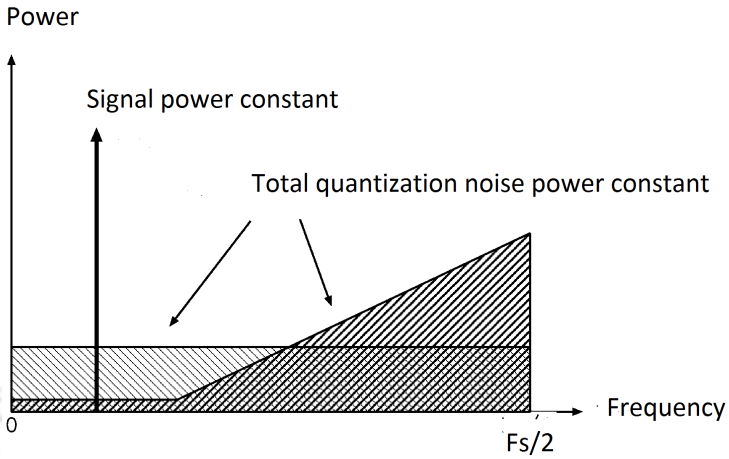

Figure 6.3: Noise shaping where low frequency noise is pushed to high frequencies

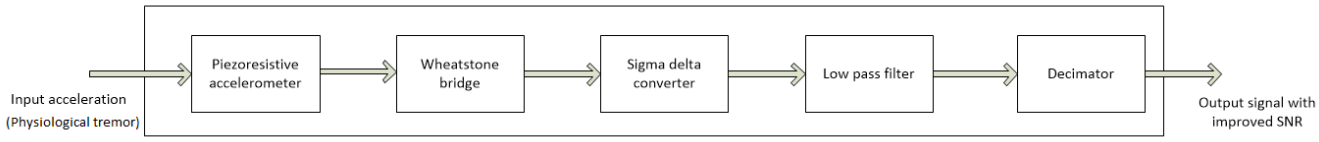

Figure 6.4: Proposed Noise reduction model with desired frequency range

summing junction. The signal is then passed through the integrator so that there can be a low pass filtering effect and we can focus on our desired frequency of 40 Hz and then this signal of desired band is fed to a comparator. The comparator acts as a one bit quantizer. The comparator output is fed back to the input summing junction via a one-bit digital-to analog converter (DAC), and it also passes through the digital filter and decimator for high resolution. The feedback loop forces the average of the signal entering from the DAC to be equal to the signal fed. The key feature of these converters is that they are the only low cost conversion method which provides both high dynamic range and flexibility in converting low bandwidth input signals.

6.3.1 Dissipation mechanism

In order to evaluate the mechanical thermal noise we should take into consideration the sources of dissipation or energy loss. Dissipation is termed as the mechanism that allows energy to escape from the orderly motion of the sensor. These include mechanical damping in the spring and support, viscous

TH-2011_11610225

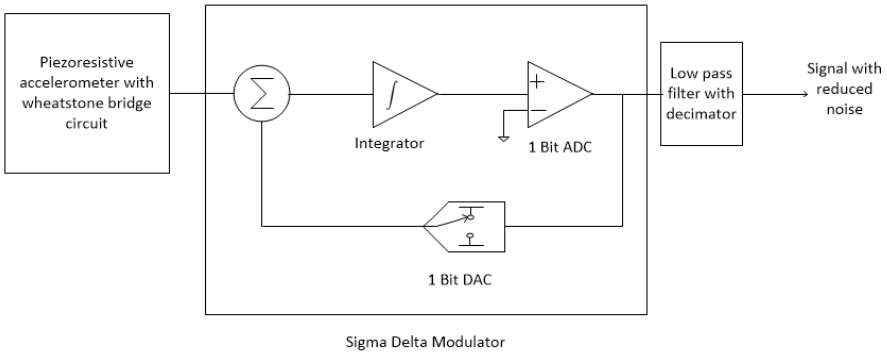

Figure 6.5: Sigma delta modulator for noise reduction

air damping, electrical leakage, magnetic eddy current damping etc. Damping determines the thermal fluctuations, hence in order to have an improvement in the signal to noise ratio the device design should have an effective and controlled damping mechanism. For the piezoresistive sensor having proof-mass and the top and bottom cover lids, damping is determined both by the spacing between them and the viscosity of the fluid used. This type of damping occurs when the proof-mass is pushed towards a fixed microstructure with the fluid in it. Squeeze film damping dominates the dissipation mechanism for gaps of several micrometers. In the present case the piezoresistive accelerometer senses the acceleration in the vertical z- axis therfore squeeze film damping is considered. The damping force arises from the squeeze film effect of the proof-mass and the air film trapped in the gap between the mass and the encapsulation. A large area to gap ratio results in higher squeeze number which results in greater damping. A small damping coefficient translates into lower energy loss, smaller damping ratio, and hence higher Q. We can improve the quality factors by reducing the operating pressure, improving the surface roughness, thermal annealing and by modifying the boundary conditions.

6.4 Results

The damping ratio is a very important design parameter for the MEMS accelerometer and its value can be determined from the geometric dimension, pressure, density and fluid viscosity. It is very important that the design should be such that the damping ratio is neither much lesser nor very much greater than unity. If we choose $\xi \ll 1$ then the structure may collapse, and if $\xi \gg 1$ then the settling time will be too large in other words it will give very slow response. In the present work the MEMS

TH-2011_11610225

accelerometer has been designed to achieve a damping of 0.7. For the designed Piezoresistive MEMS accelerometer, acceleration noise given by Eq. 6.16 is obtained as 7.65 $\mu m/s^2/\sqrt{Hz}$.

6.5 Conclusion

The performance of the microaccelerometers in terms of noise is very important. The micro accelerometer design aspects including the dissipation mechanism, signal processing circuit, temperature etc have an impact upon the noise performance. Hence careful design optimization has to be done to minimize noise which includes increasing the quality factor, reducing the resonating frequency and increasing the mass. The system must have enough dynamic range therefore the quality factor cannot be very high. A very high Q can give rise to very large out of band oscillations, and introduces ringing effect. Increasing mass increases sensitivity on one hand and a reduces natural frequency on the other hand. The bandwidth of the accelerometer has to be traded off with its sensitivity. The resonating frequency though can be decreased we must take care that it does not fall to be within the band of operating frequency. Hence proof–mass configuration should be wisely chosen by considering the trade offs. Also the device should have optimized damping by choosing appropriate damping mechanism. In order to lower the noise floor and improving the resolution the signal has to undergo low pass filtering. Thus optimization of all the designed parameters is important in order to reduce noise and improve the signal to noise ratio.

TH-2011_11610225

7

Conclusions and Future Work

Contents

TH-2011_11610225

TH-2011_11610225

7.1 Conclusion

The work carried out in this thesis is the design of piezoresistive accelerometer and analysis various facets of the same. The area studied include detailed design and analysis, reduction of cross axis sensitivity, design of damping and technique for noise reduction.

(i) Design and analysis of accelerometer: The mathematical model of accelerometer has been studied and two different structures are compared. The effect of thickness of the beams is studied and a suitable thickness of the beam is chosen for the design. In addition to the effect of thickness, the effect of placement of beam is also studied and the structure with the beams aligned with the proof-mass edge is chosen for the proposed design. The linearity of the stress with respect to the applied acceleration is evaluated for the proposed structures. Modal analysis is very important part of the design and analysis of such a device, the same is carried out for the proposed structure.

(ii) Damping analysis: Damping is a very important aspect for dynamic performance of such device. It is very important to predict the damping coefficient of accelerometer at design phase. The prediction is carried out using the existing models along with verifying the same using simulation tool. Squeeze film damping is used for the proposed accelerometer. The damping depends on the height of the thin film. Damping ratio is evaluated for different height of the thin film and height for the proposed design is decided based on the performance of the system. Time domain response is another important aspect which needs to be evaluated, the same is carried out for intended damping to establish the efficacy of damping.

(iii) Reduction of cross-axis sensitivity: Reduction of cross-axis sensitivity is very crucial for high performance accelerometer. As the worst of off axes sensitivity decides the performance; in this thesis simultaneous reduction of the cross-axis sensitivity has been done for the both the axes. This done by varying the aspect ratio of the proof-mass. The performance in terms of prime-axis and cross-sensitivity for the proposed accelerometer is compared with the ones reported in literature.

(iv) Reduction of noise: High performance accelerometer should have very low noise. In this thesis, a noise reduction scheme at the circuit level has been been proposed. Sigma delta converters are used for the purpose. It works on the basis of noise shaping, low pass filter and decimation. As the frequency of acceleration is comparatively low, the scheme is a very attractive one.

TH-2011_11610225

7.2 Further work

There are several ways, the work presented in this thesis can be extended and further investigated. Some of them are enumerated below.

(i) Study to ascertain the detailed effect of temperature on sensing.

(ii) Analysis for reducing effect of corner compensation as the beams are edge aligned to the mass

(iii) Evaluation of the proposed sensors with real signals from medical set-up

(iv) Manufacture and Test Prototype.

TH-2011_11610225

A

Appendix

Contents

TH-2011_11610225

TH-2011_11610225

A.1 Theories and Numerical Procedure Applied in COMSOL for Modelling Damping

This software tool COMSOL which shows how to couple squeeze-film gas damping, is modelled with Reynolds equation.The behavior of squeeze film is in general governed by both viscous and inertial effect within the fluid. However, for the very small geometries encountered in MEMS devices, inertial effect is often negligible. In such a case, the behavior of the fluid is governed by the well-known Reynolds equation. When the sensor squeezes the gap, the gas flows out from its edges. The narrow pathway restricts the flow, which causes gas pressure to increase. This increase in gas pressure, in turn, decelerates the plates movement, to displacements in the sensor. The pressure distribution in the narrow gap is given by modified Reynolds equation as shown in equation A.1, is a partial differential equation which describes the flow of a thin lubricant film between two surfaces. It is derived from the Navier-Stokes equations and is one of the fundamental equations of the classical lubrication theory. It was first derived by Osborne Reynolds in 1886.

$$\frac{d}{dt}(ph) + \nabla_t(phu) - p((\nabla_t h_s.u_s) - (\nabla_t h_b.u_b)) = 0 \tag{A.1}$$

The total fluid pressure p is the sum of initial/ambient pressure p_A and p_f, $h = h_0 + \Delta h_t$ is gap height consisting of the initial gap and the deformation in the normal direction of the boundary; h_s is the location of the solid wall; h_b is the location of the channel base; and u_s and u_b define the tangential velocity of the solid wall and the channel base, respectively. For MEMS devices, the temperature variation is usually negligible due to the small dimensions. Under the isothermal condition, gas density is directly proportional to its pressure P. The mean film velocity is given in equationA.2

$$u = \frac{\nabla_t p}{12\eta} h^2 Q_{ch} + \frac{u_s + u_b}{2} \tag{A.2}$$

where η denotes the fluid viscosity at normal conditions and the term Q_{ch} is the relative flow rate function that accounts for the rarefied gas effects. As COMSOL does not give the damping ratio directly so in order to predict the damping ratio, at first the height of the gap of thin film has to be calculated. It is important that at first the proper design parameters for damping

TH-2011_11610225

control is defined. The damping coefficient is obtained, for our desired damping requirement by the equation below.

$$\zeta = \frac{c}{2\sqrt{(km)}} \tag{A.3}$$

where ζ is the damping ratio, c is the damping coefficient, k is the spring constant and m is the mass. Then, using the Andrew et al's model [51], we have equation as shown below.

$$C^{Andrews} = \beta(b/a)\frac{a^2b^2\mu}{h^3} \tag{A.4}$$

where $\beta(b/a)$ is a correction factor which depends on the aspect ratio of the structure. For square proof-mass the value is 0.42.The gap of the thin film is obtained for the proposed structure as 18.6μm.

We now simulate and observe the step response in COMSOL. The damping coefficient is calculated from simulated Time domain characteristic. The response characteristic shows that damping coefficient obtained for height of 18.6μm was slightly greater than 0.7. Hence the procedure was repeated by simulating it for higher height in order to achieve a desirable damping ratio of 0.7. The simulation gives 0.7 damping coefficient for a thin film height of 23.5μm.

With this gap value, the damping coefficient is calculated using other models and also evaluated from simulation. As reported in the literature [51], that the accuracy of prediction of damping ratio varies from one model to the other, the simulation result of the proposed design is closer to the Blech model [47].

A.2 von Mises stress expression.

According to the von Mises criterion, yielding will occur when shear strain energy per unit volume reaches a critical value. The shear stress energy per unit volume is expressed in terms of three principal stresses.

$$\sigma_0 = \sqrt{\left[\frac{(\sigma_1-\sigma_2)^2+(\sigma_2-\sigma_3)^2+(\sigma_1-\sigma_3)^2}{2}\right]} \tag{A.5}$$

TH-2011_11610225

Bibliography

[1] R. J. Elble and J. McNames, "Using portable transducers to measure tremor severity," *Tremor and Other Hyperkinetic Movements*, vol. 6, May. 2016.

[2] T. A. Elwi, H. M. Al-Rizzo, D. G. Rucker, and H. R. Khaleel, "Effects of twisting and bending on the performance of a miniaturized truncated sinusoidal printed circuit antenna for wearable biomedical telemetry devices," *AEU - International Journal of Electronics and Communications*, vol. 65, no. 3, pp. 217–225., 2011.

[3] G. Grimaldi and M. Manto, *Synth. Lect. Biomed Eng.*, vol. 3, no. 1, p. 1212, 2008.

[4] C. Marsden and J. McAuley, "Physiological and pathological tremors and rhythmic central motor control," *J. of Neurology, Brain*, vol. 123, no. 8, pp. 1545–1567, 2000.

[5] C. Ramaker, J. Marinus, A. Stiggelbout, and B. J. V. Hiltenal, "Systematic evaluation of rating scales for impairment and disability in parkinson's disease," *Movement Disorders*, vol. 17, no. 5, pp. 1531–8257, 2002.

[6] N. Yazdi, F. Ayazi, and K. Najafi, "Micromachined inertial sensors," *Proceedings of the IEEE*, vol. 86, no. 8, pp. 1640–1659, Aug. 1998.

[7] L. M. Roylance and J. B. Angell, "A batch-fabricated silicon accelerometer," *IEEE Trans. Electron Devices*, vol. 26, no. 12, pp. 1911–1917, Dec. 1979.

[8] L. Findley and W. Koller, *Handbook of tremor disorders.* New York, USA: M. Dekker, 1995.

[9] M. Haris and H. Qu, "A cmos-mems piezoresistive accelerometer with large proof mass," in *2010 IEEE 5th International Conference on Nano/Micro Engineered and Molecular Systems*, Jan 2010, pp. 309–312.

[10] S. Kal, S. Das, D. Maurya, K. Biswas, A. R. Sankar, and S. Lahiri, "CMOS compatible bulk micromachined silicon piezoresistive accelerometer with low off-axis sensitivity," *Microelectronics Journal*, vol. 37, no. 1, pp. 22 – 30, 2006. [Online]. Available: http://www.sciencedirect.com/science/article/pii/S0026269205002697

TH-2011_11610225

[11] A.Partridge, J. Reynolds, B.W.Chui, E. Chow, A. Fitzgerald, L. Zhang, N. I. Maluf, and T. Kenny, "A high-performance planar piezoresistive accelerometer," *J. Microelectromech. Syst.*, vol. 9, no. 1, pp. 58–66, Mar. 2000.

[12] R. Kampen and R. Wolffenbuttel, "Modeling the mechanical behavior of bulk micromachining silicon accelerometer," *Sens. Actuators A*, vol. 64, pp. 137–150, 1998.

[13] A. Sankar, S. Das, and S.K.Lahiri, "Cross-axis sensitivity reduction of a silicon mems piezoresistive accelerometer," *Microsyst. Tech.*, vol. 15, no. 4, pp. 511–518, 2009.

[14] Y. Liu, H. Wang, H. Qin, and Y. Xie, "Performance enhancement for piezoresistive microaccelerometer by geometrical design: a focused review," *Sensor Review*, vol. 35, no. 3, pp. 310–318, 2015.

[15] Y. Luo, "Cross-axis sensitivity enhancement for a quad beam piezoresistive accelerometer," in *26th IEEE Canadian Conference on Electrical and Computer Engineering (CCECE), Regina, SK*, 2013, pp. 1–4.

[16] A. Sankar, S. Lahiri, and S. Das, "Performance enhancement of a silicon mems piezoresistive single axis accelerometer with electroplated gold on a proof mass'," *IOP.J Micromech Microeng.*, vol. 19, 2009.

[17] A. R. Sankar and S. Das, "A very-low cross-axis sensitivity piezoresistive accelerometer with an electroplated gold layer atop a thickness reduced proof mass," *Sens. Actuators, A*, vol. 189, pp. 125–133, 2013.

[18] H. Chen, M. Bao, H. Zhu, and S. Shen, "A piezoresistive accelerometer with a novel vertical beam structure," in *Proc. of Int. Solid State Sens. Actuators Conf. (Trans)*, vol. 2, Jun. 1997, pp. 1201–1204 vol.2.

[19] S. Shen, J. Chen, and M. Bao, "Analysis of twin mass structure for a piezoresistive accelerometer," *Sens. Actuators, A*, vol. 34, p. 101107, 1992.

[20] J. A. Plaza, A. Collado, E. Cabruja, and J. Esteve, "Piezoresistive accelerometers for mcm package," *J. Microelectromech. Syst.*, vol. 11, no. 6, pp. 794–801, Dec. 2002.

[21] A. Sankar, J.G.Jency, J. Ashwini, and S. Das, "Realization of a silicon piezoresistive accelerometer with proofmass edge aligned flexures using wet anisotropic etching," *IET Micro and Nano Letts.*, vol. 7, pp. 118–221, 2012.

[22] R. Amarasinghe, D. V. Dao, T. Toriyama, and S. Sugiyama, "Design and fabrication of a miniaturized six-degree-of-freedom piezoresistive accelerometer," *J. Micromech. Microeng Syst.*, vol. 15, no. 9, p. 1745, Jul. 2005.

[23] S. Kim and K. Wise, "Temperature sensitivity in silicon piezoresistive pressure transducers," *IEEE Trans. Electron Devices*, vol. 30, pp. 802–810, 1983.

TH-2011_11610225

[24] H. Chen, M. Bao, H. Zhu, and S. Shen, "A piezoresistive accelerometer with a novel vertical beam structure," *Sens. Actuators, A*, vol. 63, pp. 19–25, 1997.

[25] R.Otmani, N.Benmoussa, and B. Benyoucef, "The thermal drift characteristics of piezoresistive pressure sensor," *Physics Procedia*, vol. 21, pp. 47–52, 2011.

[26] J.C.Doll, "Self-heating in piezoresistive cantilevers," *Appl Phys Lett.*, p. 3, 2011.

[27] T. B. Gabrielson, "Mechanical-thermal noise in micromachined acoustic and vibration sensors," *IEEE Trans. Electron Devices*, vol. 40, no. 5, pp. 903–909, 1993.

[28] F.N.Hooge, "1/f noise is no surface effect," *Phys. Lett., A*, vol. 29, pp. 139–140, 1969.

[29] M. G. el Hak, *MEMS Applications*. Taylor and Francis, 2006.

[30] W. Thomson, *Theory Of Vibration with Applications*. Englewood Cliffs, New Jersey: 3rd ed., Prentice-Hall, 1988.

[31] G. Krishnan, *Displacement-amplifying Compliant mechanisms for sensor applications*, ch. Masters Thesis, Mechanical Engineering, Indian Institute of Science, Bangalore, India, 2007.

[32] Y. Cho, "Design, fabrication, and optimization of micromechanical flexures," in *PhD thesis, Univ. of California, Berkeley, CA, 1982.*

[33] H. Chen, M. Bao, H.Zhu, and S. Shaoqun, "A piezoresistive accelerometer with a novel vertical beam structure," in *Int. Conf in Solid State Sensors and Actuators 1997, TRANSDUCERS, Chicago*, 1997, pp. 1201–1204.

[34] Messina, J. Njuguna, V. Dariol, C. Pace, and G. Angeletti, "Design and simulation of a novel biomechanic piezoresistive sensor with silicon nanowires," *IEEE/ASME Trans. Mechatronics*, vol. 18, no. 3, pp. 1201–1210, 2013.

[35] Z. Zhou and X. Wang, "Analysis of squeeze-film air damping of thick perforated plate in mems devices," in *IEEE 6th International Conference on Nano/Micro Engineered and Molecular Systems, Xiamen, 2011.*

[36] M. Bao and H. Yang, "Squeeze film air damping in mems," *Sens. Actuators, A*, vol. 136, pp. 3–27, 2007.

[37] W. E. Newell, "Miniaturization of tuning forks," *Science*, vol. 161, pp. 1320–1326, 1968.

[38] J. B. Starr, "Squeeze-film damping in solid-state accelerometers," in *IEEE 4th Tech. Digest on Solid-State Sensor and Actuator Workshop*, Jun. 1990, pp. 44–47.

[39] C. Chen and W. J. Kuo, "Squeeze and viscous dampings in micro electrostatic comb drives," *Sens. Actuators, A*, vol. 107, no. 2, pp. 193–207, Oct. 2003.

TH-2011_11610225

[40] J. Mehner, S. Kurth, D. Billep, C. Kaufmann, K. Kehr, and W. Dotzel, "Simulation of gas damping in microstructures with nontrivial geometries," in *Proc. MEMS 98. IEEE. Eleventh Annual International Workshop on Micro Electro Mechanical Systems. An Investigation of Micro Structs, Sens., Actuators, Machines and Systems (Cat. No.98CH36176)*, Jan. 1998, pp. 172–177.

[41] S. M. Hutcherson, "Theoretical and numerical studies of the air damping of micro-resonators in the non-continuum regime," in *Disseration, G.W. Woodru School of Mechanical Engineering, Georgia Institute of Technology*, 2004.

[42] H. Moeenfard, "Analytical modeling of squeeze film damping in dual axis torsion microactuators," *Surf. Rev. Lett.*, vol. 22, 2015.

[43] M. I. Younis, *MEMS Linear and Non-linear Statics and Dynamics*. Newyork: Springer-Verlag New York Inc, 2011.

[44] J.Allen, *MEMS System Design*. BocaRaton Florida: Taylor Francis Group, LLC, 2005.

[45] Y. Kanda, "Piezoresistance effect of silicon," *Sensors and Actuators A: Physical*, vol. 28, no. 2, pp. 83 – 91, 1991. [Online]. Available: http://www.sciencedirect.com/science/article/pii/092442479185017I

[46] L.Chang, *Foundations of MEMS*. NG: Prentice Hall, 2006.

[47] J. J. Blech, "On isothermal squeeze films," vol. 105, p. 615, 10 1983.

[48] W. S. Griffin, H. H. Richardson, and S. Yamanami, "A study of fluid squeeze-film damping," vol. 88, 01 1966.

[49] T. Veijola, "Analytic damping model for an mem perforation cell," vol. 2, pp. 249–260, 05 2006.

[50] G. Franklin, J. Powell, and A. Emami-Naeini, *Feedback control of dynamic system*. Boston: Addison-Wesley, 1994.

[51] H. Sumali, "An experiment to determine the accuracy of squeeze-film damping models in the free-molecule regime," in *ASME 2007 International Mechanical Engineering Congress and Exposition*, vol. 11, Micro and Nano Systems, Parts A and B, November 1115 2007.

[52] L. Mol, L. A. Rocha, E. Cretu, and R. F. Wolffenbuttel, "Squeezed film damping measurements on a parallel-plate mems in the free molecule regime," in *TRANSDUCERS 2009 - 2009 International Solid-State Sensors, Actuators and Microsystems Conference*, June 2009, pp. 1425–1428.

[53] A. K. Pandey and P. Rudra, "A comparative study of analytical squeeze film damping models in rigid rectangular perforated mems structures with experimental results," *Microfluidics and Nanofluidics*, vol. 4, no. 3, pp. 205–218, Mar 2008. [Online]. Available: https://doi.org/10.1007/s10404-007-0165-4

[54] S.Kal, S. Das, D. Maurya, K.Biswas, A. R. Sankar, and S. Lahiri, "Cmos compatible bulk micromachined silicon piezoresistive accelerometer with low off-axis sensitivity," *J. Microelectronics*, vol. 37, pp. 22–30, 2005.

TH-2011_11610225

[55] Y. Kanda, "Piezoresistance effect of silicon," *Sensors and Actuators A: Physical*, vol. 28, no. 2, pp. 83 – 91, 1991. [Online]. Available: http://www.sciencedirect.com/science/article/pii/092442479185017I

[56] K. H. Kim, J. S. Ko, Y. H. Cho, K. Lee, B. M. Kwak, and K. Park, "A skew-symmetric cantilever accelerometer for automotive airbag applications," *Sensors and Actuators A: Physical*, vol. 50, no. 1, pp. 121 – 126, 1995. [Online]. Available: http://www.sciencedirect.com/science/article/pii/0924424796800951

[57] T. B. Gabrielson, "Mechanical-thermal noise in micromachined acoustic and vibration sensors," *IEEE Transactions on Electron Devices*, vol. 40, no. 5, pp. 903–909, May 1993.

[58] J. B. Johnson, "Thermal agitation of electricity in conductors," *Phys. Rev.*, vol. 32, pp. 97–109, Jul 1928. [Online]. Available: https://link.aps.org/doi/10.1103/PhysRev.32.97

[59] H. Nyquist, "Thermal agitation of electric charge in conductors," *Phys. Rev.*, vol. 32, pp. 110–113, Jul 1928. [Online]. Available: https://link.aps.org/doi/10.1103/PhysRev.32.110

TH-2011_11610225

TH-2011_11610225

TH-2011_11610225